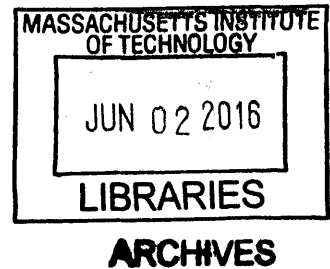


Adaptive Output-Feedback Control and Applications to Very Flexible Aircraft

by

Zheng Qu

B.S., University of Michigan, Ann Arbor (2009)
S.M., University of Michigan, Ann Arbor (2010)



Submitted to the Department of Mechanical Engineering
in partial fulfillment of the requirements for the degree of

Doctor of Philosophy in Mechanical Engineering

at the

MASSACHUSETTS INSTITUTE OF TECHNOLOGY

June 2016

© Massachusetts Institute of Technology 2016. All rights reserved.

Signature redacted

Author

Department of Mechanical Engineering

May 19, 2016

Signature redacted

Certified by

Anuradha M. Annaswamy

Senior Research Scientist

Thesis Supervisor

Signature redacted

Accepted by

Rohan Abeyaratne

Chairman, Department Committee on Graduate Students

Adaptive Output-Feedback Control and Applications to Very Flexible Aircraft

by

Zheng Qu

Submitted to the Department of Mechanical Engineering
on May 19, 2016, in partial fulfillment of the
requirements for the degree of
Doctor of Philosophy in Mechanical Engineering

Abstract

Very Flexible Aircraft (VFA) corresponds to an aerial platform whose flight dynamics critically depends on its flexible wing shape, and has been investigated as a potential solution to generate high-altitude low-endurance flights. The dominant presence of model uncertainties and potential actuator anomalies motivate an adaptive approach for control of VFA. Another particular control challenge for VFA is that its flexible modes cannot be measured accurately, which necessitates an output-feedback multi-input multi-output (MIMO) control approach. The focus of this thesis is on an adaptive output-feedback controller for a generic class of MIMO plant models with an emphasis on the control of a VFA so as to execute desired flight maneuvers. The proposed adaptive controller includes a baseline design based on observers and parameter adaptation based on a closed-loop reference model (CRM), and is applicable for a generic class of MIMO plants of arbitrary relative degree, and therefore the overall design is suitable for control in the presence of uncertainties in flexible effects, sensor dynamics, and actuator dynamics. In addition, the proposed controller can accommodate plant models whose number of outputs exceeds number of inputs. One major advantage of the proposed design is that the number of integrators required for implementation is significantly less than that of previous methods and therefore the controller can be implemented even for large-dimensional VFA models. Conditions are delineated under which asymptotic stability and command tracking can be guaranteed, and the overall design is verified using realistic simulations on a high-fidelity VFA model with unknown varying wing shape and actuator anomalies.

Thesis Supervisor: Anuradha M. Annaswamy
Title: Senior Research Scientist

Acknowledgments

I would like to extend my greatest gratitude towards my advisor, Anuradha Annaswamy, for being tremendously supportive to my research. I would like to thank Eugene Lavretsky for insight and encouragement. I would also like to thank other members of my PhD committee, Kamal Youcef-Toumi and Domitilla Del Vecchio for valuable inputs.

This thesis is dedicated to my father and mother, whose wisdom and love indulge me until today. A quote from G. K. Chesterton would be appropriate to conclude this chapter of my life:

*Fairy tales are more than true: not because they tell us that dragons exist,
but because they tell us that dragons can be beaten.*

Contents

1	Introduction	17
1.1	Large Dimension MIMO Systems	17
1.2	Very Flexible Aircraft	17
1.3	Linear Output-Feedback Control	18
1.4	Adaptive Output-Feedback Control	19
1.5	Relative Degree One Observer-Based Control Design	20
1.6	Higher Relative Degree Control Design	20
1.7	Nonsquare Plant Models	21
1.8	Synopsis of Thesis	21
1.9	Thesis Contributions by Chapter	22
2	Plant Model Description	25
2.1	A Class of Uncertain MIMO Plant Model	25
2.2	VFA Model	28
2.2.1	3-Wing VFA Model	31
2.2.2	Vulture VFA Model	32
3	Preliminaries	35
4	Relative Degree One Design	45
4.1	Relative Degree One Problem Statement	45
4.2	Relative Degree One Adaptive Control Design with SPR/LTR Properties	47

4.2.1	Controller Structure	48
4.2.2	SPR/LTR Design	51
4.2.3	Design Procedure	58
4.2.4	Comparison with Other Adaptive Output-Feedback Controllers	59
4.3	Applications to VFA	62
4.3.1	Vertical Acceleration Tracking of 3-wing VFA	62
4.3.2	Vulture VFA Bank-To-Turn Control	68
5	Relative Degree Two Design	77
5.1	Relative Degree Two Problem Statement	77
5.2	Relative Degree Two Adaptive Control Design	80
5.2.1	Control Design	80
5.2.2	Underlying SPR Error Model	83
5.2.3	Adaptive Law and Stability Proof	85
5.2.4	Design Procedure	85
5.3	With Negligible Actuator Dynamics	86
5.4	Applications to VFA	87
6	Relative Degree Three Design	93
6.1	Relative Degree Three SISO Control Design Example	93
6.1.1	Relative Degree Three SISO Plant Model	94
6.1.2	Control Design and Error Model Analysis	96
6.1.3	High Order Tuner and Stability Proof	103
6.2	Relative Degree Three MIMO Problem Statement	104
6.3	Relative Degree Three MIMO Adaptive Control Design	108
6.3.1	Control Design	108
6.3.2	Error Model Analysis	112
6.3.3	High Order Tuner and Stability Proof	115
6.3.4	Extension to Nonsquare Plant Models	117
6.3.5	Design Procedure	118
6.4	Applications to VFA	119

7 Arbitrary Relative Degree Design	129
7.1 Arbitrary Relative Degree Problem Statement	129
7.2 Extension of Control Design to Arbitrary Relative Degree	130
8 Conclusions	135
8.1 Future Work	135
A Proof for Results in Chapter 2	143
B Proof for Results in Chapter 3	147
C Proof for Results in Chapter 4	151
D Proof for Results in Chapter 5	167
E Proof for Results in Chapter 6	177
F Proof for Results in Chapter 7	193

List of Figures

2-1	The illustration of 3-Wing VFA	31
2-2	The illustration of Vulture VFA	33
4-1	The architecture of the adaptive output-feedback controller: an adaptive component is added to a baseline observer-based controller . . .	51
4-2	The Bode plot of the SPR system $\{(A - LC), B, S_1 C\}$ for the 3-wing VFA model using the SPR/LTR observer parameter $L = L_\rho$	67
4-3	L_ρ in the baseline controller is able to recover the phase condition of $\{(A + B\Lambda^*\Theta^* - L_\rho C), B, S_1 C\}$ with unknown Θ^* and Λ^* for the 3-wing VFA model	67
4-4	The Nyquist plot of the loop gain at input, $L_u(s)$, of the baseline controllers, compared with that of the LQR controller for the 3-wing VFA model	67
4-5	The simulation results of the vertical acceleration tracking of the 3-wing VFA using the adaptive output-feedback controller, compared with the baseline SPR/LTR controller	69
4-6	The “snapshots” of the closed-loop systems for the 3-wing VFA model in the simulation shown in Figure 4-5b	70
4-7	Comparison of the maximum and minimum singular values of the transfer function matrix between the original Vulture VFA model and the reduced-order model	71
4-8	The zoom-in map of poles and transmission zeros of $\{(A - L_\rho C), B, S_1 C\}$ for the Vulture VFA	72

4-9	The frequency domain analysis of the closed-loop system using the baseline SPR/LTR controller on the Vulture VFA model, compared with a LQR	72
4-10	The flight path and flexible wing shape of the Vulture VFA in the BTT maneuver, controlled by the adaptive SPR/LTR controller.	74
4-11	The tracking of roll angle (ψ) and side-slip angle (β) in the BTT maneuver of the Vulture VFA through thrust (T_1) and tail (δ_1) using the adaptive controller, compared with the baseline controller and a LQR.	75
4-12	The adapted parameters settle down to steady-state values after three step commands of BTT for the Vulture VFA	76
5-1	The tracking of η and A_z using the relative degree two adaptive controller for the nonlinear 3-wing VFA model	90
5-2	The parameter trajectories of the relative degree two adaptive controller in the simulation shown in Figure 5-1b for the nonlinear 3-wing VFA model	91
5-3	The frequency domain analysis of the snapshot closed-loop system shows that adaptation mitigates the effects of model uncertainties on the robustness of the “snapshot” closed-loop systems for the 3-wing VFA model	91
6-1	The tracking of η and A_z using the relative degree three adaptive controller on the nonlinear VFA model	123
6-2	The parameter trajectories of the relative degree three adaptive controller in the simulation shown in Figure 6-1b for the nonlinear 3-wing VFA model	124
6-3	The spectrum of the aileron δ_a response in the simulation shown in Figure 6-1b for the nonlinear 3-wing VFA model	124
6-4	The frequency response of the snapshot closed-loop system with the relative degree three adaptive controller, from δ_e to V_z , and the effects of $\Psi_i(0)$ for the 3-wing VFA model	124

6-5 The frequency domain analysis of the snapshot closed-loop system shows that adaptation mitigates the effects of model uncertainties on robustness for the 3-wing VFA model	125
6-6 The time domain response of η and δ_a when subject to sinusoidal disturbance/noise of magnitude 0.2 and frequencies 0.3, 2, 3 rad/sec for the nonlinear 3-wing VFA model	127
6-7 The mean of the moving window standard deviation (MMSTD) of η tracking and δ_a control when subject to sinusoidal disturbance/noise of various frequencies for the nonlinear 3-wing VFA model	127

List of Tables

6.1 Total number of integrators required for each controller	122
--	-----

Chapter 1

Introduction

1.1 Large Dimension MIMO Systems

To achieve engineering marvels, modern machines are made of a huge number of intricate components and mechanism, and therefore include complicated dynamics. Control designs that are based on a simplified low-order plant model cannot produce stable performance in all operation range while applied on the real machine, while control designs based on high-fidelity high-order models usually yield a much higher order controller that defies efficient implementation. These large dimension systems are also equipped with a large number of sensors and actuators, and are required to perform a complex maneuver that involve all sensors and actuators simultaneously, which defies classical single-input-single-output (SISO) decoupling approach and therefore motivates a MIMO approach. One of such large dimension MIMO control challenge is Very Flexible Aircraft (VFA) [1, 2].

1.2 Very Flexible Aircraft

VFA platforms are being investigated with increased attention in the last decade, motivated to a large extent by the desire to generate high-altitude long-endurance (HALE) flights [1, 3, 4]. VFA corresponds to an aerial platform whose equilibrium flight condition (*trim*) critically depends on the flexible modes of wings [3, 5]. One

of the challenges of VFA is a significant change in the rigid-body dynamics around a trim as its wing morphs. For example, the pitch (short period) mode of VFA can become unstable when wing dihedral is trimmed at a high value [5, 6]. As a consequence, control designs based on low-order rigid-body dynamics only may face unexpected adversities. An example of this adversity occurred in 2003 during the second test flight of Helios when the flight controller failed to regulate the wing dihedral and eventually, allowed the unstable pitch mode to diverge [6]. The lesson learned from the mishap is that the model for control designs has to include body flexible effects [5, 6].

Nonlinear VFA models have been investigated in [5, 7, 8] with focus on capturing the flexibility effects while VFA navigates through multiple trims. For maneuvers around a single trim, high-fidelity linear model, such as the one for Vulture VFA [2], is also introduced with the focus on verification of the control design for large dimension systems. All these platforms feature a particular challenge that only a set of state measurements can be used for control because body flexible modes have to be included in the model but none of them are measurable. The restriction necessitates control designs based on output-feedback, such as linear observer-based controllers.

1.3 Linear Output-Feedback Control

Output-feedback MIMO control designs have been studied extensively because of their ability to control a plant with only incomplete state measurements. One strategy is to use an observer to generate state estimates, and use the estimates to perform state-feedback-like control [9]. Observer-based controllers have been widely employed for aircraft control and their performance is quite satisfactory for a nominal linear time invariant (LTI) plant model, which are able to capture most of the rigid body dynamics [10, 11]. Combined with the “full-state” loop transfer recovery (LTR) technique [9, 12] (referred as the LTR technique hereafter), the resulting controllers, denoted as observer-based LTR, recover the guaranteed stability margins of linear quadratic regulators (LQR) asymptotically [9, 12, 13], and therefore can tolerate a

certain amount of model uncertainties. Application of observer-based LTR controllers to VFA, however, faces unique difficulties. First, since flexible wings can deform to an unknown shape, the actual trim and the corresponding flight dynamics can drift far away from the nominal trim and its nominal dynamics (*trim drift*). Second, a HALE flight can cause severe actuator anomalies such as power surge in motors or structure damage on control surfaces. Both unknown adversities can exceed stability margins of observer-based LTR controllers, and therefore make these controllers inadequate for VFA.

1.4 Adaptive Output-Feedback Control

The limitations of linear controllers motivate an adaptive control solution that is able to accommodate the unknowns associated with VFA flights. Those unknowns include unknown structure stiffness and compliance change caused by unknown trim drift, which is another consequence of unmeasurable states, and unknown scaling of lift/thrust force caused by actuator anomalies. This thesis will show that both types of the unknown adversities can be modeled as parametric uncertainties in the underlying plant model.

For uncertain plant models, adaptive control has been investigated as a candidate improvement over linear controllers for the reason that it guarantees to recover both stability and performance despite the presence of large parametric uncertainties [14]. The classical approach to MIMO adaptive controllers (see [14, Chapter 10] and [15, Chapter 9]) is based on the underlying plant transfer function matrix. Such a design typically requires the knowledge of plant's Hermite form [16, 17] and uses a non-minimal observer along with a reference model, resulting in a significant number of integrators (a high order controller). These high order designs prohibit their applications to VFA since VFA model usually features large amount of flexible states.

1.5 Relative Degree One Observer-Based Control Design

In contrast to the classical method, recent literature proposes a new approach of adaptive control based on state-space representation, which uses a minimal observer to generate the underlying state estimates [18, Chapter 14]. The state estimates are then used for both feedback (similar to observer-based linear controllers) and parameter adaptation. Unlike the classical approach, the observer is also used as a reference model, by appealing to the notion of a closed-loop reference model (CRM), which is recently shown to be a highly promising direction in adaptive control due to improved transients [19–21]. The presence of CRM allows the new controllers to use much fewer integrators than the classical ones, and is therefore an attractive alternative in the case of MIMO plant models (see [18, 22–24]). The proposed controllers in these references guarantee stable adaptation based on an underlying strict positive real (SPR) condition and therefore can be applied on a plant model with relative degree one. Implementation of the proposed controllers requires solutions for its parameters, which are subject to a matrix inequality, and therefore are solved using numerical methods in these references. As a result, applications to a large dimension plant model, or analysis of LTR properties, are not available.

1.6 Higher Relative Degree Control Design

The adaptive controllers proposed in the above-mentioned references [18, 23–25] are based on a restrictive assumption that the underlying relative degree of the plant is unity. This implies that any actuator dynamics that may be present has to be sufficiently fast, and also that the set of sensors must result in the number of net integrations to not exceed one (for example, velocity sensors for mechanical systems). Since actuator dynamics or sensor dynamics are hardly negligible in real applications, especially for HALE flight where actuator/sensor aging could take place, high relative degree plant models with uncertainties in both the plant dynamics and the actua-

tor/sensor dynamics need to be considered. While adaptive controllers for such kind of plant models have been addressed in SISO plants [21], currently very few results exist for this case in MIMO plants. Classical adaptive control approach (see [14, Chapter 10] and [15, Chapter 9]) addresses MIMO plant models with high relative degree at the cost of huge amount of integrators and therefore are not suitable for large dimension systems such as VFA applications.

1.7 Nonsquare Plant Models

Square systems play a key role in control theory development because of some unique properties they may possess such as SPR properties [26], which serves a crucial role in guaranteeing stability. Therefore, in adaptation design for MIMO plant models [14, 15], square plant models with stable transmission zeros are commonly assumed. Nonsquare plant models, whose number of outputs exceeds number of inputs, become increasingly popular in industry since sensors are cheap and can be massively deployed. The fact that nonsquare plant models usually do not have transmission zeros makes them a good candidates for adaptive control design. To extend control design to non-square systems, a squaring-up method is usually needed, which effectively produces an artificial square system through addition suitable inputs. Literature on squaring-up methods were rather sparse until the work by [27, 28]. The squaring-up method in these references, however, are subject to a restrictive assumption that the underlying plant models have uniform relative degree one, which prevents the design to be applicable to plants that have actuator dynamics, i.e. higher relative degree.

1.8 Synopsis of Thesis

The main contribution of the thesis is the development of an adaptive output-feedback controller for a class of MIMO plant models with unequal number of inputs and outputs and arbitrary relative degree, and the demonstration of the design on a high-fidelity large dimension VFA model for high-altitude flight with body flexible effects.

First, a generic class of MIMO plant models that are suitable for control purpose, in particular for VFA control, is examined in Chapter 2. Then mathematical preliminaries necessary for control design and analysis are introduced in Chapter 3. While assuming no actuator dynamics present, we develop an adaptive controller for the plant model with relative degree one in Chapter 4. In Chapter 5, we then explicitly consider actuator dynamics and extend the control design to plant models with relative degree two. The control design is further extended to relative degree three in Chapter 6, which serves as a corner stone to extend the whole design to arbitrary relative degree in Chapter 7. Squaring-up method are provided in each section such that the overall method can be applied on nonsquare plant models. Simulations with high-fidelity VFA model are presented at the last section of each chapter for each of the control designs. All proof of the Propositions, Lemma, Theorem can be found in the Appendix.

1.9 Thesis Contributions by Chapter

The main contributions of the thesis is described in Section 1.8. The following paragraphs are thesis contributions by chapter.

Chapter 2

A class of nonlinear VFA model as proposed in [8] is properly linearized and is shown to contain parametric uncertainties due to unmeasurable flexible effects. This class of linearized VFA model is shown to belong to a generic class of MIMO plant models.

Chapter 3

Based on a series of definitions and properties pertain to relative degree [29, 30], an implementable state-space realization is developed for a plant model with its input being differentiated, which is a crucial part for high relative degree control design.

Chapter 4

Based on the previous adaptive control design for relative degree one plant models [18], a new explicit closed-form solution for its parameters is proposed and shown to guarantee an underlying SPR condition while retaining the LTR properties in the baseline controller. The design is also extended to plant models with nonlinear parametric uncertainties. Demonstration of the control design on a large-dimension nonsquare VFA model is carried out around a single trim.

Chapter 5

Using a recursive property of the new control parameter design, the relative degree one adaptive control design is extended to plant models with relative degree two. Extension to nonsquare plant models whose number of outputs exceeding number of inputs is also integrated into the design. Demonstration of the control design on a nonlinear VFA model is carried out while the VFA navigating through multiple trim.

Chapter 6

The relative degree two adaptive control design is extended to nonsquare plant models with relative degree three. Demonstration of the control design on a VFA model verifies that significantly less number of integrators are used compared with the classical adaptive controllers.

Chapter 7

The adaptive control design is extended to nonsquare plant models with arbitrary relative degree.

Chapter 2

Plant Model Description

This section describes a class of MIMO plant models that are commonly seen in real world applications. First a generic class of uncertain MIMO plant models is examined in Section 2.1. The main focus of this thesis is presented in Section 2.2, where a class of VFA model is examined and shown to be a MIMO plant model with parametric uncertainties. Then Section 2.2.1 presents a 3-Wing VFA model that belongs to the class and will be used for our simulation validation. Section 2.2.2 describes another example of the class, the Vulture VFA model, that will be used for the verification of the design on a large dimension plant model.

2.1 A Class of Uncertain MIMO Plant Model

Dynamics of a MIMO plant around an equilibrium flight condition can be described by a linear time invariant (LTI) model as

$$\begin{aligned}\dot{x} &= Ax + Bu \\ y &= Cx\end{aligned}\tag{2.1}$$

where $x \in \mathbb{R}^n$ are states, $u \in \mathbb{R}^m$ are control inputs, and $y \in \mathbb{R}^p$ are measurement outputs. $A \in \mathbb{R}^{n \times n}$, $B \in \mathbb{R}^{n \times m}$, $C \in \mathbb{R}^{p \times n}$ are known matrices which represent a nominal model. Since in most flight control applications, there are more sensors than actuators (as sensors are much cheaper than actuators), and all states are not

measurable, we assume that $n > p \geq m$.

Eq.(2.1) corresponds to the ideal case where all plant matrices are known. In reality, these matrices are unknown and are identified through various methods. The state matrix A can be determined through experiments fairly accurately, such as wind-tunnel tests for aircraft frame. C is well known as well since the relation between measured outputs and states is well defined. The input matrix B , in contrast, may not be accurate as the net effect of control inputs are subjected to perturbations. We address two of the dominant issues in this section.

The first source of uncertain perturbations we consider is the unknown structural stiffness, compliance or weight distribution change. In most cases, this effect can be modeled as an additive term $\Theta^{*T}\Phi(x)$ where $\Phi(\cdot) : \mathbb{R}^n \rightarrow \mathbb{R}^h$ is a known nonlinear function regressor and $\Theta^* \in \mathbb{R}^{h \times m}$ is an unknown parametric uncertainty. The second source of uncertainties that we consider is actuator anomalies caused by electronic power surge or control surface damage. This is modeled as an unknown multiplicative factor $\Lambda^* \in \mathbb{R}^{m \times m}$. Together, both uncertainties lead to a modified plant model given by

$$\begin{aligned}\dot{x} &= Ax + B\Theta^{*T}\Phi(x) + B\Lambda^*u \\ y &= Cx\end{aligned}\tag{2.2}$$

The class of plant model as in (2.2) is generic and can model a variety of real dynamics. For example, it can model the response of vertical acceleration of aircraft when elevators move, in which case Θ^* are the uncertainties in the CG position of the aircraft [18, Chapter 2]. Another example is the response of pitch/roll/yaw angles of a quadrotor when some of its motors change power output, which is summarized below.

Example 2.1. [31]The 6 DOF dynamics of quadrotor helicopters around a hover orientation can be described by a linear model that belongs to (2.2) as

$$\begin{aligned}\ddot{w} &= g\theta, \quad \ddot{y} = -g\phi, \quad \ddot{z} = \frac{1}{m}(U_1 + \Delta U_1) \\ \ddot{\phi} &= \frac{L}{I_x}(U_1 + \Delta U_1), \quad \ddot{\theta} = \frac{L}{I_y}(U_3 + \Delta U_3), \quad \ddot{\psi} = \frac{1}{m}(U_3 + \Delta U_4)\end{aligned}\tag{2.3}$$

where variables w, y, z are the positions of CG in the inertial frame; Variables ϕ, θ, ψ are the Euler angles of the body frame; Constants m, I_x, I_y, I_z are the mass and moments of inertia of the quadrotor, respectively; Constant L is the length of rotor arm; Variables U_1, U_2, U_3, U_4 are the collective, roll, pitch and yaw forces generated by the four rotors, and $\Delta U_1, \Delta U_2, \Delta U_3, \Delta U_4$ are their associated uncertainties caused by motor/propeller deficiency.

Another example is the response of cart position when the mounted inverted pendulum is pushed, as summarized below.

Example 2.2. The dynamics of cart position around the unstable equilibrium $\theta_0 = 0$, $p_0 = 0$, where θ is the angle between the bar and the vertical line, p is the horizontal displacement of the cart, belongs to the class of (2.2) and can be written as

$$\underbrace{\begin{bmatrix} \dot{p} \\ \ddot{p} \\ \dot{\theta} \\ \ddot{\theta} \end{bmatrix}}_{\dot{x}} = \underbrace{\begin{bmatrix} 0 & 1 & 0 & 0 \\ 0 & 0 & \frac{mg}{M} & 0 \\ 0 & 0 & 0 & 1 \\ 0 & 0 & \frac{g(M+m)}{Ml} & 0 \end{bmatrix}}_{A} \underbrace{\begin{bmatrix} p \\ \dot{p} \\ \theta \\ \dot{\theta} \end{bmatrix}}_{x} + \underbrace{\begin{bmatrix} 0 \\ \frac{1}{M} \\ 0 \\ \frac{1}{Ml} \end{bmatrix}}_{B} u + \underbrace{\begin{bmatrix} 0 \\ \frac{1}{M} \\ 0 \\ \frac{1}{Ml} \end{bmatrix}}_{\Theta^* x} \quad (2.4)$$

$$y = [p] = \underbrace{\begin{bmatrix} 1 & 0 & 0 & 0 \end{bmatrix}}_{C} x$$

where u is the force input and Θ^* are the uncertainties in the weights of cart or point mass at the tip of pendulum.

In all the cases discussed above, $\Phi(x)$ can be as simple as x , and Λ^* are the uncertainties in the control effectiveness due to motor or control surface damage. Detail assumptions on the class of plant models (2.2) will be discussed in the beginning of each control design section. Among these assumptions, the relative degree of the plant model is the major topic of this thesis.

2.2 VFA Model

This section will show that a generic VFA model, if linearized around a trim, also belongs to the class of MIMO plant models presented in (2.2). Our starting point is a nonlinear VFA model including its complete rigid body dynamics and flexible component dynamics, which is derived in [8] using the virtual work method as

$$\begin{bmatrix} M_{FF} & M_{FB} \\ M_{BF} & M_{BB} \end{bmatrix} \begin{bmatrix} \ddot{\epsilon} \\ \dot{\beta} \end{bmatrix} + \begin{bmatrix} C_{FF} & C_{FB} \\ C_{BF} & C_{BB} \end{bmatrix} \begin{bmatrix} \dot{\epsilon} \\ \beta \end{bmatrix} + \begin{bmatrix} K_{FF} & 0 \\ 0 & 0 \end{bmatrix} \begin{bmatrix} \epsilon \\ b \end{bmatrix} = \begin{bmatrix} B_F \\ B_B \end{bmatrix} F^{load}, \quad (2.5)$$

assuming:

Assumption 2.1. *The coupling between rigid body and flexible elements are caused by inertia and compliance property change only;*

Assumption 2.2. *Control surfaces span the entire wing;*

Assumption 2.3. *Properties of aircraft vary slowly with respect to the rigid body position and orientation;*

Assumption 2.4. *External loads weakly depend on body acceleration;*

Assumptions 2.1 and 2.4 implies that aerodynamic coupling is negligible. ϵ are states of the flexible wing with elements being states of each discretized flexible segments, and $\dot{b} = \beta$ are states of rigid body with β being velocities and b being positions/orientations. K_{FF} is the stiffness of the joints. Define $J_{h\epsilon}(\epsilon, b) = \frac{\partial h}{\partial \epsilon}$ and $J_{hb}(\epsilon, b) = \frac{\partial h}{\partial b}$ as the Jacobian matrices with $h(\epsilon, b)$ being the lumped coordinate transformation effects integrated along wing span. Since $\dot{J}_{h\epsilon} = \frac{\partial^2 h}{\partial \epsilon^2} \dot{\epsilon} + \frac{\partial^2 h}{\partial \epsilon \partial b} \dot{b}$ and $\dot{J}_{hb} = \frac{\partial^2 h}{\partial b \partial \epsilon} \dot{\epsilon} + \frac{\partial^2 h}{\partial b^2} \dot{b}$, the compliance matrices $C_{(\cdot)(\cdot)}$ are functions of $(\epsilon, \dot{\epsilon}, b, \beta)$. More

specifically,

$$\begin{aligned}
M_{FF}(\epsilon) &= J_{h\epsilon}^T M_e J_{h\epsilon}, \quad M_{BF}(\epsilon) = J_{hb}^T M_e J_{h\epsilon} \\
M_{FB}(\epsilon) &= J_{h\epsilon}^T M_e J_{hb}, \quad M_{BB}(\epsilon) = J_{hb}^T M_e J_{hb} + M_{RB} \\
C_{FF}(\epsilon, \dot{\epsilon}, \beta) &= J_{h\epsilon}^T M_e \dot{J}_{h\epsilon} + C_e, \quad C_{BF}(\epsilon, \dot{\epsilon}, \beta) = J_{hb}^T M_e \dot{J}_{h\epsilon} \\
C_{FB}(\epsilon, \dot{\epsilon}, \beta) &= J_{h\epsilon}^T M_e \Omega_B J_{hb} + 2 J_{h\epsilon}^T M_e \dot{J}_{hb} \\
C_{BB}(\epsilon, \dot{\epsilon}, \beta) &= J_{hb}^T M_e \Omega_B J_{hb} + 2 J_{hb}^T M_e \dot{J}_{hb} + C_{RB} \\
B_F(\epsilon) &= J_{h\epsilon}, \quad B_B(\epsilon) = J_{hb},
\end{aligned} \tag{2.6}$$

where $M_{(\cdot)}$ is the effective inertia, $C_{(\cdot)}$ is the effective compliance, $F^{load}(\ddot{\epsilon}, \dot{\epsilon}, \epsilon, \dot{\beta}, \beta, u_s)$ is the aerodynamic load (see [8] for detail derivations), and u_s is the control surface input. Since Assumption 2.3 holds, $J_{(\cdot)(\cdot)}$, $M_{(\cdot)(\cdot)}$ and $B_{(\cdot)}$ are only function of ϵ , and the compliance matrices $C_{(\cdot)(\cdot)}$ are only functions of $\epsilon, \dot{\epsilon}, \beta$. The generalized aerodynamic loading F^{load} are calculated locally at wing segments and then summed along the wing span. It is noted that because inertia, compliance and external load effects are all subject to local coordinate transformation, $M_{(\cdot)(\cdot)}$, $C_{(\cdot)(\cdot)}$ and $B_{(\cdot)}$ all have J_{hb} or $J_{h\epsilon}$ as their leading factors.

To design a controller for a trim $[\ddot{\epsilon}_0, \dot{\epsilon}_0, \epsilon_0, \dot{\beta}_0, \beta_0, u_0]^T$, we first define deviation states and inputs as $x_p = [\epsilon - \epsilon_0, \dot{\epsilon} - \dot{\epsilon}_0, \beta - \beta_0]^T \in \mathbb{R}^{n_p}$ and $u_p = (u_s - u_0) \in \mathbb{R}^m$, respectively, and perform model linearization (ignoring high-order error terms), which generally leads to a linear parameter varying (LPV) plant as

$$Q_1 \dot{x}_p = Q_2 x_p + Q_3 u_p, \tag{2.7}$$

where Q_1 includes inertia matrices, Q_2 includes compliance and stiffness matrices and both are functions of $(\ddot{\epsilon}_0, \dot{\epsilon}_0, \epsilon_0, \dot{\beta}_0, \beta_0)$ (see [8] for detail derivations). Q_3 is a function of $(\epsilon_0, \beta_0, u_0)$. Control of the LPV plant requires gain scheduling [32] with respect to $(\ddot{\epsilon}_0, \dot{\epsilon}_0, \epsilon_0, \dot{\beta}_0, \beta_0, u_0)$, which faces difficulties since only $(\epsilon_0, \beta_0, u_0)$ are measurable, while $(\ddot{\epsilon}_0, \dot{\epsilon}_0, \dot{\beta}_0)$ are not. The controller has to calculate its parameters using an assumed trim point $(0, 0, \epsilon_0, 0, \beta_0)$, which can be far away from the actual trim. This

introduces model uncertainties as

$$\begin{aligned} Q_1 &= \bar{Q}_1(0, 0, \epsilon_0, 0, \beta_0) + \Delta Q_1^*(\ddot{\epsilon}_0, \dot{\epsilon}_0, \dot{\beta}_0) \\ Q_2 &= \bar{Q}_2(0, 0, \epsilon_0, 0, \beta_0) + \Delta Q_2^*(\ddot{\epsilon}_0, \dot{\epsilon}_0, \dot{\beta}_0). \end{aligned} \quad (2.8)$$

where \bar{Q}_1 and \bar{Q}_2 are the known to the controller as well as Q_3 , while ΔQ_1^* and ΔQ_2^* are the unknown to the controller. Eq.(2.8) transforms the plant (2.7) into a special form as specified in Lemma 2.1, whose proof can be found in Appendix A.

Lemma 2.1. *The nonlinear VFA model (2.5)(2.6) that satisfies Assumptions 2.1 to 2.4, has the unknown ΔQ_1^* and ΔQ_2^* that can be parametrized as*

$$\Delta Q_1^* = Q_3 \Theta_{q_1}^{*T}(\ddot{\epsilon}_0, \dot{\epsilon}_0, \dot{\beta}_0), \quad \Delta Q_2^* = Q_3 \Theta_{q_2}^{*T}(\ddot{\epsilon}_0, \dot{\epsilon}_0, \dot{\beta}_0), \quad (2.9)$$

and the model can be linearized around an unknown trim $(\ddot{\epsilon}_0, \dot{\epsilon}_0, \epsilon_0, \beta_0, \dot{\beta}_0, \beta_0, u_0)$, producing an uncertain LPV plant as

$$\begin{aligned} \dot{x}_p &= (A_p + B_p \Theta_p^{*T})x_p + B_p \Lambda^* u_p \\ y_p &= C_p x_p \end{aligned} \quad (2.10)$$

where $A_p(\epsilon_0, \beta_0, u_0) = \bar{Q}_1^{-1} \bar{Q}_2$, $B_p(\epsilon_0, \beta_0, u_0) = \bar{Q}_1^{-1} Q_3$ are known plant parameters, while $\Theta_p^{*T} = \Theta_{q_2}^{*T} - \bar{\Theta}_{q_1}^{*T} A_p - \bar{\Theta}_{q_1}^{*T} B_p \Theta_{q_2}^{*T}$, where $\bar{\Theta}_{q_1}^{*T} = (I + \Theta_{q_1}^{*T} Q_1^{-1} Q_3)^{-1} \Theta_{q_1}^{*T}$, and $\Lambda^* = \Lambda_p^*$, where $\Lambda_p^* = (I - \bar{\Theta}_{q_1}^{*T} B_p)$, are unknown.

Eq.(2.9) implies that the local body inertia and compliance changes caused by local wing deformation can be approximated by similar changes caused by external loads. In realistic applications, Λ^* can include control effectiveness loss Λ_d^* as $\Lambda^* = \Lambda_p^* \Lambda_d^*$ where Λ_d^* can be present due to possible control surface damage. Eq.(2.10) is the actual uncertain LPV plant model when aircraft flies through different trims. If we assume that

Assumption 2.5. *All aircraft properties vary slowly around a trim,*

then all matrices in Eq.(2.10) are constant and Eq.(2.5) becomes a linear time invariant model, which belongs to the class of plant models in (2.2). The following

two subsections present two VFA model examples that belong to the generic VFA model class (2.10).

2.2.1 3-Wing VFA Model

Consider a simple VFA comprised of three rigid wings with elastic pivot connections adjoining them [5]. The longitudinal and vertical dynamics of the 3-wing VFA is coupled with the dynamics of rotational movement of outer wings with respect to the center wing about the chord axis, as shown in Figure 2-1. The angle between the two wing planes is denoted as wing *dihedral* (η).



Figure 2-1: The illustration of 3-Wing VFA

The platform captures essential flexible wing effects and can be viewed as building blocks of large VFA. A 6-state nonlinear model has been developed in [5, Eq.s (45) and (46)] including aircraft's pitch mode and dihedral dynamics. Define V as airspeed, α as the angle of attack, θ as pitch angle and q as pitch rate. The nonlinear model can be rewritten in the form of (2.5) with $\epsilon = \eta$ and $\beta = [V, \alpha, q]^T$:

$$\begin{bmatrix} d_3(\eta) & s\alpha c\eta & 0 & 0 \\ 0 & m & 0 & 0 \\ 0 & 0 & mV & 0 \\ 0 & 0 & 0 & c_1 + c_2 s^2 \eta \end{bmatrix} \begin{bmatrix} \dot{\eta} \\ \dot{V} \\ \dot{\alpha} \\ \dot{q} \end{bmatrix} + \begin{bmatrix} k_c - \frac{m^* s}{3} c\eta s\eta \dot{\eta} & \frac{m^* s}{2} c\eta c\alpha \dot{\alpha} & 0 & \frac{m^* s}{2} c\eta c\alpha \\ 0 & 0 & 0 & g \\ 0 & 0 & 0 & 0 \\ 2c_2 c\eta s\eta q & 3c_2 c\eta s\alpha \dot{\alpha} & 0 & 3c_2 c\eta s\alpha \end{bmatrix} \begin{bmatrix} \dot{\eta} \\ V \\ \alpha \\ q \end{bmatrix} + \begin{bmatrix} k_k & 0 & 0 & 0 \\ 0 & 0 & 0 & -g \\ 0 & 0 & 0 & 0 \\ 0 & 0 & 0 & 0 \end{bmatrix} \begin{bmatrix} \eta \\ \int V dt \\ \int \alpha dt \\ \theta \end{bmatrix} + \begin{bmatrix} c\eta s\eta & c\eta c\alpha \\ 0 & 0 \\ 0 & 0 \\ c^2 \eta & c\eta s\alpha \end{bmatrix} \begin{bmatrix} \delta_e \\ \delta_a \end{bmatrix}, \quad (2.11)$$

where $s(\cdot) = \sin(\cdot)$, $c(\cdot) = \cos(\cdot)$ and δ_e and δ_a are properly scaled. Parameter c_1 and c_2 are inertia constants that depends on aircraft physical properties, and $d_3(\eta)$ is the rotation inertia about longitudinal axis and therefore a function of η (see [5]). Measurements are vehicle vertical acceleration A_z , η and q . Other states, α and $\dot{\eta}$, are unmeasurable and are unavailable for control. The nonlinear model was trimmed at 30ft/sec airspeed, 40,000 ft altitude and different dihedrals, and the corresponding linearized models with respect to each dihedral were obtained [5] and were used as our design model. For example, the linearized model around the trim at $\eta = 10^\circ$ can

be written as

$$\begin{bmatrix} V \\ \dot{\alpha} \\ \dot{\theta} \\ \dot{q} \\ \dot{\eta} \\ \ddot{\eta} \end{bmatrix} = \begin{bmatrix} -0.279 & 3.476 & -32.2 & -0.015 & 0.514 & 0.525 \\ -0.070 & -4.104 & 0 & 1.013 & 0.193 & 0.100 \\ 0 & 0 & 0 & 1 & 0 & 0 \\ 0 & -54.04 & 0 & 0.255 & 1.845 & 21.41 \\ 0 & 0 & 0 & 0 & 1 & 0 \\ 0.002 & 0.044 & 0 & 0.819 & -0.075 & -6.518 \end{bmatrix} \begin{bmatrix} V \\ \alpha \\ \theta \\ q \\ \eta \\ \dot{\eta} \end{bmatrix} + \begin{bmatrix} -2.57 & -6.47 \\ -0.795 & -0.079 \\ 0 & 0 \\ 5.991 & -6.363 \\ 0 & 0 \\ 0.195 & -0.034 \end{bmatrix} \begin{bmatrix} \delta_e \\ \delta_a \end{bmatrix} \quad (2.12)$$

$$y = \begin{bmatrix} q \\ \eta \end{bmatrix} = \begin{bmatrix} 0 & 0 & 0 & 1 & 0 & 0 \\ 0 & 0 & 0 & 0 & 1 & 0 \end{bmatrix} x.$$

where three aileron are bundled as one control δ_a and three elevators are bundled as one control δ_e . The pitch mode is stable for this trim. Local stability analysis shows that when the dihedral is above 15° , the pitch mode becomes unstable [5]. Let's consider the uncertainties that may exist in the plant model. First, there might be a control surface damage that reduces control effectiveness to 10% ($\Lambda^* = 0.1$). Second, since the outer elevators are connected to the outer wings, their control effectiveness is locally linearly proportional to η and therefore is a function of Θ^*x (in which case, the regressor $\Phi(x) = x$). To verify the model form of (2.10) in the presence of uncertainties, we obtained the linearized model for $\eta = 16^\circ$ and $\dot{\eta} = 0.2$ deg/sec, which can be parametrized with in the form of (2.12) with (A_p, B_p, C_p) for $\eta = 10^\circ$ and $\dot{\eta} = 0$ deg/sec, and

$$\Lambda^* = 0.1; \quad \Theta_p^{*T} = \begin{bmatrix} 0.02 & -31.94 & 0.12 & 0.91 & 9.1 & -9.28 \end{bmatrix}. \quad (2.13)$$

2.2.2 Vulture VFA Model

Recently, a large VFA platform, denoted as Vulture, has been under development to meet the goals of HALE maneuvers. Vulture is an experimental aircraft with a wingspan of 400ft. Its entire wing is made of light low-yield material and is flexible to deform. 3-wing VFA example shown in the previous subsection represents building blocks of the Vulture VFA. One can consider the wings of the Vulture as hundreds of 3-wing segments adjoined together. The huge wings are in junction with 4 long booms in the middle of wingspan and 2 end devices at the tips, as shown in Figure 2-2.

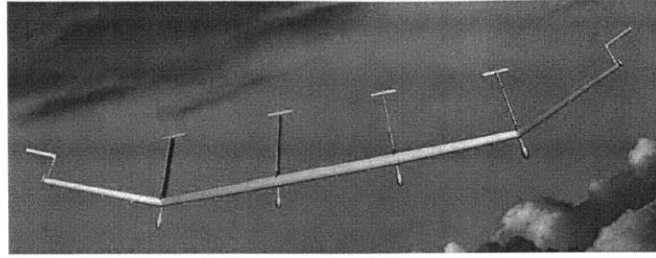


Figure 2-2: The illustration of Vulture VFA

A large dimension model has been developed for Vulture with 707 states, 21 control inputs and 212 outputs, representing the VFA trim at a nominal HALE flight condition at a cruise speed of 34.6 ft/sec, an altitude of 66,000 ft, and with zero dihedral [2]. The 21 inputs includes 15 engine propellers evenly placed across the wingspan and 6 tail elevators at the end of each boom (see Ref. [2] for details). If dividing the 707 states into three groups, i.e. 12 rigid body dynamics states x_{RB} for 6 vehicle degrees of freedom, 340 flexible positions x_{flex} , and 340 flexible velocities v_{flex} , the Vulture model manifests itself in the following block matrix form:

$$\begin{bmatrix} \dot{x}_{RB} \\ \dot{x}_{flex} \\ \dot{v}_{flex} \end{bmatrix} = \underbrace{\begin{bmatrix} \times & * & \times \\ 0 & 0 & I \\ \times & \times & o\backslash o \end{bmatrix}}_{A_p} \begin{bmatrix} x_{RB} \\ x_{flex} \\ v_{flex} \end{bmatrix} + \underbrace{\begin{bmatrix} \times \\ 0 \\ \times \end{bmatrix}}_{B_p} u_p + \underbrace{\begin{bmatrix} * \\ 0 \\ \times \end{bmatrix}}_{C_p} \dot{u}_p + \underbrace{\begin{bmatrix} * \\ 0 \\ \times \end{bmatrix}}_{D_p} \ddot{u}_p$$

$$y_p = \underbrace{\begin{bmatrix} \times & 0 & 0 \end{bmatrix}}_{C_p} x + D_p u_p + D_1 \dot{u}_p + D_2 \ddot{u}_p \quad (2.14)$$

where \times represents dense entries, $*$ represents sparse entries and $o\backslash o$ represents diagonal entries. Some observations are made. First, the flexible modes are strongly coupled with rigid-body dynamics. Second, the control u only acts on flexible component. Third, there are control rate \dot{u}_p and control acceleration \ddot{u}_p effects, which represent aero-elastic-coupling between unsteady aerodynamics and flexible effects of boom. These features imposes great control challenges. For the control design, we will pretend that the \dot{u}_p and \ddot{u}_p terms are not present and therefore the resulting model (called the design model) belongs to the class of MIMO plant models as in

(2.10). For the actual simulation we will bring back the \dot{u}_p and \ddot{u}_p terms (called the evaluation model).

Chapter 3

Preliminaries

This section presents definitions and lemma that will be used to handle high relative degree systems. Proofs of all results in this section are redirected to the corresponding references. First we define index notations in superscript and subscript that are often used in a zero polynomial.

Definition 3.1. No bracket is number of power operation, i.e. $x^{n+1} = x^{\{n+1\}} = x^n \cdot x$; [] bracket is index for variable notation, for example, $x^{[2+1]} = x^{[3]}$; and () bracket is the number of derivative, for example $x^{(2)} = \ddot{x}$.

Define s as the differentiation operator, i.e. $s^i[\cdot] = \frac{d^i}{dt^i}[\cdot] = [\cdot]^{(i)}$, and define $\pi_r^i(s)$ as what follows.

Definition 3.2. Define $\pi_r^i(s)$ as a i th order polynomial in s with a_r^i as the its coefficients, i.e.

$$\pi_r^i(s) = (s + \alpha_1)(s + \alpha_2) \cdots (s + \alpha_i) = \sum_{j=0}^i a_r^{r-j} s^{i-j} \quad (3.1)$$

for $i = 1, 2, \dots, r$, and $\alpha_i \in \mathbb{C}$; Define d_r^i as the coefficients of differentiation operation, i.e. $s^r(xy) = d_r^r x^{(r)}y + d_r^{[r-1]} x^{(r-1)}y^{(1)} + \dots + d_r^0 xy^{(r)}$.

Remark 3.1. In particular, $s^{(-1)}[\cdot] = \int [\cdot] dt$. $\pi_r^i(s)$ arrange coefficients in a reverse way (for example, $\pi_2^0(s) = a_2^2$, $\pi_2^1(s) = a_2^2s + a_2^1$ and $\pi_2^2(s) = a_2^2s^2 + a_2^1s + a_2^0$) so that

$$\pi_r^i(s) \cdot s^{r-i} + \sum_{j=0}^{r-i-1} a_r^j s^j = \pi_r^{i+1}(s) \quad (3.2)$$

has a recursive property.

Consider a state space representation $\{A, B, C\}$ with m inputs and p outputs. Square systems have $m = p$ while nonsquare systems have $m \neq p$. The notation $\{A, B, C, D\}$ is defined as the transfer function matrix $G(s) = C(sI - A)^{-1}B + D$. The case when $D = 0$ is denoted as $\{A, B, C\}$. Degenerate systems are defined as follows.

Definition 3.3. If for an m -input p -output linear system $G(s) = C(sI - A)^{-1}B + D$, the rank of $G(s)$ is strictly less than $\min(m, p)$ for any $s \in \mathbb{C}$, where \mathbb{C} is the set of complex number, then the system is degenerate.

Most real linear plant models are non-degenerate, whose transmission zeros can be defined as follows.

Definition 3.4. [33] For a non-degenerate m -input and p -output linear system with minimal realization $A \in \mathbb{R}^{n \times n}$, $B \in \mathbb{R}^{n \times m}$, $C \in \mathbb{R}^{p \times n}$ and $D \in \mathbb{R}^{p \times m}$, the transmission zeros are defined as the finite values of z such that $\text{rank}[R(z)] < n + \min[m, p]$, where

$$R(z) = \begin{bmatrix} zI - A & B \\ C & D \end{bmatrix}. \quad (3.3)$$

Transmission zeros represent a state trajectory that cannot be detected by any of the outputs. Most non-square linear systems don't have transmission zeros; square systems are more likely to lose rank and therefore more likely to have transmission zeros [34]. Generally, for MIMO plants transmission zeros and individual transfer function zeros are different. An example below illustrates the difference.

Example 3.1. In Example 2.2, the SISO plant model $\{A, B, C\}$ has four poles at $0, 0, \sqrt{\frac{g(M+m)}{Ml}}, -\sqrt{\frac{g(M+m)}{Ml}}$, and two zeros at $\sqrt{\frac{q}{l}}, -\sqrt{\frac{q}{l}}$. Suppose an additional measurement of the tilt angle rate $\dot{\theta}$ is included in y as

$$y = \begin{bmatrix} p \\ \dot{\theta} \end{bmatrix} = \begin{bmatrix} 1 & 0 & 0 & 0 \\ 0 & 0 & 0 & 1 \end{bmatrix} x. \quad (3.4)$$

Then the resulting single-input-multiple-output does not have any transmission zeros.

However, choosing an additional mixing measurement as

$$y = \begin{bmatrix} p \\ -\sqrt{\frac{q}{l}}\theta + \dot{\theta} + p \end{bmatrix} = \begin{bmatrix} 1 & 0 & 0 & 0 \\ 1 & 0 & 1 & -\sqrt{\frac{q}{l}} \end{bmatrix} x \quad (3.5)$$

results in a plant model with a transmission zeros at $\sqrt{\frac{q}{l}}$. The ratio of mixing has to be exact for the transmission zero to exist.

We part B into columns as $B = [b_1, b_2, \dots, b_m]$ with b_i corresponding to the i th input u_i . The input relative degree of the plant model is defined as following.

Definition 3.5. A linear square plant model $\{A, B, C\}$ has

a) input relative degree $\tau = [r_1, r_2, \dots, r_m]^T \in \mathbb{N}^{m \times 1}$ if and only if

i) $\forall j \in \{1, \dots, m\}, \forall k \in \{0, \dots, r_j - 2\} :$

$$CA^k b_j = 0_{m \times 1}, \text{ and} \quad (3.6)$$

$$ii) \text{ rank } \begin{bmatrix} CA^{r_1-1} b_1 & CA^{r_2-1} b_2 & \dots & CA^{r_m-1} b_m \end{bmatrix} = m; \quad (3.7)$$

b) uniform input relative degree $r \in \mathbb{N}$ if and only if it has input relative degree $\tau = [r_1, r_2, \dots, r_m]^T$ with $r = r_1 = r_2 = \dots = r_m$.

Remark 3.2. If $\{A, B, C\}$ has u_i of input relative degree r_i , one needs to differentiate u_i r_i th time to make u_i shows up in the y equation, i.e.

$$\begin{aligned} C(sI - A)^{-1} b_i \cdot s &= C(sI - A)^{-1} A b_i \\ &\vdots \\ C(sI - A)^{-1} b_i \cdot s^{r_i-1} &= C(sI - A)^{-1} A^{r_i-1} b_i \\ C(sI - A)^{-1} b_i \cdot s^{r_i} &= C(sI - A)^{-1} A^{r_i} b_i + C A^{r_i-1} b_i \end{aligned} \quad (3.8)$$

where we have used Definition 3.5 and the identity $(sI - A)^{-1}s = I + (sI - A)^{-1}A$. The term “relative degree” is referred to input relative degree in this paper.

Generically, any MIMO plant model has input relative degree since condition i)

and *ii*) are generically satisfied. The input relative degree relates to the transmission zeros of the plant model in the following Lemma (see [35, Corollary 2.6] for proof).

Lemma 3.1. *For a square system $\{A, B, C\}$ with uniform input relative degree r , define*

$$\mathfrak{C} := \begin{bmatrix} C \\ CA \\ \vdots \\ CA^{r-1} \end{bmatrix}, \quad \mathfrak{B} := \begin{bmatrix} B & AB & \cdots & A^{r-1}B \end{bmatrix}, \quad (3.9)$$

with $\mathfrak{C} \in \mathbb{R}^{mr \times n}$, $\mathfrak{B} \in \mathbb{R}^{n \times mr}$, $\mathfrak{M} \in \mathbb{R}^{n \times (n-mr)}$ as the right null space of \mathfrak{C} such that $\mathfrak{C}\mathfrak{M} = 0$, and

$$\mathfrak{N} = (\mathfrak{M}^T \mathfrak{M})^{-1} \mathfrak{M}^T [I_n - \mathfrak{B}(\mathfrak{C}\mathfrak{B})^{-1} \mathfrak{C}] \in \mathbb{R}^{(n-mr) \times n} \quad (3.10)$$

such that $\mathfrak{N}\mathfrak{B} = 0$ and $\mathfrak{N}\mathfrak{M} = I_{n-mr}$. Then $\mathfrak{C}\mathfrak{B}$ is full rank, and the eigenvalues of

$$Z = \mathfrak{N}A\mathfrak{M} \in \mathbb{R}^{(n-mr) \times (n-mr)} \quad (3.11)$$

are the transmission zeros of the $\{A, B, C\}$.

Lemma 3.1 can be directly extended to the plant model with nonuniform relative degree. It follows Lemma 3.1 that the number of transmission zeros are related to the relative degree in the following way (see [35] for proof).

Corollary 3.1. *The number of transmission zeros n_z of a plant model with relative degree $\mathbf{r} = [r_1, r_2, \dots, r_m]^T$ satisfies*

$$n_z = n - r_s \quad (3.12)$$

where $r_s = \sum_{i=1}^m r_i$ and n is the number of states.

Realization of a transfer function matrix is not unique. Two realizations of linear time invariant systems are equivalent if they share a same transfer function. A special state space realization, called “input normal form”, will be used to write system

matrices with respect to its relative degree, as stated in the Following Lemma, whose proof can be found in [35, Theorem 2.4].

Lemma 3.2. *[Input Normal Form] For plant models $\{A, B, C\}$ with uniform relative degree r , there exists an invertible coordinate transformation matrix*

$$T_{in} = \begin{bmatrix} (\mathfrak{C}\mathfrak{B})^{-1}\mathfrak{C} \\ \mathfrak{N} \end{bmatrix}, \quad T_{in}^{-1} = \begin{bmatrix} \mathfrak{B} & \mathfrak{M} \end{bmatrix}, \quad (3.13)$$

where \mathfrak{M} and \mathfrak{N} are defined in Lemma 3.1, that can transform the plant model into

$$\begin{bmatrix} \dot{\xi}_1 \\ \dot{\xi}_2 \\ \vdots \\ \dot{\xi}_r \\ \dot{\eta} \end{bmatrix} = \underbrace{\begin{bmatrix} 0 & \cdots & 0 & R_1 & V \\ I_m & \cdots & 0 & R_2 & 0 \\ \vdots & \ddots & \vdots & \vdots & 0 \\ 0 & \cdots & I_m & R_r & 0 \\ 0 & \cdots & 0 & U & Z \end{bmatrix}}_{A_{in}} \begin{bmatrix} \xi_1 \\ \xi_2 \\ \vdots \\ \xi_r \\ \eta \end{bmatrix}_{x_{in}} + \underbrace{\begin{bmatrix} I_m \\ 0 \\ \vdots \\ 0 \\ 0 \end{bmatrix}}_{B_{in}} u$$

$$y = \underbrace{\begin{bmatrix} 0 & \cdots & 0 & CA^{r-1}B & 0 \end{bmatrix}}_{C_{in}} x_{in} \quad (3.14)$$

using $x_{in} = T_{in}x$, $A_{in} = T_{in}AT_{in}^{-1}$, $B_{in} = T_{in}B$, and $C_{in} = CT_{in}^{-1}$, where $Z \in \mathbb{R}^{(n-3m) \times (n-3m)}$ has eigenvalues that are transmission zeros of $\{A, B, C\}$.

$\{A, B, C\}$ and $\{A_{in}, B_{in}, C_{in}\}$ are two equivalent realizations. Systems with differentiator s added to inputs also have equivalent realizations, as stated in the following Lemma, whose proof can be found in the Appendix B.

Lemma 3.3. *Given a linear system $\{A, B, C\}$ with uniform input relative degree r , the following two realizations are equivalent:*

i)

$$\begin{aligned} \dot{x} &= Ax + B\pi_{r-1}^{r-i}(s)[u] \\ y &= Cx \end{aligned} \quad (3.15)$$

where $\pi_{r-1}^{r-i}(s)$ is defined in (3.1) for $i = 1, 2, \dots, r-1$;

ii)

$$\begin{aligned}\dot{x}' &= Ax' + B_r^i u \\ y &= Cx'\end{aligned}\tag{3.16}$$

where

$$B_r^i = \sum_{j=0}^{r-i} A^{r-j} B a_{r-1}^{r-i-j} = \pi_{r-1}^{r-i}(A) B.\tag{3.17}$$

and x' is a new state coordinate.

Remark 3.3. It is noted $\{A, B_r^i, C\}$ has relative degree i , and as a result, we name B_r^i as “the input path with relative degree i ”. It is noted that the implementation of representation (3.15) usually requires differentiating input u first and therefore is not feasible, while the implementation of (3.16) does not require differentiating u first and is generally feasible. For this reason, we will design controllers using (3.16), and will use (3.15) for analysis. Two state coordinates are related as

$$x' = x - \sum_{j=i+1}^r (B_r^j s^{j-i-1})[u].\tag{3.18}$$

(3.15) differentiates inputs of a relative degree r system $\{A, B, C\}$ $(r - i)$ times, which adds $(r - i)$ transmission zeros to $\{A, B, C\}$, as stated in the following proposition, whose proof can be found in the B.

Proposition 3.1. Define $Z\{\cdot\}$ as the set of transmission zeros of transfer function $\{\cdot\}$ and $Z[\cdot]$ as that of a polynomial $[\cdot]$; if $\{A, B, C\}$ and B_r^i are given in Lemma 3.3, then

$$Z\{A, B_r^i, C\} = Z\{A, B, C\} \cup Z[\pi_{r-1}^{r-i}(s)]$$

One special category of plant models with relative degree is the relative degree one plant models. Relative degree one plant models have the following property, which is a special case of Lemma 3.1 (see Ref. [29] for the proof).

Corollary 3.2. [29] For a square system $\{A, B, C\}$ with CB full rank (uniform relative degree one), there exist matrices $M \in \mathbb{R}^{n \times (n-m)}$ and $N \in \mathbb{R}^{(n-m) \times n}$ such that

$NB = 0_{(n-m) \times m}$, $CM = 0_{m \times (n-m)}$, $NM = I_{(n-m) \times (n-m)}$ and the eigenvalues of (NAM) are the transmission zeros of $\{A, B, C\}$.

One special category of relative degree one transfer functions is a strictly positive real (SPR) transfer function. This thesis uses Ref. [14, Definition 2.10] for the definition of SPR. Kalman–Yakubovich–Popov (KYP) lemma links the frequency domain properties of an SPR transfer function to its realization.

Lemma 3.4. *[KYP Lemma] A system $\{A, B, C\}$ is strictly positive real if and only if there exists a $P = P^T > 0$ such that*

$$PA + A^T P < 0 \quad (3.19)$$

$$PB = C^T. \quad (3.20)$$

An SPR $\{A, B, C\}$ is a square system satisfying $CB = B^T PB = (CB)^T > 0$. With the definition of N , Eq.(3.20) of KYP Lemma can be fully characterized as following (see Ref. [36] for the proof).

Lemma 3.5. *[36] Given a pair of B and C , if there exists a $P = P^T > 0$ such that $PB = C^T$, then $P \in \mathcal{P}$ where*

$$\mathcal{P} = \{P > 0 \mid P = C^T(CB)^{-1}C + N^T W_p N, \quad W_p > 0\}, \quad (3.21)$$

N is the right null space of B and W_p is an arbitrary symmetric positive definite matrix.

Lemma 3.5 implies that given a pair of B and C such that $CB = (CB)^T > 0$, a $P > 0$ that satisfies $PB = C^T$ can be calculated using (3.21). From Lemma 3.2, it can be concluded that having stable transmission zeros is a necessary condition for the system to be SPR. This can be shown by pre and post-multiplying Eq.(3.19) with M^T and M , respectively, and appealing to Eq.(3.21), which yields

$$W_p NAM + M^T A^T N^T W_p < 0. \quad (3.22)$$

For Eq.(3.22) to hold for an symmetric positive definite (SPD) W_p , *NAM* has to be Hurwitz.

Another special category of plant models with relative degree is the relative degree zero plant models $\{A, B, C, D\}$. Relative degree zero plant model can also have SPR properties. The following states the multivariable case of Lefschetz-Kalman-Yakubovich (LKY) Lemma regarding to SPR relative degree zero plant models.

Lemma 3.6. [26, 37, 38] Assume (A, B, C, D) is a minimal realization of $G(s)$; Then $G(s)$ is SPR if and only if a $\gamma > 0$, a matrix $P = P^T > 0$, a matrix $L > 0$, and matrices W and K exist such that

$$PA + A^T P = -W^T W - L \quad (3.23)$$

$$PB = C^T + W^T K \quad (3.24)$$

$$K^T K = D + D^T \quad (3.25)$$

Lemma 3.4 and Lemma 3.6 leads to a Corollary that states the close relation between a SPR relative degree one plant model and a SPR relative degree zero plant model.

Corollary 3.3. If a transfer function matrix $\{A, B, C\}$ is SPR, then there exists a $\alpha^* > 0$ such that the transfer function matrix $\{A, B_a^0, C, aCB\}$, where $B_a^0 = aAB + B$ is SPR for all $a < \alpha^*$; and $\{A, B, C\}$ and $\{A, B_a^0, C, aCB\}$ share a same $P = P^T > 0$ that satisfies the results of Lemma 3.4 and the results of Lemma 3.6, respectively.

The following proposition provides formulation of parameter errors in the presence of s , which will be used in parameter adaptation design and error model formulation. The proof is rather straight forward and therefore is omitted here.

Proposition 3.2. Suppose s is the differentiation operator, ϕ^{*T} is a constant parameter matrix, $\phi(t)$ is a function of time, $\omega(t)$ is another function of time t , then

$$\pi_r^i(s) [\phi^T(t)\omega(t)] - \phi^{*T} \pi_r^i(s) [\omega(t)] = \pi_r^i(s) [\tilde{\phi}^T(t)\omega(t)] \quad (3.26)$$

where $\tilde{\phi}^T(t) := \phi^T(t) - \phi^{*T}$, and $\pi_r^i(s)$ is defined in (3.1) for $i = 1, 2, \dots, r$.

The \mathcal{L}_1 , \mathcal{L}_2 and \mathcal{L}_∞ bound of a time series signal $x(t)$ is defined in [14, Section 2.7].

Chapter 4

Relative Degree One Design

This section presents the adaptive control design for relative degree one plant models, and is organized as follows. Section 4.1 formulates the control problem in the context of VFA. Section 4.2 presents the adaptive controller design and its SPR/LTR properties, and also includes stability analysis of the adaptive system. Section 4.3 demonstrates the response of the resulting closed-loop system with the adaptive controller using two numerical examples, including the 3-wing VFA model and the Vulture VFA model [2] around a single flight condition.

4.1 Relative Degree One Problem Statement

Following the description in Chapter 2, an application-driven nominal plant model with relative degree one is described as

$$\begin{aligned}\dot{x}_p &= A_p x_p + B_p u \\ y_p &= C_p x_p \\ z &= C_{pz} x_p + D_{pz} u\end{aligned}\tag{4.1}$$

where $x_p \in \mathbb{R}^{n_p}$ are states, $u_p \in \mathbb{R}^m$ are control inputs, and $y_p \in \mathbb{R}^{p_p}$ are measurement outputs. In addition, tracking outputs $z \in \mathbb{R}^d$ are also measured. An example of z is the vertical acceleration measurement in aircraft. We assume $n_p > p_p$ and $p_p + d \geq m \geq d$. Since z typically includes non-strictly proper outputs such as

accelerations, a constant matrix D_{pz} is assumed to be present. If in some cases, y_p includes non-strictly proper outputs, they are integrated to become strictly proper outputs. $C_{pz} \in \mathbb{R}^{d \times n_p}$ and $D_{pz} \in \mathbb{R}^{d \times m}$ and are assumed to be known.

While Eq.(4.1) represents a nominal plant model, the actual plant model considered in this section is written as

$$\begin{aligned}\dot{x}_p &= A_p x_p + B_p \Lambda^* [u + \Theta^{*T} \Phi(x_p)] \\ y_p &= C_p x_p \\ z &= C_{pz} x_p + D_{pz} \Lambda^* [u + \Theta^{*T} \Phi(x_p)]\end{aligned}\tag{4.2}$$

where $\Theta^{*T} \Phi(x_p)$ and Λ^* are unknown control perturbations. In particular for VFA control as derived in Section 2.2, $\Phi(x_p) = x_p$, and Θ^{*T} are the uncertainties in structural compliance caused by unmeasurable flexible effects, while Λ^* are the uncertainties in control effectiveness caused by unknown control surface damage. Since z are usually measured in earth coordinate frame, they are subject to unknown coordinate transformation caused by unmeasurable flexible effects and therefore has Θ^* . The underlying control problem is to design $u(t)$ such that in the presence of the uncertainties, $z(t)$ follows a specified reference $z_m(t)$, i.e. *reference tracking*.

The adaptive controller that we will present in this section requires the following assumptions regarding the plant model in (4.2):

Assumption 4.1. (A_p, B_p) is controllable and (A_p, C_p) is observable;

Assumption 4.2. $\{A_p, B_p, C_p\}$ has stable transmissions;

Assumption 4.3. $\{A_p, B_p, C_{pz}, D_{pz}\}$ does not have a transmission zero at the origin;

Assumption 4.4. $\text{rank}(C_p B_p) = m$.

Assumption 4.5. Λ^* is diagonal, full rank, bounded by a known value, $\|\Lambda^*\| < \Lambda_{\max}^*$ and the sign of each element $\text{sign}(\Lambda^*)$ is known;

Assumption 4.6. Θ^* is bounded by a known value, $\|\Theta^*\| < \Theta_{\max}^*$; $\Phi(\cdot)$ is globally differentiable, and is globally Lipschitz continuous, i.e. there exists a finite constant

$l_\phi \in \mathbb{R}$ such that $\forall x_1, x_2 \in \mathbb{R}^{n_p}$,

$$\|\Phi(x_1) - \Phi(x_2)\| \leq l_\phi \|x_1 - x_2\|. \quad (4.3)$$

Assumption 4.1 is standard. The fact that the underlying plant model is non-square and typically has no transmission zeros [34] makes Assumption 4.2 reasonable. Assumption 4.3 usually holds, especially when $D_{pz} \neq 0$.

For nominal MIMO plant models satisfying Assumptions 4.1 to 4.3, a baseline observer-based controller (such as LQG/LTR [9]) can be designed to achieve a satisfactory tracking performance with adequate stability margins. Assumptions 4.4 to 4.6 are needed for the proposed adaptive controller. Of these, Assumption 4.4 is perhaps the most restrictive one since it implies that all actuator dynamics are negligible and sensors result in net integration of one, and can be viewed as the MIMO counterpart of a relative degree one assumption (see Ref. [14, Chapter 5]). Assumption 4.5 implies that the actuator anomalies are bounded and independent from each other. Assumption 4.6 is commonly satisfied for the aerial platforms with flexible wingshape as they are usually approximated as a combination of different sinusoidal functions.

4.2 Relative Degree One Adaptive Control Design with SPR/LTR Properties

This section presents the adaptive output-feedback controller. Section 4.2.1 first introduces the architecture of the controller, which includes an observer that also serves as a CRM. The adaptation law is also shown in this section. Section 4.2.2 presents the design of observer parameters and their SPR and LTR properties, as well as stability analysis of the adaptive system. Section 4.2.3 summarizes the overall design procedure, and Section 4.2.4 compares our design with other adaptive output-feedback controllers recently proposed (see [18, Chapter 14] and [23, 24]). The main challenge in our controller design is in the selection of the observer parameters so as

to ensure that an underlying transfer function matrix is SPR. This is carried out in Section 4.2.2, and described in Lemmas 4.5 and Theorem 4.1.

4.2.1 Controller Structure

Following the design procedure in Ref. [18, Chapter 14], the controller is divided into two parts, a baseline observer-based controller with an integral error modification, and an adaptive component augmentation.

Addition of Integral Error

Suppose a piecewise continuous command $z_{cmd}(t)$ is prescribed. For the purpose of command tracking, we first introduce an integral error state $e_{pz} = z - z_{cmd}$ and $w_{pz} := \int e_{pz} dt$, which leads to a modified plant model:

$$\begin{aligned} \begin{bmatrix} \dot{x}_p \\ \dot{w}_{pz} \end{bmatrix} &= \underbrace{\begin{bmatrix} A_p & 0 \\ C_{pz} & 0 \end{bmatrix}}_A \underbrace{\begin{bmatrix} x_p \\ w_{pz} \end{bmatrix}}_x + \underbrace{\begin{bmatrix} B_p \\ D_{pz} \end{bmatrix}}_B \Lambda^*[u + \Theta^{*T}\Phi(x_p)] + \underbrace{\begin{bmatrix} 0 \\ -I \end{bmatrix}}_{B_z} z_{cmd} \\ y &= \underbrace{\begin{bmatrix} C_p & 0 \\ 0 & I \end{bmatrix}}_C x \\ z &= \underbrace{\begin{bmatrix} C_{pz} & 0 \end{bmatrix}}_{C_z} x + \underbrace{[D_{pz}]}_{D_z} \Lambda^*[u + \Theta^{*T}\Phi(x_p)]. \end{aligned} \tag{4.4}$$

Eq.(4.4) can be written compactly as

$$\begin{aligned} \dot{x} &= Ax + B\Lambda^*[u + \Theta^{*T}\Phi(x_p)] + B_z z_{cmd} \\ y &= Cx \\ z &= C_z x + D_z \Lambda^*[u + \Theta^{*T}\Phi(x_p)]. \end{aligned} \tag{4.5}$$

Define $n := n_p + r$ and $p := p_p + d$. Then $x \in \mathbb{R}^n$ and $y \in \mathbb{R}^p$. It is noted that the augmented plant model in (4.5) manifests itself as the plant model we will address in this thesis as discussed in (2.2) and has $p \geq m$. We note that (A, B) is controllable

because of Assumptions 4.1 and 4.3, and (A, C) is observable because Assumption 4.1 holds and the additional error states are also measured. Moreover, $\text{rank}(CB) = m$ since Assumption 4.4 holds.

Augmentation Architecture

We choose the control input u in (4.5) as

$$u = u_{bl} + u_{ad}, \quad (4.6)$$

where u_{bl} is determined by a baseline observer-based controller and u_{ad} by an adaptive controller. The baseline control u_{bl} is chosen as

$$u_{bl} = -Kx_m \quad (4.7)$$

where K is designed by applying the linear quadratic regulator (LQR) technique on the nominal plant model $\{A, B, C\}$, and x_m is the output of the state observer

$$\begin{aligned} \dot{x}_m &= Ax_m + Bu_{bl} + B_z z_{cmd} + L_\rho(y - y_m) \\ y_m &= Cx_m \\ z_m &= C_z x_m + D_z u_{bl}. \end{aligned} \quad (4.8)$$

which also serves as a CRM [19, 21, 39]. One can see the form of a CRM in (4.8) by substituting u_{bl} with Eq.(4.7). Eq.(4.8) serves two purposes, one of an observer, where L_ρ is equivalent to an observer gain, whose purpose is to provide state estimates, and the other of a reference model, whose purpose is to provide a reference for the states. While L_ρ can be chosen using the LTR techniques when the uncertainties Λ^* and Θ^* are zero, its design in the presence of uncertainties will depend also on an underlying SPR transfer function, which will be discussed in greater detail in Section 4.2.2 and 4.2.2.

The adaptive component u_{ad} is chosen as

$$u_{ad} = -u_{bl} + \Lambda^T(t)u_{bl} - \Theta^T(t)\Phi(x_{mp}), \quad (4.9)$$

where x_{mp} is the first n_p elements of x_m , corresponding to the estimate of x_p . $\Lambda^T(t)$ and $\Theta^T(t)$ are estimates of Λ^{*-1} and Θ^{*T} , respectively, both of which are to be suitably adjusted. To determine their adjustment, we derive the error model for $e_x = x - x_m$ by subtracting (4.8) from (4.5) as

$$\begin{aligned} \dot{e}_x &= Ax + Bu_{bl} + B_z z_{cmd} + B\Lambda^*[u_{ad} + (I - \Lambda^{*-1})u_{bl} + \Theta^{*T}\Phi(x_p)] \\ &\quad - Ax_m - Bu_{bl} - B_z z_{cmd} - L_\rho(y - y_m) \\ &= (A - L_\rho C)e_x + \mathfrak{U}(x_p, x_{mp}) + B\Lambda^*[\tilde{\Lambda}^T u_{bl} - \tilde{\Theta}^T \Phi(x_{mp})], \end{aligned} \quad (4.10)$$

where $\mathfrak{U}(x_p, x_{mp}) := B\Lambda^*\Theta^{*T}[\Phi(x_p) - \Phi(x_{mp})]$, $\tilde{\Lambda}^T(t) := \Lambda^T(t) - \Lambda^{*-1}$, and $\tilde{\Theta}^T(t) := \Theta^T(t) - \Theta^{*T}$. The structure of (4.10) suggests the following adaptive laws,

$$\begin{aligned} \dot{\Theta}(t) &= \Gamma_\theta \Phi(x_{mp}) e_y^T S_1^T \text{sign}(\Lambda^*) \\ \dot{\Lambda}(t) &= -\Gamma_\lambda u_{bl} e_y^T S_1^T \text{sign}(\Lambda^*), \end{aligned} \quad (4.11)$$

where $\Gamma_\theta > 0$, $\Gamma_\lambda > 0$ are update gains, $e_y = y - y_m$ and $S_1 \in \mathbb{R}^{m \times p}$ is an output-mixing matrix which will be designed together with L_ρ in Section 4.2.2. The adaptation law in (4.11), which follows Ref. [18, page 430], uses state estimate $x_m(t)$ and the output errors e_y only, which enables output feedback adaptation. Under the SPR conditions on an underlying transfer function matrix and with Assumptions 4.5 and 4.6, it can be shown that the adaptive controller given by (4.6)(4.7)(4.8)(4.9) and (4.11) (shown in Figure 4-1) leads to global asymptotic stability and reference tracking. This is addressed in detail in Section 4.2.2, along with the design of L_ρ and S_1 .

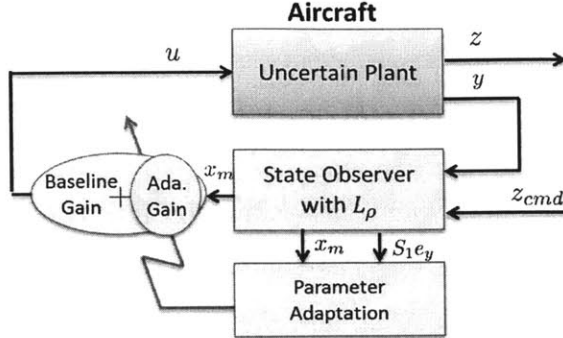


Figure 4-1: The architecture of the adaptive output-feedback controller: an adaptive component is added to a baseline observer-based controller

4.2.2 SPR/LTR Design

L_ρ in the observer/CRM (4.8) and S_1 in the adaptation law (4.11) will be chosen such that an underlying transfer function matrix, which will be defined in this section, is SPR. Section 4.2.2 presents the SPR design for a simpler case when $\Theta^* = 0$ in (4.5), and Section 4.2.2 addresses the general case when $\Theta^* \neq 0$. The SPR designs for both cases as well as the stability analysis of the adaptive system are presented in these sections as well. The LTR properties of L_ρ in the baseline controller are introduced in Section 4.2.2. All proofs in this section can be found in the Appendix C.

Nominal SPR Design: $\Theta^* = 0$

Since $\Theta^* = 0$, we choose $\Theta(t) \equiv 0$ and denote L_ρ as L . The only uncertainty existing in the plant model (4.5) is Λ^* . Lemma 4.1 guarantees the stability of the adaptive design under the SPR conditions of $\{(A - LC), B, S_1 C\}$. Define $e_x = x - x_m$.

Lemma 4.1. *For the uncertain plant model (4.5) with $\Theta^* = 0$, satisfying Assumptions 4.1 to 4.5, if a pair of L and S_1 are chosen such that the underlying transfer function $\{(A - LC), B, S_1 C\}$ is SPR, the adaptive SPR/LTR controller (4.6), (4.7), (4.8), (4.9), and (4.11) with $L = L_\rho$ and $\Theta(t) \equiv 0$, guarantees that i) the closed-loop system has bounded solutions and ii) $e_x(t) \rightarrow 0$ as $t \rightarrow \infty$.*

Since $\tilde{\Theta} = 0$ and $L_\rho = L$, the error model (4.10) becomes

$$\dot{e}_x = (A - LC)e_x + B\Lambda^*\tilde{\Lambda}^T u_{bl}. \quad (4.12)$$

Eq.(4.12) reveals that the underlying transfer function $\{(A - LC), B, S_1C\}$ represents the signal path from $\tilde{\Lambda}^T u_{bl}$ to $S_1 e_y$. The conditions of Lemma 4.1 imply that this signal path is SPR, meaning that $\tilde{\Lambda}^T u_{bl}$ and $S_1 e_y$ is always in the same direction [26] (i.e. the phase between the two signals is bounded by $\pm 90^\circ$). The directionality is utilized in the adaptation law (4.11) to adjust parameters suitably.

The matrices L and S_1 that make the required signal path SPR are referred to as “SPR pairs” and are to be determined. Using Lemma 3.4 (KYP Lemma), the design goal can be transformed into: given $\{A, B, C\}$, find an SPR pair such that there exists a $Q > 0$ that can produce a solution $P = P^T > 0$ to the following equations:

$$(A - LC)^T P + P(A - LC) = -Q < 0 \quad (4.13)$$

$$PB = C^T S_1^T. \quad (4.14)$$

The design in (4.13)(4.14) is the “feedback SPR design” that has been attempted previously [23, 24, 36, 40]. In contrast to the designs in Ref. [36, 40] that requires $CB > 0$, the method in this section extends the results to non-square plant models with CB being full rank. Comparison between our method and Ref. [23, 24] is discussed in detail in Section 4.2.4. We now describe how an SPR pair can be designed.

First, a \bar{B} is designed by appending B with a $B_{s1} \in \mathbb{R}^{n \times (p-m)}$, i.e.

$$\bar{B} = [B, B_{s1}] \quad (4.15)$$

where B_{s1} represents the pseudo-inputs that are designed to square-up the system $\{A, \bar{B}, C\}$. The following Lemma provides a constructive method to find the B_{s1} such that stable transmission zeros are produced, whose proof (by construction) can be found in Appendix C (see [41] for a detail proof and a construction method).

Lemma 4.2. *Given a system $\{A, B, C\}$ satisfying Assumptions 4.1 to 4.4, a $B_{s1} \in$*

$\mathbb{R}^{n \times (p-m)}$ can be constructed such that $\{A, \bar{B}, C\}$ has stable transmission zeros and $C\bar{B}$ is full rank.

An output-mixing matrix S and \bar{C} are designed as

$$S := [S_1, S_2] = (C\bar{B})^T \quad (4.16)$$

$$\bar{C} := SC. \quad (4.17)$$

$S_1 \in \mathbb{R}^{m \times p}$ is a sub-matrix of S . A $\mu^* \in \mathbb{R}$ is chosen such that

$$0 < \mu^* < |\mu_{max}| \quad (4.18)$$

where μ_{max} is the maximum real part of the transmission zeros of $\{A, \bar{B}, \bar{C}\}$. An \bar{A} is designed as

$$\bar{A} = A + \mu^* I. \quad (4.19)$$

A finite L is calculated as

$$L = \bar{B}R^{-1}S \quad (4.20)$$

where R^{-1} is designed by applying the output-feedback SPR method [40] on $\{\bar{A}, \bar{B}, \bar{C}\}$:

$$R^{-1} = (\bar{C}\bar{B})^{-1}((\bar{C}\bar{A}\bar{B})^T + \bar{C}\bar{A}\bar{B})(\bar{C}\bar{B})^{-1} + \epsilon I > 0. \quad (4.21)$$

The finite constant ϵ in (4.21) should be chosen to be large enough such that

$$\begin{aligned} \varepsilon &> \bar{\varepsilon}, \quad \bar{\varepsilon} = \max [\varepsilon_1, \varepsilon_2] \\ \varepsilon_1 &= \lambda_{max} \{ -(\bar{C}\bar{B})^{-1}((\bar{C}\bar{A}\bar{B})^T + \bar{C}\bar{A}\bar{B})(\bar{C}\bar{B})^{-1} \} \\ \varepsilon_2 &= \lambda_{max} \{ (\bar{C}\bar{B})^{-1}H^TQ_I^{-1}H(\bar{C}\bar{B})^{-1} \} \end{aligned} \quad (4.22)$$

where $\lambda_{max}(\cdot)$ stands for the maximum real part of the eigenvalues and

$$H := M^T \bar{A}^T \bar{C}^T + P_I N \bar{A} \bar{B}. \quad (4.23)$$

N is the null space of \bar{B} and M is the null space of \bar{C} satisfying $NM = I$ (see Lemma

3.2). P_I is the unique solution to a Lyapunov equation

$$P_I N \overline{A} M + M^T \overline{A}^T N^T P_I = -Q_I. \quad (4.24)$$

Once a $Q_I > 0$ is chosen, a finite $P_I > 0$ can always be found since $N \overline{A} M$ is the zero dynamics of $\{\overline{A}, \overline{B}, \overline{C}\}$ and hence is Hurwitz. It is noted that Q_I scales P_I . Different from Ref. [40], we choose a $Q_I > 0$ such that

$$P_I \geq \lambda_{\max} \left\{ M^T [I + \overline{B}^T (\overline{C} \overline{B})^{-1} \overline{B}^T] M \right\} I_{(n-m)}. \quad (4.25)$$

Eq.(4.15) to Eq.(4.25) complete our design of L and S_1 . Numerical examples will show L has a reasonable magnitude. It is noted that the pseudo-input matrix B_2 is only used to design L and not used as real control inputs (see also [18, page 426]). Intuitively, in (4.12) a large enough LC , which is in the output-feedback direction $\overline{B}R^{-1}\overline{C}$, will overwhelm the error state dynamics and aligns the directions of $\tilde{\Lambda}^T u_{bl}$ and $S_1 e_y$. This is formally summarized in Lemma 4.3.

Lemma 4.3. *Given a MIMO plant model $\{A, B, C\}$ that satisfies Assumptions 4.2 to 4.4, the finite pair of $L \in \mathbb{R}^{n \times p}$ as in (4.20) and $S_1 \in \mathbb{R}^{m \times p}$ as in (4.16) guarantees that $\forall \mu \in \mathbb{R}$ satisfying $0 \leq \mu \leq \mu^*$, the transfer function matrix $\{(A + \mu I - LC), B, S_1 C\}$ is strictly positive real.*

Lemma 4.3 extends the results in Ref. [40] to a non-square plant model with a class of $(A + \mu I)$. Lemma 4.3 (choosing $\mu = 0$) and Lemma 4.1 complete the controller design for the $\Theta^* = 0$ case.

Robust SPR Design: $\Theta^* \neq 0$

When $\Theta^* \neq 0$, the L_ρ design in CRM (4.8) depends on the bound of Ψ^* , where Ψ^* is defined as

$$\Psi^* := \frac{l_\phi^2}{4} \Lambda^* \Theta^{*T} \Theta^* \Lambda^{*T} S_1 C. \quad (4.26)$$

l_ϕ is defined as in (4.3), and S_1 is defined in (4.16). From Assumptions 4.5 and 4.6, a bound of Ψ^* can be calculated as

$$\|\Psi^*\| \leq \frac{l_\phi^2}{4} \Lambda_{\max}^{*2} \Theta_{\max}^{*2} \|S_1 C\| = \Psi_{\max}^*. \quad (4.27)$$

Ψ_{\max}^* is finite and known. We introduce the following Lemma on the stability of the adaptive system, which provides the guidelines for the design of L_ρ .

Lemma 4.4. *For the uncertain plant model (4.5) satisfying Assumptions 4.1 to 4.6, if a pair of L_ρ and S_1 are chosen such that the underlying uncertain transfer function $\{(A + \eta I + \frac{1}{\eta}B\Psi^* - L_\rho C), B, S_1 C\}$ is guaranteed to be SPR for some $\eta > 0$, the adaptive SPR/LTR controller (4.6), (4.7), (4.8), (4.9), and (4.11) guarantees that i) the closed-loop system has bounded solutions and ii) $e_x(t) \rightarrow 0$ as $t \rightarrow \infty$.*

The error model for the general case $\Theta^* \neq 0$ has been presented in (4.10). Conditions of Lemma 4.4 imply that the underlying directionality between $\tilde{\Lambda}^T u_{bl}$ (or $\tilde{\Theta}^T \Phi(x_{mp})$) and $S_1 e_y$ can still be utilized to adjust the adaptive parameters. The directionality, however, becomes implicit because of the presence of the nonlinear term $\mathfrak{U}(x_p, x_{mp})$ (see (4.10)). Previous adaptive output-feedback control designs [23] use the directionality implicitly in proving the stability. Lemma 4.4 in this thesis reveals the underlying directionality explicitly, and synthesizes observer parameter designs with stability analysis, which is the central idea of our method. Lemma 4.1 is a special case of Lemma 4.4 when $\Psi^* = 0$. The case when $\Phi(x_p) = x_p$ (as considered in Ref. [23, 24]), can be treated as a special case of Lemma 4.4 with $\Psi^* = \Lambda^* \Theta^*$, (where Θ^* should be augmented with additional r columns of zeros because of the augmentation of integral errors), which is summarized in the following corollary with proof omitted.

Corollary 4.1. *Following the setup of Lemma 4.4 with plant model (4.5) and $\Phi(x_p) = x_p$, if a pair of L_ρ and S_1 are chosen such that $\{(A + B\Psi^* - L_\rho C), B, S_1 C\}$ is guaranteed to be SPR, the closed-loop system with the adaptive controller guarantees $e_x(t) \rightarrow 0$ as $t \rightarrow \infty$.*

We now present the design of an SPR pair for the case when $\Theta^* \neq 0$. First, we use Eq.(4.20) and Eq.(4.16) to design an SPR pair of L and S_1 . Then we introduce an additional term to L as

$$L_\rho = L + \rho \bar{B} S = \bar{B}(R^{-1} + \rho I)S \quad (4.28)$$

where ρ is a design parameter that is chosen to be sufficiently large:

$$\rho > \rho^*, \quad \rho^* = \frac{\Psi_{max}^{*2} \|S_1\|^2}{2\mu^{*2} \lambda_{min}(\tilde{Q}) \lambda_{min}(S^T S)}. \quad (4.29)$$

μ^* is chosen in (4.18), and \tilde{Q} is found using

$$\tilde{Q} = -N^T H (\bar{C} \bar{B})^{-1} \bar{C} - \bar{C}^T (\bar{C} \bar{B})^{-1} H^T N + \bar{C}^T (R^{-1} + \varepsilon I) \bar{C} + N^T Q_I N. \quad (4.30)$$

Numerical examples will show L_ρ has a reasonable magnitude. It is noted that ϵ and ρ has the same effect on L_ρ , and L_ρ depends on Ψ_{max}^* instead of Ψ^* . In general, μ^* in (4.29) can be chosen to be any scalars smaller than μ^* . Lemma 4.5 validates the SPR design.

Lemma 4.5. *Given an uncertain plant model (4.5) that satisfies Assumptions 4.1 to 4.6, the finite pair of $L_\rho \in \mathbb{R}^{n \times p}$ as in (4.28) and $S_1 \in \mathbb{R}^{m \times p}$ as in (4.16) guarantees that $\forall \mu \in \mathbb{R}$ satisfying $0 \leq \mu \leq \mu^*$ and $\forall \Psi \in \mathbb{R}^{m \times n}$ bounded by $\|\Psi\| \leq \Psi_{max}^*$, the uncertain transfer function matrix $\{(A + \mu I + \frac{1}{\mu^*} B \Psi - L_\rho C), B, S_1 C\}$ is strictly positive real.*

With Lemma 4.5 (choosing $\mu = \mu^*$ and $\Psi = \Psi^*$) and Lemma 4.4 (choosing $\eta = \mu^*$), we are able to summarize the design, and realize the control goal, which is presented in Theorem 4.1, whose proof can be found in Appendix C. Define $e_y(t) = y - y_m$ and $e_z(t) = z - z_m$.

Theorem 4.1. *For an uncertain plant model (4.2) that satisfies Assumptions 4.1 to 4.6 and for any $z_{cmd}(t)$ that is piecewise continuous, the adaptive controller (4.6), (4.7), (4.8), (4.9), and (4.11), with L_ρ as in (4.28) and S_1 as in (4.16), guarantees*

that i) the closed-loop system has bounded solutions, ii) $e_y(t) \rightarrow 0$ as $t \rightarrow \infty$ and iii) $e_z(t) \rightarrow 0$ as $t \rightarrow \infty$.

LTR Properties

The observer parameter L_ρ as in (4.28) can replace the observer parameter in the baseline observer-based controller. The following Lemma shows that the resulting baseline controller approaches “full-state” LTR asymptotically. In what follows, the notation $A \rightarrow B$, where A and B are matrices of same size, implies that $(\underline{\sigma}[A] - \underline{\sigma}[B]) \rightarrow 0$, where $\underline{\sigma}[\cdot]$ denotes the minimum singular value of matrix $[\cdot]$.

Lemma 4.6. *For a nominal plant model $\{A, B, C\}$ (without uncertainties Λ^* or Θ^*) satisfying Assumptions 4.1 to 4.4, suppose that a LQR controller with a parameter K has a loop gain at input $L_u^*(s)$ and a loop gain at output $L_o^*(s)$, and that the baseline observer-based controller (4.7)(4.8) with K and L_ρ as in (4.28), has loop gains $L_u(s)$ and $L_o(s)$; then as $\epsilon \rightarrow \infty$ or $\rho \rightarrow \infty$, i)*

$$L_u(s) \rightarrow L_u^*(s) \quad (4.31)$$

and ii)

$$L_o(s) \rightarrow C [L_o^*(s)] C^\dagger(s, \bar{B}) \quad (4.32)$$

pointwisely for all finite non-zero s in the closed right half of the complex plain, i.e.

$$s \in \mathcal{D} := \{s \neq 0, \quad s \in \mathbb{C}^{0+}, \quad |s| < +\infty\}, \quad (4.33)$$

where $C^\dagger(s, \bar{B}) \in \mathbb{R}^{n \times p}$ is a function of s and \bar{B} satisfying $CC^\dagger(s, \bar{B}) = I_p$.

Remark 4.1. Since i) is a standard LTR result [9] and ii) holds for any LQG/LTR controllers using a squared-up \bar{B} , Lemma 4.6 implies that L_ρ retains the LTR properties of a LQG/LTR controller. LQR controllers can be designed to have a $L_u^*(s)$ that yields good stability margins, and have a $L_o^*(s)$ that yields low output sensitivities at the integral loops (see Ref. [18, Chapter 2 and Chapter 5]). As a result, Lemma 4.6

implies that once a large enough L_ρ is chosen, the stability margins of the baseline controller are guaranteed, and the output sensitivities at the integral loops can be tuned by designing \bar{B} and K together, which is currently under investigation. However, one should be cautious to use a large L_ρ because $L_o^*(s)$ can have high output sensitivities at some other loops and so can $L_o(s)$.

Lemma 4.6 and Lemma 4.5 imply that the baseline controller and the adaptive controller can share the same observer and the controllers can switch between each other by simply turning u_{ad} on or off. When u_{ad} is off, the controller is denoted as the baseline SPR/LTR controller. The L_ρ design as in (4.28) has been preliminarily reported in Ref. [23]. This thesis formally proves its SPR properties and its LTR properties.

4.2.3 Design Procedure

The overall control design in this section can be summarized into the following step-wise procedure:

Step 4.1. Given a plant model $A_p, B_p, C_p, C_{pz}D_{pz}$, check Assumptions 4.1 to 4.4;

Step 4.2. Add integral error states to the plant model and obtain A, B, C, C_z, D_z using (4.4);

Step 4.3. Design a baseline observer-based controller (4.7)(4.8) and choose K and an observer parameter using the LQR and the LTR techniques, respectively;

Step 4.4. Pick a B_{s1} using Lemma 4.2 and produce a squared-up \bar{B} as in (4.15);

Step 4.5. Design a μ^* using (4.18) and ε using (4.22), then design a nominal SPR pair L using Eq.(4.20) and S_1 using Eq.(4.16);

Step 4.6. Calculate Ψ_{\max}^* using Eq.(4.27) and pick ρ using Eq.(4.29); then design a L_ρ using Eq.(4.28) and replace the observer gain in the baseline controller (4.8) with L_ρ ;

Step 4.7. Design parameter adaptation (4.11) and add the adaptive control (4.9) to the baseline control (4.6).

Step 4.1 to Step 4.3 are conventional observer-based controller designs. Step 4.5 to Step 4.7 are for the adaptive component addition, which completes our adaptive SPR/LTR control design. It is noted that for both the baseline controller and the adaptive controller, the L_ρ design is independent from the K design. We can generally consider that K is designed for performance, and L_ρ is designed for stability. It is also noted that for the case that $\Phi(x_p) = x_p$, Step 4.5 can be simplified that μ^* is no longer needed. The overall controller structure is shown in Figure 4-1.

4.2.4 Comparison with Other Adaptive Output-Feedback Controllers

Previous sections have presented the complete design of the proposed adaptive controller. The controller framework in Section 4.2.1 has been proposed in Ref. [18, Chapter 14] and [18, 23, 24] but with different procedures for choosing L and S_1 . We now compare our SPR/LTR method described in Section 4.2.3 with the previous approaches.

In order to carry out the comparison, we first return to the solution P of (4.13) and (4.14) for the choice of L_ρ as in (4.28) and S_1 as in (4.16). We rewrite the unique solution P to (4.13) and (4.14) as

$$P = \bar{C}^T (\bar{C}\bar{B})^{-1} \bar{C} + N^T P_I N \quad (4.34)$$

where $P_I > 0$ is defined in (4.24) (see proof of Lemma 4.3 and Lemma 4.5). P validates our SPR design.

An alternate procedure for choosing L and S_1 , denoted as the adaptive observer-based LTR (OBLTR) control method, is presented in Ref. [18, Chapter 14]. The

procedure is presented as follows. A \bar{B} is first designed using (4.15), then the weights

$$Q_v = Q_{v0} + \frac{v+1}{v} \bar{B}\bar{B}^T; \quad R_v = \frac{v}{v+1} R_{v0} \quad (4.35)$$

are chosen using arbitrary constant matrices $Q_{v0} > 0$ and $R_{v0} > 0$, and a sufficiently small scalar v . The following ARE is solved

$$P_v \bar{A}^T + \bar{A} P_v - P_v C^T R_v^{-1} C P_v + Q_v = 0. \quad (4.36)$$

for a unique SPD solution P_v . We choose \bar{A} using (4.19) in Eq.(4.36), which is similar to Ref. [5], but with a bound that $0 < \mu^* < |\mu_{max}|$ to ensure SPR properties (see below). L is chosen to be L_v as

$$L_v = P_v C^T R_v^{-1}, \quad (4.37)$$

and S_1 is chosen to be $W_1 \in \mathbb{R}^{m \times p}$ as

$$W R_{v0}^{-\frac{1}{2}} = [W_1, W_2] \quad (4.38)$$

where $W \in \mathbb{R}^{p \times p}$ is designed as

$$W = U_w V_w, \quad U_w \Lambda_w V_w = svd(\bar{B}^T C^T R_{v0}^{\frac{1}{2}}) \quad (4.39)$$

where *svd* stands for singular value decomposition. Combined with the control architecture in Section 4.2.1, the procedure from (4.35) to (4.39) completes the design of the adaptive OBLTR controller. The OBLTR design has been shown in Ref. [18, Theorem 13.2] to lead to

$$P_v = P_0 + O(v) \quad (4.40)$$

where $P_0 > 0$ is an unknown SPD matrix satisfying

$$P_0 C^T = \bar{B} W R_{v0}^{\frac{1}{2}} \quad (4.41)$$

and $O(v)$ represents an unknown symmetric matrix which approaches to zero as $v \rightarrow 0$, which further leads to

$$L_v = P_v C^T R_v^{-1} \rightarrow \frac{1}{v} \bar{B} W R_{v0}^{-\frac{1}{2}} \rightarrow \infty, \quad \text{as } v \rightarrow 0. \quad (4.42)$$

and therefore retains the LTR properties asymptotically (see Section 4.2.2). Moreover, the OBLTR adaptive design has been shown in Ref. [18, Theorem 14.1] to lead to the existence of a v that guarantees bounded reference tracking for a plant model (4.5) in the presence of uncertainties. The same OBLTR adaptive design has been shown in Ref. [23] (see Theorem 3 and its proof in Ref. [23], and combine with (4.19) and (4.36) in this thesis) to lead to the existence of a non-zero v that guarantees the SPR property of $\{(A + \mu^* I + \frac{1}{\mu^*} B \Psi^* - L_v C), B, W_1 C\}$ and in turn, guarantees asymptotic reference tracking.

Now we compare our SPR/LTR method with the OBLTR method. Both methods can produce a finite SPR pair of L and S_1 . From Section 4.2.2, one can conclude that both methods lead to a L that retains the LTR properties of LQG/LTR controllers. However, the OBLTR method relies on the existence of a small v for which the SPR properties are guaranteed. In practice, it may not be easy to determine how small v needs to be. In contrast, our method (see (4.28)) provides a closed-form solution for both L and S_1 .

An alternative procedure of designing L and S_1 based on the linear-matrix-inequality optimization techniques has been proposed in Ref. [24]. The parameter L is determined using a numerical procedure [24]; no closed-form solution for L or guaranteed LTR properties of the baseline controller are provided, unlike our SPR/LTR method.

4.3 Applications to VFA

This section presents the applications of the adaptive SPR/LTR controller on two VFA platforms that are discussed in Section 2.2. Section 4.3.1 presents the 3-wing VFA, whose low order model allows us to illustrate the LTR properties and the SPR properties of the controller. Section 4.3.1 introduces the application on the Vulture VFA, whose high order model demonstrates the numerical stability of the proposed control design.

It should be noted that the adaptive SPR/LTR controller required Assumptions 4.1 to 4.6. It can be shown that all of these assumptions can be met by the VFA models of both platforms considered below. Of these, Assumption 4.4 is the most restrictive one, as it requires the aircraft sensors to include measurements of linear velocities and angular velocities of the body components very close to actuators, and neglects actuator dynamics altogether.

4.3.1 Vertical Acceleration Tracking of 3-wing VFA

This section applies the control design described in Section 4.2 on the 3-Wing VFA model as in (2.12). The control goal is to use elevators δ_e to achieve the tracking of a vertical acceleration command of the center wing while keeping the dihedral regulated.

We performed sensitivity analysis (using the method in Ref. [42] Chapter 9) on the linearized model (2.12) and found that the pitch mode and the dihedral dynamics (pitch-dihedral dynamics) can be decoupled from the phugoid mode. Assuming that the airspeed was maintained by auto-thrust, we truncated the phugoid mode from the model and obtained a 4-state LTI model with states as $x_p = [\alpha, q, \eta, \dot{\eta}]$, where α is the angle of attack and q is the pitch rate. Measurements are vehicle vertical acceleration (A_z), and q . However, α , η and its rate $\dot{\eta}$ cannot be measured accurately and are not available for control. For Step 4.1, we obtained a plant model for $\eta = 10^\circ$

as

$$\begin{bmatrix} \dot{\alpha} \\ \dot{q} \\ \dot{\eta} \\ \ddot{\eta} \\ A_z \end{bmatrix} = \begin{bmatrix} -4.104 & 1.013 & 0.193 & 0.100 & 0 \\ -54.04 & 0.255 & 1.845 & 21.41 & 0 \\ 0 & 0 & 0 & 1 & 0 \\ 0.044 & 0.819 & -0.075 & -6.518 & 0 \\ -123.12 & 0 & 0 & 0 & 0 \end{bmatrix} \begin{bmatrix} \alpha \\ q \\ \eta \\ \dot{\eta} \\ V_z \end{bmatrix} + \begin{bmatrix} -0.795 \\ 5.991 \\ 0 \\ 0.195 \\ -23.84 \end{bmatrix} \delta_e$$

$$y = \begin{bmatrix} q \\ V_z \end{bmatrix} = \begin{bmatrix} 0 & 1 & 0 & 0 & 0 \\ 0 & 0 & 0 & 0 & 1 \end{bmatrix} x. \quad (4.43)$$

where we have augmented an integrated A_z (V_z , the climb rate measurement) state for command tracking. Eq.(4.43) is $\{A, B, C\}$ by Step 4.2. The analysis of the potential uncertainties in the HALE flight, as described in Section 2.2.1), leads to the following uncertain model

$$\begin{aligned} \dot{x} &= (A + B\Lambda^*\Theta^{*T})x + B\Lambda^*u \\ \Lambda^* &= 0.1; \quad \Theta^{*T} = \begin{bmatrix} -31.94 & 0.91 & 9.1 & -9.28 & 0 \end{bmatrix}. \end{aligned} \quad (4.44)$$

Λ^* and Θ^* are unknown to control design. The pitch mode of (4.44) is unstable and therefore loosing control effectiveness is a threat to stability. The uncertain plant model (4.44) belongs to the class of models in (4.5) satisfying Assumptions 4.1 to 4.6.

We now proceed to control design based on (4.44) with uncertain Λ^* and Θ^* . Some classical adaptive approaches can only handle a square system with all stable individual zeros (Ref. [15, Chapter 9]), which is inapplicable here since the SISO transfer function from δ_e to V_z has unstable zeros. The proposed controller in this chapter can be applied here since the additional q measurement makes (2.12) a non-square plant with stable transmission zeros. Now we present our control design step by step. Step 4.3 used the LQR technique with a penalty $diag [1 \ 1 \ 0.01 \ 0.01 \ 0.01]$ on the states and a penalty 10 on the input, which yielded

$$K = \begin{bmatrix} -0.9154 & 0.2534 & 0.1382 & 0.5614 & -0.0316 \end{bmatrix}. \quad (4.45)$$

The following matrices are produced in Step 4.5:

$$B_2 = \begin{bmatrix} 0 & 0.9699 & 0 & 0 & 0.2437 \end{bmatrix}^T \quad (4.46)$$

$$S = \begin{bmatrix} 0.2437 & -0.9699 \\ 0.9699 & 0.2437 \end{bmatrix}. \quad (4.47)$$

We used (4.38) to design S . It was confirmed that $\{A, \bar{B}, \bar{C}\}$ has stable transmission zeros and $\bar{C}\bar{B} = (\bar{C}\bar{B})^T > 0$. Using Eq.(4.20) with $\bar{A} = A$ and $\varepsilon = 10$ yielded

$$L = \begin{bmatrix} -4.116 & 6.949 \\ 41.94 & -52.53 \\ 0 & 0 \\ 1.011 & -1.708 \\ -120.74 & 208.44 \end{bmatrix} \quad (4.48)$$

$$S_1 = \begin{bmatrix} 0.2437 & -0.9699 \end{bmatrix}. \quad (4.49)$$

A P was found using Eq.(4.34) as

$$P = \begin{bmatrix} 82.71 & 0.689 & -139.7 & -19.21 & -2.741 \\ * & 0.9489 & -1.372 & -0.2030 & 0.2036 \\ * & * & 963.9 & 140.3 & 5.462 \\ * & * & * & 26.70 & 0.8079 \\ * & * & * & * & 0.1898 \end{bmatrix} \quad (4.50)$$

where $*$ represents symmetric elements. Quick examination confirmed that $P > 0$, and that P , L and S_1 satisfy Eq.(4.13) and Eq.(4.14), which validates the SPR properties of $\{(A - LC), B, S_1 C\}$.

We assumed the uncertainties Λ^* and Θ^* can be bounded by $\Lambda_{max}^* = 1.1$ and $\Theta_{max}^* = 32$. Also, it was assumed that $\Phi(x_p) = x_p$ and therefore $l_\phi = 1$ and $\Psi^* = \Lambda^* \Theta^*$. Step 4.6 produced $\Psi_{max}^* = 11.9$ and $\rho^* \approx 4.92$, and therefore $\rho = 5$ is chosen

and

$$L_\rho = \begin{bmatrix} -5.084 & 10.80 \\ 53.94 & -80.40 \\ 0 & 0 \\ 1.249 & -2.655 \\ -148.6 & 324.37 \end{bmatrix}. \quad (4.51)$$

The same P as in (4.50) guarantees the SPR properties of $\{(A+B\Lambda^*\Theta^*-L_\rho C), B, S_1C\}$. This completes our SPR/LTR control design.

For comparison, the design using the OBLTR method (4.37) with $v = 0.0006$, $Q_{v0} = I$ and $R_{v0} = 10000I$ was also obtained as

$$L_v = \begin{bmatrix} -3.200 & 12.41 \\ 42.07 & -94.32 \\ 0.286 & -0.109 \\ 1.325 & -3.187 \\ -94.32 & 382.3 \end{bmatrix} \quad (4.52)$$

$$W_1 = \begin{bmatrix} 0.2437 & -0.9699 \end{bmatrix}. \quad (4.53)$$

To validate that the pair of L_v and W_1 produces an SPR $\{(A - L_v C), B, W_1 C\}$, we propose a semidefinite programming procedure (see Ref. [43, 44]) that can be added to the OBLTR method: reduce v until a P_0^* can be found using

$$\min \quad Tr(\overline{W}_p^T \overline{W}_p) \quad (4.54)$$

$$s.t. \quad \overline{W}_p > 0,$$

$$(A - L_v C)^T P_0^* + P_0^* (A - L_v C) < 0,$$

and

$$P_0^* \in \overline{\mathcal{P}},$$

$$\text{where } \overline{\mathcal{P}} := \{P > 0 \mid P = \overline{C}_w^T (\overline{C}_w \overline{B})^{-1} \overline{C}_w + N^T \overline{W}_p N, \quad \overline{W}_p > 0\}$$

where Tr stands for the trace of a matrix and $\overline{C}_w = WR_{v0}^{\frac{1}{2}}C$. A parser, Yalmip [45],

was used to execute the program (4.54) with L_v as in (4.52) and W as in (4.53). A P_0^* was found as

$$P_0^* = \begin{bmatrix} 41.72 & 0.3328 & -1.5328 & -2.162 & -1.325 \\ * & 0.9457 & -0.0177 & -0.0194 & 0.2161 \\ * & * & 16.35 & 2.881 & 0.0703 \\ * & * & * & 1.215 & 0.0772 \\ * & * & * & * & 0.1398 \end{bmatrix} \quad (4.55)$$

which guarantees that $\{(A - L_v C), B, W_1 C\}$ is SPR. However, to guarantee that $\{(A + B\Lambda^*\Theta^* - L_v C), B, W_1 C\}$ is SPR, we need to further reduce v , for which the OBLTR method does not have a closed-form solution, whereas our SPR/LTR method does. The total number of integrators used in our adaptive controller is shown in Table 6.1.

Figure 4-2 shows that the two designs, L_ρ and L_v , were able to constrain the phase of the target SPR transfer function within ± 90 degree, which is a necessary condition of the SPR properties. Figure 4-3 shows that the uncertainties in (2.12) broke the ± 90 phase condition, and that replacing L with L_ρ was able to recover the phase condition. It is observed in Figure 4-4 that the loop gain at input of the baseline SPR/LTR controller almost overlays that of the LQR controller in terms of both phase and magnitude. The gain margin and phase margin of the baseline controller is $[-44, 42]$ dB and ± 59 deg, respectively. Also shown in the Figure 4-4 is the baseline OBLTR controller. Both baseline controllers, as well as the LQR controller, have adequate stability margins since their $L_u(s)$ all avoid the unit circle around -1 (where the gray dash line is a part of the unit circle around -1).

The uncertain VFA model (4.44) with different η was simulated with the baseline SPR/LTR controller and with the adaptive addition. An actuator model with a bandwidth 10 rad/sec was added in each simulation. The nominal case with the 10° dihedral plant model is shown in Figure 4-5a. Both controllers were able to maneuver the aircraft following an A_z command and eventually achieved zero tracking error. Only small amount of control and control rates were used. The same controllers were

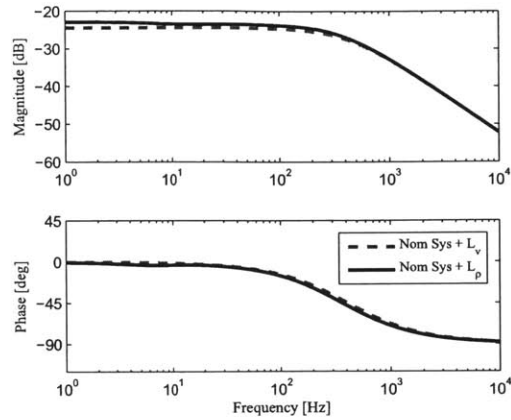


Figure 4-2: The Bode plot of the SPR system $\{(A - LC), B, S_1 C\}$ for the 3-wing VFA model using the SPR/LTR observer parameter $L = L_p$

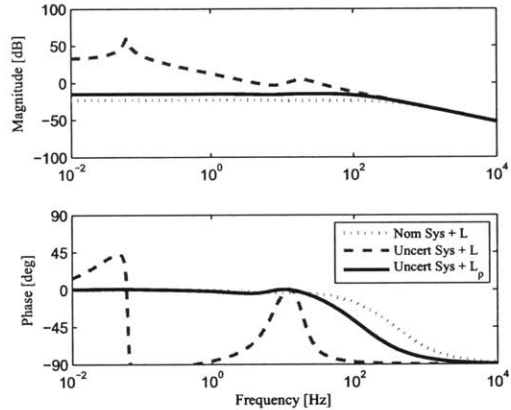


Figure 4-3: L_p in the baseline controller is able to recover the phase condition of $\{(A + B\Lambda^*\Theta^* - L_p C), B, S_1 C\}$ with unknown Θ^* and Λ^* for the 3-wing VFA model

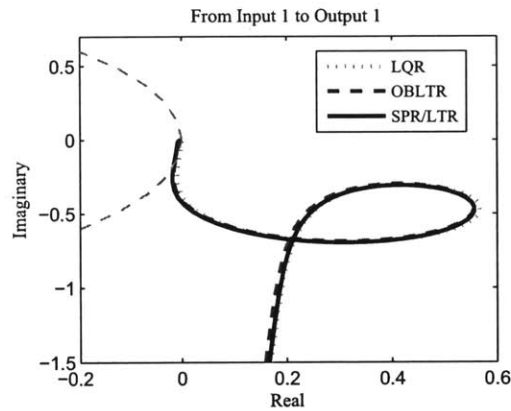


Figure 4-4: The Nyquist plot of the loop gain at input, $L_u(s)$, of the baseline controllers, compared with that of the LQR controller for the 3-wing VFA model

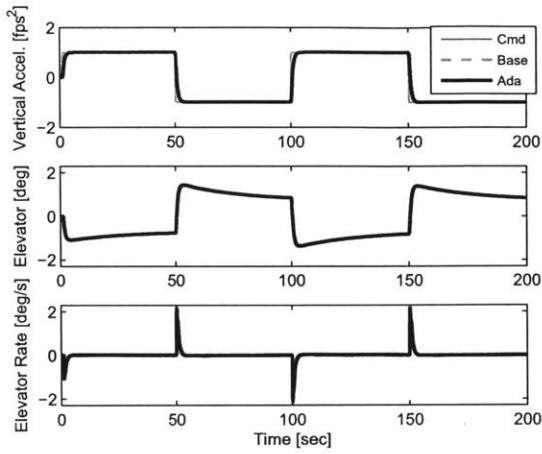
used to control the 16° dihedral, whose results are shown in Figure 4-5b. In this case, the baseline controller was not able to suppress the unstable pitch mode, while the adaptive controller was able to do so. Figure 4-5c shows the adaptive controller was robust in the presence of noise and random disturbance (white noise with 0.15 standard deviation) in all input and measurement channels. The total number of integrators used in each of the controller is summarized in Table 6.1, which shows that our new design uses significantly less integrators compared with the classical one.

The parameter trajectories are shown in Figure 4-12. After four step commands, the parameters settled down to their steady states. If we freeze $\Theta(t)$ and $\Lambda(t)$ at different moments and use these instantaneous values in u_{ad} (4.9), the resulting closed-loop systems represent the “snapshots” of the adaptive system in the time history. The examination in frequency domain confirmed that these “snapshot” closed-loop systems approach the nominal closed-loop system as time evolves, as shown in Figure 4-6b.

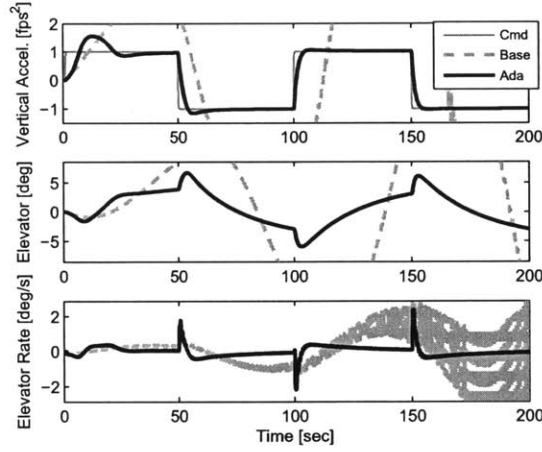
4.3.2 Vulture VFA Bank-To-Turn Control

This section applies adaptive control design in Section 4.2 on the Vulture VFA model described in Section 2.2.2. The desired maneuver is to bank the VFA to turn (BTT). The controller needs to force the VFA to follow a roll angle while keeping the aircraft oriented. In order to do so, we used tails to roll the aircraft and used engine thrusts to keep the side slip angle at zero. The 6 tails were divided into two groups, 3 on right and 3 on left. Same magnitude but opposite sign of movement was issued to each group. The 15 engines were also divided into two groups with an even number of engines in each group. This treatment reduced the number of input to 2, one for engine and one for tail. B_p was suitably treated. The control rate and acceleration effects were ignored in the design model and were brought back in the evaluation model for simulation.

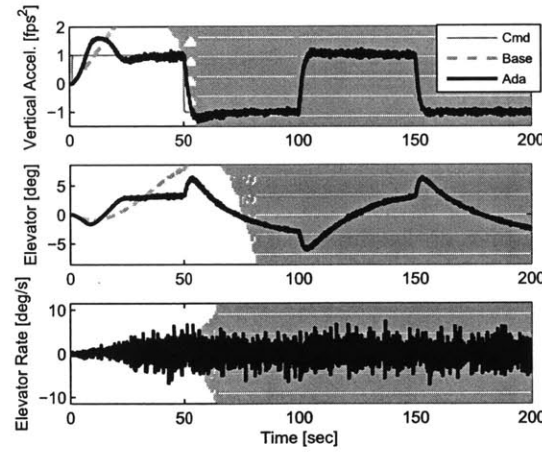
The high-order nature of the model necessitates a state-space reduced-order approach. Using the balanced realization method [46] (which is summarized in Appendix C), we obtained a 80-state model. It is noted that the unstable modes in the original Vulture model were separated from the plant before model reduction, and were



(a) The nominal case

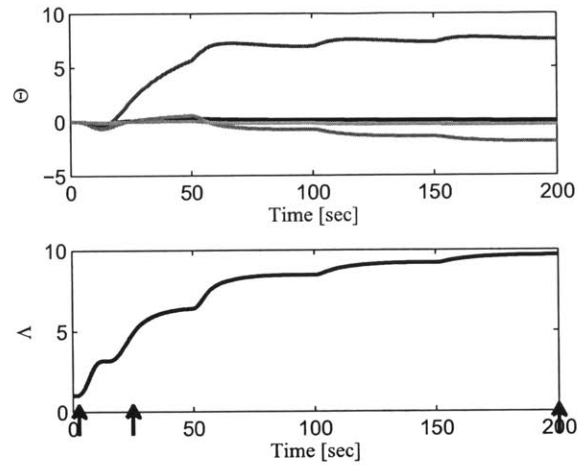


(b) The uncertain case

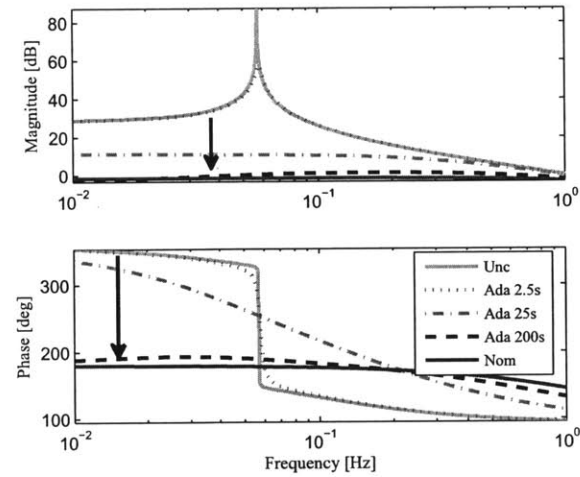


(c) The uncertain case with noise and disturbance

Figure 4-5: The simulation results of the vertical acceleration tracking of the 3-wing VFA using the adaptive output-feedback controller, compared with the baseline SPR/LTR controller



(a) The parameter trajectory in time domain



(b) The frequency domain “snapshots” of the closed-loop system at the three instants of time marked on (a)

Figure 4-6: The “snapshots” of the closed-loop systems for the 3-wing VFA model in the simulation shown in Figure 4-5b

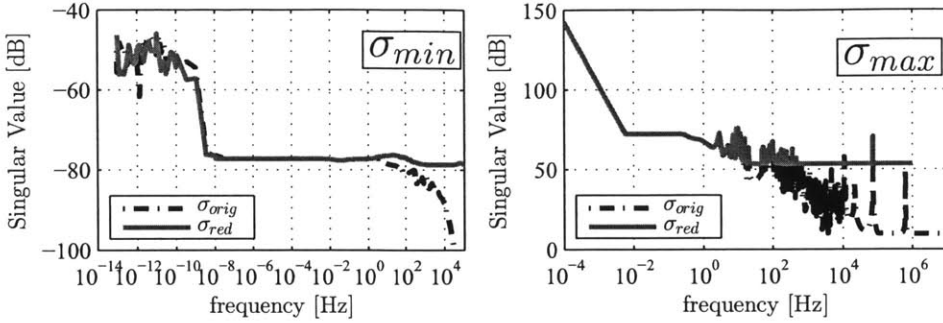


Figure 4-7: Comparison of the maximum and minimum singular values of the transfer function matrix between the original Vulture VFA model and the reduced-order model

augmented back after. Figure 4-7 examines the maximum and minimum singular values of the transfer function matrix for both the original model and the reduced model. The 80-state plant model preserves sufficient input-output characteristics of the original model in low frequencies smaller than 100 Hz. Further state decoupling was not possible as the input-state sensitivity matrix, calculated by the method in the reference, [42] was found to be fully coupled.

Using sensitivity analysis on the reduced model (see [42, Chapter 9]), we determined the 12 independent outputs that yields CB full rank. They are roll rate, pitch rate, yaw rate, longitudinal, lateral and vertical accelerations at the wingroot, and corresponding angular rates and accelerations measured at tail number two. The measurements at tail two are used to satisfy Assumption 4.4. After integrating non-strictly proper outputs, we obtained a strictly proper LTI model with $n_p = 92$ states, $m = 2$ inputs and $p_p = 12$ outputs.

We designed the adaptive controller based on the reduced-order model. Quick examination confirmed that the reduced-order model satisfies Assumptions 4.2 to 4.4. The effects of the dihedral drift and actuator anomalies were modeled by $\Theta^*\Phi(x_p)$ and Λ^* , respectively. Assumptions 4.5 and 4.6 are satisfied with $l_\phi = 10$. The state-feedback gain K was found using a penalty of 1.45 on each of the outputs and a penalty of 1 on each of the inputs. The gain matrix L_ρ and S_1 were found with $\mu^* = 0.01$, $\epsilon = 50$ and $\rho = 10$. Figure 4-8 shows the poles and transmission zeros of the baseline controller with L_ρ .

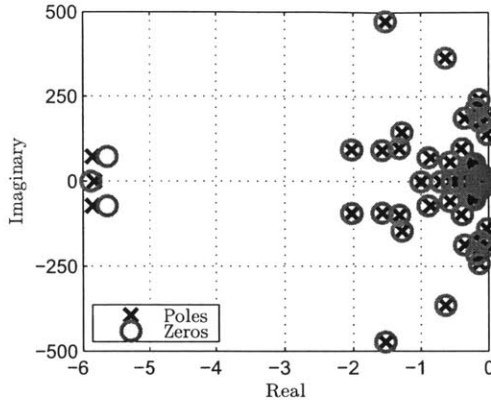


Figure 4-8: The zoom-in map of poles and transmission zeros of $\{(A - L_\rho C), B, S_1 C\}$ for the Vulture VFA

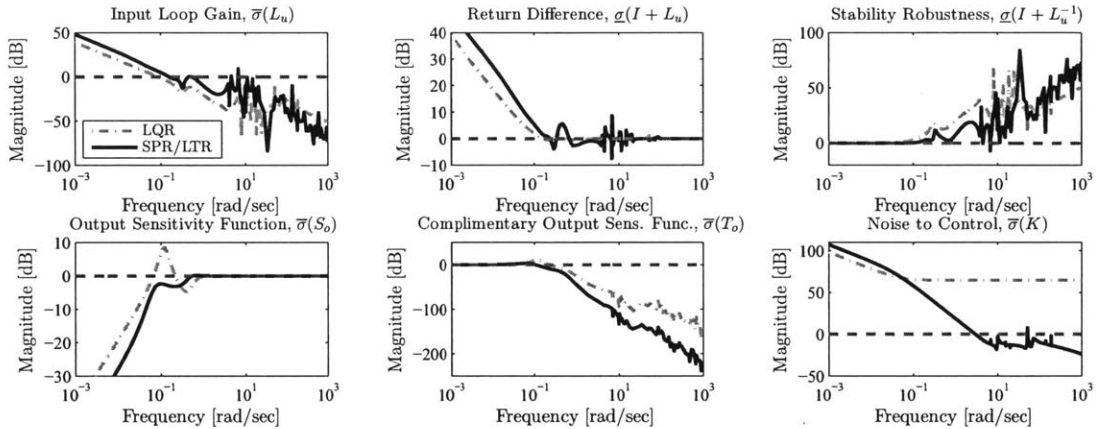


Figure 4-9: The frequency domain analysis of the closed-loop system using the baseline SPR/LTR controller on the Vulture VFA model, compared with a LQR

To show the robustness of the baseline controller, the “Gang-of-Six” transfer functions [47] are examined in Figure 4-9. The ideal LQR controller is also shown in the figure for comparison. The figure shows that the loop gain at input $L_u(s)$ of the baseline SPR/LTR controller almost recovers that of a LQR; gain margin and phase margin are found to be $[-5.04, 4.75]$ dB and ± 25 deg, respectively. The crossover frequency of $L_u(s)$ is around 0.1 rad/sec. The output sensitivity function $S_o(s)$ (only the integral loops are shown in the figure) has low magnitude. The magnitude of the noise-to-control transfer function gradually rolls off at high frequencies.

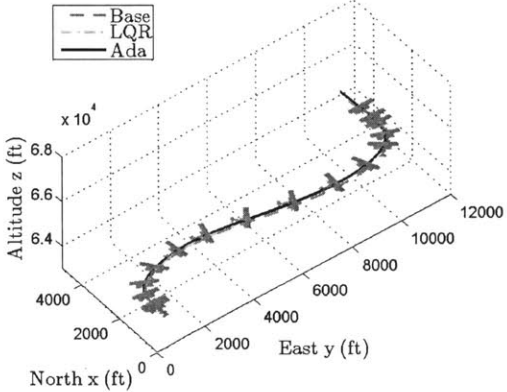
Three controllers, i.e. the LQR controller, the baseline SPR/LTR controller, and

the adaptive SPR/LTR controller were simulated on the original Vulture model. We included control rate and control acceleration effects in the evaluation model for simulation. Also, second-order actuators with a natural frequency of 50 rad/sec and a damping ratio of 0.6 were introduced to all control channels. Magnitude saturation of ± 10 deg and rate saturation of ± 40 deg/s were imposed on the tail. Magnitude saturation of $[-50, 40]$ lbs and rate saturation of ± 20 lbs/s were imposed on the engine. For additional robustness, a projection algorithm [48] was incorporated into the adaptation law (4.11)

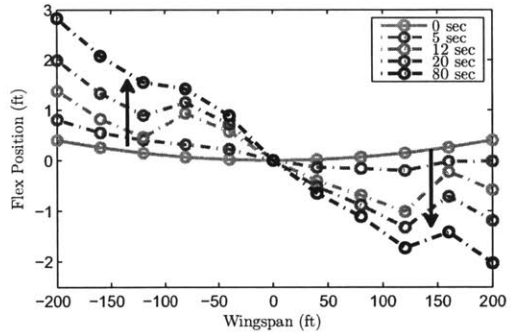
$$\begin{aligned}\dot{\Theta}(t) &= \text{proj}[\Theta; \vartheta, \epsilon; \Gamma_\theta \Phi(x_{mp}) e_y^T S_1^T \text{sign}(\Lambda)] \\ \dot{\Lambda}(t) &= \text{proj}[\Lambda; \vartheta, \epsilon; -\Gamma_\lambda u_{ble} e_y^T S_1^T \text{sign}(\Lambda)]\end{aligned}\quad (4.56)$$

to bound $\Theta(t)$ and $\Lambda(t)$ without altering the stability and tracking results in Theorem 4.1. Previous analysis shows that the projection algorithm improve the robustness of the controller over nonparametric uncertainties [49]. The projection parameters were set as $\Gamma_\theta = 0.01I$, $\Gamma_\lambda = 0.01I$, $\vartheta = 10^{-3}I$ and $\epsilon = 10^{-3}I$.

The simulation results of the nominal plant model (without uncertainty) is shown in Figure 4-11a. All three controllers had exactly the same performance and achieve perfect command tracking for both roll angle and side slip angle. The non-minimum-phase behavior in the responses were caused by the flexible effect of booms and by the interaction between wing sections. Figure 4-11b shows the performance of controllers in the presence of uncertainties. At the start of the simulation, we let the aircraft settle down to a different dihedral angle, emulating turbulence-driven dihedral drift. 10ft dihedral on the outer wing was present at $t = 0$, as shown in the wing shape evolution Figure 4-10b. Correspondingly, $\Phi(x)$ was a parabolic function with suitable coefficients to represent the concave wingshape. Also, there was a power surge in all actuators with $\Lambda^* = 1.5$. In the presence of uncertainties, neither LQR or the baseline SPR/LTR controller was able to stabilize the aircraft, as shown in the Figure 4-11a and 4-11b,. On the other hand, the adaptive controller not only stabilized the aircraft but also recovered the reference performance (as that in Figure 4-11a). The adaptive controller did so by actively reducing its control gains and therefore using much less



(a) The flight path and attitude of the center wing (not in scale)



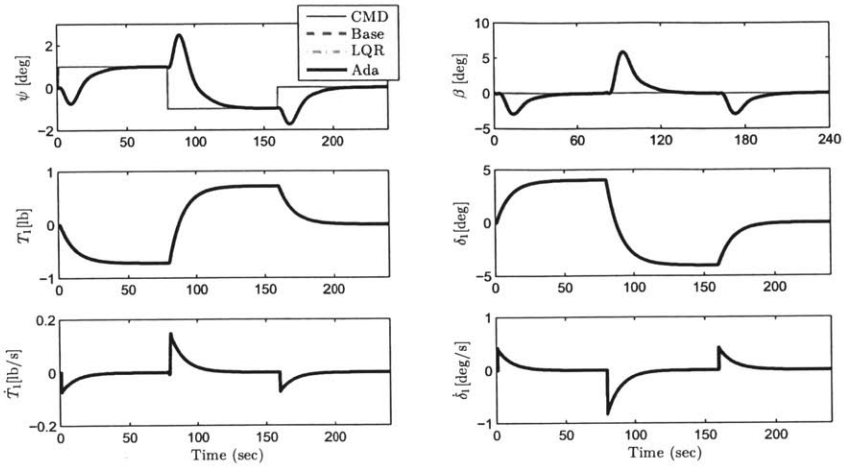
(b) The wing dihedral shape evolution (rear view)

Figure 4-10: The flight path and flexible wing shape of the Vulture VFA in the BTT maneuver, controlled by the adaptive SPR/LTR controller.

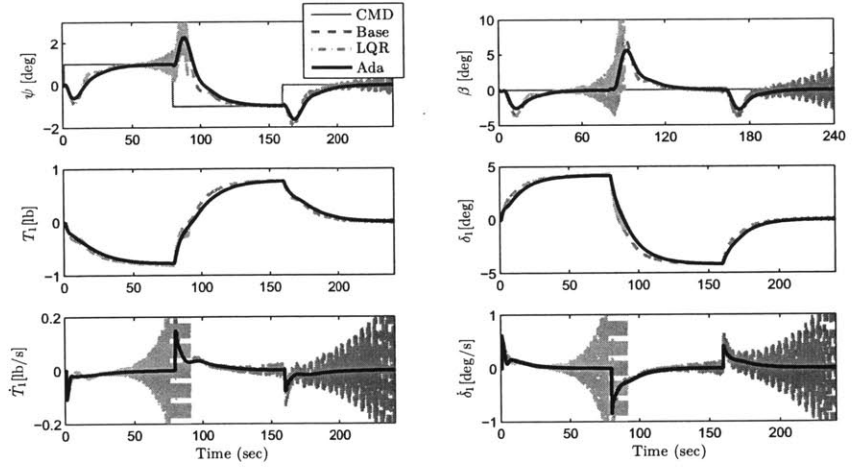
control rates than the other two controllers.

Figure 4-11c shows the same uncertain case with gust wind (white noise with a standard deviation of 10^{-3}) and measurement noise (white noise with a standard deviation of 10^{-3}) in all 12 measurement channels. It is shown in the figure that adaptive controller is robust under these adversities.

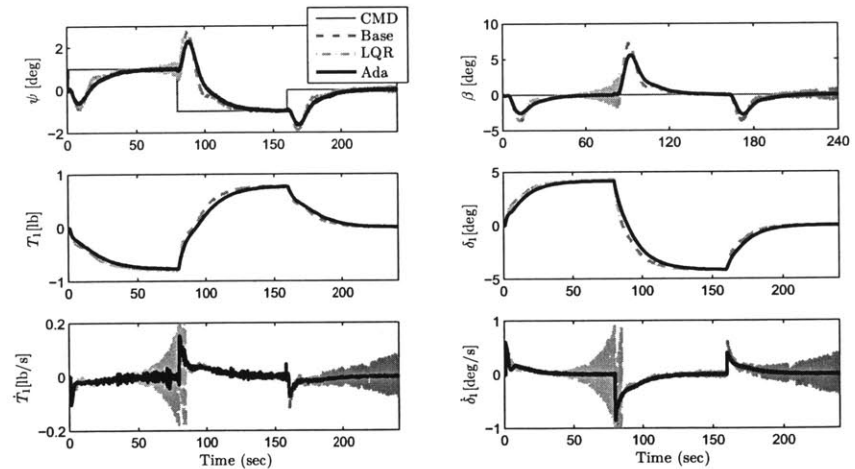
Figure 4-12 shows the parameter trajectories in this simulation. The 89 adaptive parameters settled down to steady-state values after three step commands. The smooth trajectories show that the noise and disturbance was attenuated by the controller. Figure 4-10a shows the flight path and attitude of the VFA in 3D space. The rendered aircraft represents the center section of the VFA, and the roll angle of the



(a) The nominal case



(b) The uncertain case



(c) The uncertain case with noise and disturbance

Figure 4-11: The tracking of roll angle (ψ) and side-slip angle (β) in the BTT maneuver of the Vulture VFA through thrust (T_1) and tail (δ_1) using the adaptive controller, compared with the baseline controller and a LQR.

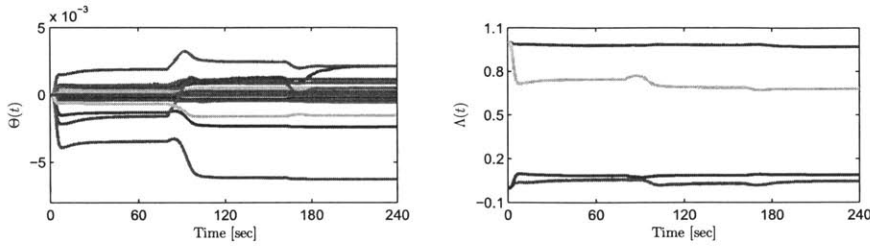


Figure 4-12: The adapted parameters settle down to steady-state values after three step commands of BTT for the Vulture VFA

wing section in the figure only represents the local roll angle very close to the center wingroot (only about 1 deg). The actual dihedral shape of the entire wingspan was found by recording the flexible positions of the wing and is shown in Figure 4-10b. The dihedral was trimmed at a parabolic shape at $t = 0$ sec and ended at a nonlinear form at $t = 80$ sec. After that it gradually returned to the trim value (not shown in the figure). The total number of integrators used in each of the controller is summarized in Table 6.1, which shows that our new design uses significantly less integrators compared with the classical one.

Chapter 5

Relative Degree Two Design

An adaptive control design for relative degree one plant (referred as relative degree one adaptive controller hereafter) has been developed in Chapter 4. This chapter extends the control design to relative degree two plant models where first-order actuator dynamics are present. This chapter is organized as follows. Section 5.1 formulates a generic control problem motivated by VFA control challenges. Section 5.2 develops an adaptive controller and presents the stability analysis. Section 6.4 presents simulation results.

5.1 Relative Degree Two Problem Statement

In Chapter 4, the plant model as we considered in (4.5) ignore all actuator dynamics.

In this section, we consider a plant model as

$$\begin{aligned}\dot{x}_p &= A_p x_p + B_p \Lambda^*[u_p + \Theta_p^{*T} x_p] \\ y_p &= C_p x_p \\ z &= C_{pz} x_p + D_{pz} \Lambda^*[u_p + \Theta_p^{*T} x_p]\end{aligned}\tag{5.1}$$

(see Section 4.1 for descriptions) that is subject to first order actuator dynamics as

$$\dot{u}_p + c(I + \Theta_a^{*T}) u_p = cu\tag{5.2}$$

where c is the nominal actuator time constant and $\Theta_a^* \in \mathbb{R}^{m \times m}$ are its uncertainties. For command tracking, we augment the plant model (2.10) with integral tracking error states $w_z := \int(z - z_{cmd})dt$. The augmented plant is shown as

$$\begin{aligned} \begin{bmatrix} \dot{x}_p \\ \dot{w}_u \\ \dot{w}_z \end{bmatrix} &= \underbrace{\begin{bmatrix} A_p & B_p & 0 \\ 0 & -cI & 0 \\ C_{pz} & D_z & 0 \end{bmatrix}}_A \underbrace{\begin{bmatrix} x_p \\ w_u \\ w_z \end{bmatrix}}_x + \underbrace{\begin{bmatrix} B_p \\ 0 \\ D_z \end{bmatrix}}_{B_1} \Lambda^* \Theta_p^{*T} x_p \\ &\quad + \underbrace{\begin{bmatrix} 0 \\ cI \\ 0 \end{bmatrix}}_{B_2} \Lambda^* [u + \Theta_a^{*T} \Lambda^{*-1} w_u] + \underbrace{\begin{bmatrix} 0 \\ 0 \\ -I \end{bmatrix}}_{B_z} z_{cmd} \quad (5.3) \\ y &= \underbrace{\begin{bmatrix} C_p & 0 & 0 \\ 0 & 0 & I \end{bmatrix}}_C x, \quad z = \underbrace{\begin{bmatrix} C_{pz} & D_z & 0 \end{bmatrix}}_{C_z} x + D_z \Lambda^* \Theta_p^{*T} x_p. \end{aligned}$$

which is rewritten in a compact form as

$$\begin{aligned} \dot{x} &= Ax + B_1 \Psi_1^{*T} x + B_2 \Psi_2^{*T} x + B_2 \Lambda^* u + B_z z_{cmd} \quad (5.4) \\ y &= Cx, \quad z = C_z x + D_z \Psi_1^{*T} x. \end{aligned}$$

It is noted that the plant model (5.4) belongs to the class of (2.2). There exists another class of relative degree three plant models that include relative degree one plant dynamics, no actuator dynamics and first order sensors, which can also be written as (6.47) (with some slight modifications, see Appendix D). In this section, we consider that the plant model has linear parametric uncertainties $B_1 \Psi_1^{*T} x$ and $B_2 \Psi_2^{*T} x$ for simplicity. For extension to nonlinear parametric uncertainties, the reader is referred to the relative degree one case in Section 4.1 and Section 4.2. w_u are scaled actuator states defined as $w_u = \Lambda^* u_p$. $x \in \mathbb{R}^n$ are augmented states, $u \in \mathbb{R}^m$ are new control inputs, and $y \in \mathbb{R}^m$ are augmented measurement outputs. Matrices $A \in \mathbb{R}^{n \times n}$, $B_1 \in \mathbb{R}^{n \times m}$, $B_2 \in \mathbb{R}^{n \times m}$, $C \in \mathbb{R}^{p \times n}$, $B_z = \mathbb{R}^{n \times d}$, $C_z \in \mathbb{R}^{d \times n}$ and $D_z \in \mathbb{R}^{d \times m}$ are known. Uncertainty matrices have the form of $\Psi_1^{*T} = [\Theta_p^{*T}, 0, 0] \in \mathbb{R}^{m \times n}$, $\Psi_2^{*T} =$

$[0, \Lambda^* \Theta_a^{*T} \Lambda^{*-1}, 0] \in \mathbb{R}^{m \times n}$, and $\Lambda^* \in \mathbb{R}^{m \times m}$ and they include unknown elements. $B_1 \Psi_1^{*T}$ are uncertainties in the plant dynamics and $B_2 \Psi_2^{*T}$ are the uncertainties in the actuator dynamics. The control goal is to design u such that z tracks a trajectory z_m from a reference model.

The adaptive controller that we will present requires the following assumptions regarding the plant model (5.4):

Assumption 5.1. (A, B_2, C) is a minimal realization;

Assumption 5.2. All $\{A, B_2, C\}$'s transmission zeros (a total of n_z) are stable and satisfies $(n - n_z - 2m) \geq (p - m)$;

Assumption 5.3. $\{A, B_2, C\}$ has uniform relative degree two;

Assumption 5.4. B_1 can be spanned by a linear combination of B_2 and AB_2 ,

Assumption 5.5. Ψ_1^* satisfies $\Psi_1^{*T} B_2 = 0$;

Assumption 5.6. Ψ_1^* and Ψ_2^* are bounded by a known value, i.e. $\|\Psi_1^*\| < \Psi_{max}$ and $\|\Psi_2^*\| < \Psi_{max}$;

Assumption 5.7. Λ^* is symmetric positive definite and bounded by a known value, i.e. $\|\Lambda^*\| < \Lambda_{max}$.

Assumption 5.1 and 5.2 is always satisfied if (A_p, B_p, C_p) and $\{A_p, B_p, C_{pz}, D_z\}$ are minimal realizations and have stable transmission zeros (see Section 4.1 for justifications). The fact that (A, B_2, C) is non-square makes Assumption 5.2 reasonable [34]. Assumption 5.5 is always satisfied if the plant model has the structure as in (5.3), in which case $B_1 = \frac{1}{c} AB_2 + B_2$ and $\Psi_1^{*T} = [\times, 0, 0]$. (This is further explained using a SISO case in Proposition 6.1). For nominal plant models satisfying Assumptions 5.1 and 5.2, a robust baseline observer-based controller (such as LQG [9]) can be designed to achieve the control goal.

For adaptive control, additional assumptions on the plant model are needed. For (5.3), Assumption 5.3 implies $[(C_p B_p)^T, D_z^T]$ has column rank m (see [25] for justifications and [50] for the relaxation to rank deficiency). The inequality $(n - n_z - 2m) \geq$

$(p - m)$ allows a squaring-up method to be carried out. Assumption 5.6 is commonly satisfied for aerial platforms with physical constraints on the maximum structural deformation rate. Assumption 5.7 is satisfied if $\Theta_{q_1}^{*T}$ has a small magnitude, which implies that inertia properties of aircraft varies slowly, and Λ_d^* is positive definite and diagonal, which implies that control surface damage should be independent from each other.

5.2 Relative Degree Two Adaptive Control Design

This section will develop an adaptive controller for the relative degree two plant model. The adaptive controller is developed in Section 5.2.1 and its parameters are designed in Section 5.2.1 to guarantee the SPR properties of an underlying SPR error model shown in Section 5.2.2. Adaptive law and stability analysis can be found in Section 5.2.3. The overall design procedure is summarized in Section 5.2.4. Analysis of the limiting case when the actuator dynamics is negligible is presented in Section 5.3. Proofs of all lemmas and theorems in this section can be found in Appendix D.

5.2.1 Control Design

The control design will extend the design in Section 4.2 to relative degree two plant models by adding one transmission zeros as $(a_1^1 s + a_1^0)$ to the error model without explicitly differentiating given signals. We choose the control input u as

$$u = u_{bl} + u_{ad} \quad (5.5)$$

where u_{bl} is determined using a baseline observer-based controller and u_{ad} by an adaptive controller. The baseline control u_{bl} is chosen as

$$u_{bl} = -K^T x_m \quad (5.6)$$

where $K^T \in \mathbb{R}^{m \times n}$ is designed by the linear quadratic regulator (LQR) technique. u_{ad} is designed as

$$u_{ad} = -u_{bl} + (a_1^1 s + a_1^0) \Omega^T(t) \bar{\xi}(t), \quad (5.7)$$

where $a_1^1 > 0$ and $a_1^0 > 0$ are free to choose, and

$$\begin{aligned} \Omega^T(t) &= [\Lambda^T, \Psi_1^T, \Psi_2^T] \\ \bar{\xi}^T &= [\bar{u}_{bl}^T, -x_m^T, -\bar{x}_m^T]; \end{aligned} \quad (5.8)$$

$\Omega^T(t)$ is an estimate of $\Omega^{*T} = [\Lambda^{*-1}, \bar{\Psi}_1^{*T}, \bar{\Psi}_2^{*T}]$ where $\bar{\Psi}_1^{*T}$ and $\bar{\Psi}_2^{*T}$ will be defined in Section 5.2.2. x_m are the states of a modified closed-loop reference model (CRM, based on [39]) as

$$\begin{aligned} \dot{x}_m &= Ax_m + B_2 u_{bl} + B_2 (a_1^1 s + a_1^0) [\psi_2^{1T}(t) \bar{e}_{sy}] \\ &\quad + B_z z_{cmd} + L(y - y_m) \\ y_m &= C x_m, \quad z_m = C_z x_m + D_z u_{bl} \end{aligned} \quad (5.9)$$

where $\psi_2^{1T}(t) \in \mathbb{R}^{m \times p}$ is an estimate of $\bar{\psi}_2^{1*T}$, which is a linear function of Ψ_2^{*T} and will be defined in Section 5.2.2, and

$$e_{sy} := R^{-1} S e_y, \quad \text{and } e_y := y - y_m. \quad (5.10)$$

Signals denoted as $(\bar{\cdot})$ are a filtered version of signals (\cdot) as

$$\bar{u}_{bl} = \frac{1}{a_1^1 s + a_1^0} u_{bl}, \quad \bar{x}_m = \frac{a_1^1}{a_1^1 s + a_1^0} x_m, \quad \bar{e}_{sy} = \frac{a_1^1}{a_1^1 s + a_1^0} e_{sy}. \quad (5.11)$$

Control parameters L , R and S will be designed in Section 5.2.1 to guarantee the SPR properties of an underlying error model shown in Section 5.2.2. Adjustable parameters $\Omega^T(t)$ and $\psi_2^{1T}(t)$ will be adapted online by prescribing their time derivatives, which will be presented in Section 5.2.3.

Design of L and S

The design of L in (5.9) and S in (5.10) will eventually guarantee a SPR property and therefore will be based on a square system, which necessitates a squaring-up procedure being carried out on $\{A, B_2, C\}$ as discussed in Lemma 5.1 (see Appendix D for the proof and a construction method).

Lemma 5.1. *For plant models satisfying Assumptions 5.1 to 5.3, there exists a $B_{s1} \in \mathbb{R}^{n \times (p-m)}$ such that $\{A, \bar{B}_2, C\}$, where $\bar{B}_2 = [B_2, B_{s1}]$, has stable transmission zeros and nonuniform input relative degree as $r_i = 2$ for $i = 1, 2, \dots, m$ and $r_i = 1$ for $i = m+1, m+2, \dots, p$.*

B_{s1} will only be used to design L and S , which are

$$B_2^1 = AB_2a_1^1 + B_2a_1^0, \quad \bar{B}_2^1 = [B_2^1, B_{s1}] \quad (5.12)$$

$$S = (C\bar{B}_2^1)^T, \quad \bar{C} := SC, \quad (5.13)$$

$$R^{-1} = (\bar{C}\bar{B}_2^1)^{-1} \left[\bar{C}A\bar{B}_2^1 + (\bar{C}A\bar{B}_2^1)^T \right] (\bar{C}\bar{B}_2^1)^{-1} + \varepsilon I \quad (5.14)$$

$$L = \bar{B}_2^1 R^{-1}(\varepsilon) S. \quad (5.15)$$

where $\varepsilon > 0$ is chosen to be large enough as

$$\begin{aligned} \varepsilon &> \bar{\varepsilon}, \quad \bar{\varepsilon} = \max [\varepsilon_1, \varepsilon_2] \\ \varepsilon_1 &= \lambda_{\max} \left\{ -(\bar{C}\bar{B}_2^1)^{-1} \left[\bar{C}A\bar{B}_2^1 + (\bar{C}A\bar{B}_2^1)^T \right] (\bar{C}\bar{B}_2^1)^{-1} \right\} \\ \varepsilon_2 &= \lambda_{\max} \left\{ (\bar{C}\bar{B}_2^1)^{-2} \left[a^2 \left\| \bar{C}A\bar{B}_2^1 \right\|^2 \Psi_{\max}^2 + H_{\max}^2 \right] \right\} \\ H_{\max} &= (1 + 2\Psi_{\max} \|P_I\|) \|P_I\| \left(\left\| N^1 A \bar{B}_2^1 \right\| \right. \\ &\quad \left. + (1 + a + aR_{\max}) \Psi_{\max} \right) + \left\| \bar{C}A M \right\|. \end{aligned} \quad (5.16)$$

where $a = a_1^1/a_1^0$, $N^1 = (M^T M)^{-1} M^T \left[I - \bar{B}_2^1 (\bar{C}\bar{B}_2^1)^{-1} \bar{C} \right]$, M is the null space of C , P_I is a solution of $P_I N^1 A M + (N^1 A M)^T P_I = -I$ (see Lemma 3.1 for its existence), $\bar{\Psi}_{\max} = \Psi_{\max} \left\| \begin{bmatrix} \mathfrak{B} & \mathfrak{M} \end{bmatrix} \right\|$, and $R_{\max} = \|(\mathfrak{C}\bar{\mathfrak{B}})^{-1} \mathfrak{C} A B\|$, where $\mathfrak{C}^T = \begin{bmatrix} C^T & (CA)^T \end{bmatrix}^T$, $\bar{\mathfrak{B}} = \begin{bmatrix} \bar{B}_2 & A\bar{B}_2 \end{bmatrix}$ and \mathfrak{M} is the null space of \mathfrak{C} (see Lemma 3.1). The solution of $\bar{\varepsilon}$ is derived from Lemma 4.5, which can be applied here since

$\{A, \bar{B}_2^1, C\}$ has uniform $r = 1$. $\bar{\varepsilon}$ is so designed to guarantee the SPR properties of an underlying error model as will be shown next. Numerical examples will show L has a reasonable magnitude.

5.2.2 Underlying SPR Error Model

This section will present the analysis of underlying error model and its SPR properties. The error model is derived by subtracting (5.9) from (5.4) as

$$\begin{aligned}\dot{e}_x &= A_{L^*}^* e_x + B_2 a_1^1 \psi_2^{1*T} e_{sy} + B_1 \Psi_1^{*T} x_m + B_2 \Psi_2^{*T} x_m \\ &\quad + B_2 \Lambda^*(u_{bl} + u_{ad}) - B_2 u_{bl} - B_2 (a_1^1 s + a_1^0) \psi_2^{1*T}(t) \bar{e}_{sy}\end{aligned}\quad (5.17)$$

where $e_x = x - x_m$ are state errors, $A_{L^*}^* := A^* - L^* C$ and $A^* = A + B_1 \Psi_1^{*T} + B_2 \Psi_2^{*T}$.

Define

$$L^* = \bar{B}_2^{1*} R^{-1}(\varepsilon) S \quad (5.18)$$

$$\bar{B}_2^{1*} = [B_2^{1*}, B_{s1}], \quad B_2^{1*} = A_{L^*}^* B_2 a_1^1 + B_2 a_1^0. \quad (5.19)$$

It is noted that \bar{B}_2^{1*} is invariant for $\forall L^*$. L^* is needed for the SPR property of $\{A_{L^*}^*, \bar{B}_2^{1*}, SC\}$ that has uniform $r = 1$ (see Lemma 4.1). The difference between L^* in (5.18) and L in (5.15) can be parameterized using a recursive property of B_2^i , as stated in Lemma 5.2, whose proof can be found in Appendix D.

Lemma 5.2. *[Recursive Properties of B_2^i] The difference between B_2^{1*} and B_2^i can be parameterized as*

$$B_2^{1*} - B_2^i = B_2^2 \psi_2^{1*T} \quad (5.20)$$

and therefore

$$L^* - L = [(B_2^{1*} - B_2^i), 0] R^{-1} S = B_2^2 \bar{\psi}_2^{1*T} R^{-1} S \quad (5.21)$$

where $B_2^2 = B_2 a_1^1$, and ψ_2^{1*T} and $\bar{\psi}_2^{1*T} = \begin{bmatrix} \psi_2^{1*T} & 0_{m \times (p-m)} \end{bmatrix}$ are a linear function of Ψ_2^{*T} .

Remark 5.1. If $\Psi_2^* = 0$, then $\psi_2^{1*} = 0$ and $\bar{\psi}_2^{1*} = 0$; as a result, we can choose $\psi_2^1(t) \equiv 0$ in the CRM (5.9).

The uncertainties is shown to lie in the range of B_2^2 and hence the name “recursive”. Substituting u_{ad} with (5.7) and L with (5.21), and applying (5.10)(5.11), the error model (5.17) can be derived as

$$\begin{aligned}\dot{e}_x &= A_{L^*}^* e_x + B_2^{1*} \Lambda^* \bar{\Psi}_1^{*T} x_m + B_2^2 \Lambda^* \bar{\Psi}_2^{*T} x_m \\ &\quad + B_2 \Lambda^* (a_1^1 s + a_1^0) [\Lambda^T(t) \bar{u}_{bl} - \Psi_1^T(t) x_m - \Psi_2^T(t) \bar{x}_m] \\ &\quad - B_2 (a_1^1 s + a_1^0) [\tilde{\psi}_2^{1T}(t) \bar{e}_{sy}] \end{aligned}\tag{5.22}$$

where $\tilde{\psi}_2^{1T}(t) = \psi_2^{1T}(t) - \bar{\psi}_2^{1*T}$ are parameter estimation errors and we have used an equality that $B_1 \Psi_1^{*T} + B_2 \Psi_2^{*T} = B_2^{1*} \Lambda^* \bar{\Psi}_1^{*T} + B_2^2 \Lambda^* \bar{\Psi}_2^{*T}$; Such parametrization always exists since Assumption 5.5 and Lemma 5.2 hold. Substituting u_{ad} in (5.22) with (5.7) and applying Lemma 3.3 with (5.19) yields

$$\dot{e}_{mx} = A_{L^*}^* e_{mx} - B_2^{1*} \tilde{\psi}_2^{1T}(t) \bar{e}_{sy} + B_2^{1*} \Lambda^* \tilde{\Omega}^T \bar{\xi} \tag{5.23}$$

$$e_y = C e_{mx} = C e_x \tag{5.24}$$

where $e_{mx} = e_x + B_2[\cdot]$ (see Lemma 3.3 for a detail expression), $\tilde{\Omega}^T(t) = \Omega^T(t) - \Omega^{*T}$ are parameter estimation errors. It is noted that (5.24) holds because $CB_2 = 0$. Eq.s (5.23) and (5.24) are our underlying error model.

Proposition 3.1 implies that transmission zeros are added at $(-a_1^0/a_1^1)$ through using the filtered signals $\bar{[\cdot]}$ as in (5.11), and therefore $\{A^*, B_2^{1*}, C\}$ has all stable transmission zeros. The following Lemma states that ϵ in (5.16) is so designed such that L^* and S guarantee a SPR property. Proof of Lemma 5.3 can be found in Appendix D.

Lemma 5.3. *Given Assumptions 5.1 to 5.7, the finite pair of $L^* \in \mathbb{R}^{n \times m}$ as in (5.18) and $S \in \mathbb{R}^{m \times m}$ as in (5.15), with ϵ chosen in (5.16), guarantees that the transfer function $\{(A^* - L^* C), \bar{B}_2^{1*}, SC\}$ is strictly positive real.*

Define partition $S^T = [S_2^T, S_1^T]$ with $S_2 \in \mathbb{R}^{m \times p}$ and $S_1 \in \mathbb{R}^{(p-m) \times p}$. Lemma 5.3

also implies that $\{(A^* - L^*C), B_2^{1*}, S_2C\}$ is also SPR.

5.2.3 Adaptive Law and Stability Proof

This section will present the adaptive law for the adjustable parameters in u_{ad} (5.7) and \dot{x}_m (5.9). The structure of the SPR error model (5.23) suggests that the uncertainty estimates $\Omega(t)$ and $\Psi_m(t)$ should be adjusted using

$$\begin{aligned}\dot{\Omega}(t) &= -\Gamma_{\psi_\lambda} \bar{\xi} e_y^T S_2^T \\ \dot{\psi}_2^1(t) &= \Gamma_{\psi_m} \bar{e}_{sy} e_y^T S_2^T\end{aligned}\tag{5.25}$$

where $\Gamma_{\psi_\lambda} > 0$ and $\Gamma_{\psi_m} > 0$ are adaptation gains. The following theorem guarantees the stability and tracking performance of the adaptive system, whose proof can be found in Appendix D. Define $e_z(t) = z - z_m$ as tracking errors.

Theorem 5.1. *For an uncertain MIMO plant model (5.4) that satisfies Assumptions 5.1 to 5.7, and for any $z_{cmd}(t)$ that is piecewise continuous, the adaptive controller (5.5), (5.6), (5.7), (5.9), and (5.25), with L and S designed in (5.15), guarantees that i) the closed-loop system has bounded solutions, ii) $e_y(t) \rightarrow 0$ as $t \rightarrow \infty$, and iii) $e_z(t) \rightarrow 0$ as $t \rightarrow \infty$.*

5.2.4 Design Procedure

The overall control design in this section can be summarized into the following step-wise procedure:

Step 5.1. *Given a plant model (A, B, C, C_z, D_z) , check Assumptions 5.1 to 5.7;*

Step 5.2. *Add integral error states to the plant model using (5.3);*

Step 5.3. *Design a baseline observer-based controller (5.6)(5.9) (without adaptive terms) and choose K and an observer parameter using the LQR and the LTR techniques, respectively;*

Step 5.4. *(For nonsquare plant models only). Pick a B_{s1} using Lemma 5.1 and produce a squared-up \bar{B}_2 ;*

Step 5.5. Design a ε using (5.16), then design a SPR pair L using Eq.(5.15) and S_1 using Eq.(5.13), and replace the observer gain in the baseline controller (5.9) with L ;

Step 5.6. Design parameter adaptation (5.25) and add the adaptive portion (5.7) to the baseline control (5.5) and to the CRM.

Step 5.1 to Step 5.3 are conventional observer-based controller designs. Step 5.5 to Step 5.6 are for the adaptive component addition, which completes our adaptive control design. It is noted that for both the baseline controller and the adaptive controller, the L design is independent from the K design. We can generally consider that K is designed for performance, and L is designed for stability. The overall controller structure diagram is shown in Figure 4-1.

5.3 With Negligible Actuator Dynamics

In the limiting case that the actuator dynamics in the relative degree two plant model (5.4) is eligible, the plant model can be written as

$$\begin{aligned}\dot{x} &= Ax + B_1 \Psi_1^{*T} x + B_2 \Psi_2^{*T} x + B_2^{1*} \Lambda^* u + B_z z_{cmd} \\ y &= Cx.\end{aligned}\tag{5.26}$$

where B_2^{1*} is defined in (5.19) and is relative degree one input path. Using the relative degree two adaptive controller presented in Section 5.2, the error model becomes

$$\begin{aligned}\dot{e}_x' &= A_{L*}^* e_x' - B_2^{1*} \left[\tilde{\psi}_2^{1T}(t) \bar{e}_{sy} \right] + B_2^{1*} \Lambda^* (a_1^1 s + a_1^0) \left[\tilde{\Omega}^T \bar{\xi} \right] \\ e_y &= C e_x'\end{aligned}\tag{5.27}$$

Performing another coordinate transformation using Lemma 3.3 as

$$e_{mx} := e_x' - B_2^{1*} \Lambda^* a_1^1 \left[\tilde{\Omega}^T \bar{\xi} \right]\tag{5.28}$$

yields

$$\dot{e}_{mx} = A_{L^*}^* e_{mx} - B_2^{1*} \left[\tilde{\psi}_2^{1T}(t) \bar{e}_{sy} \right] + B_2^{0*} \Lambda^* \left[\tilde{\Omega}^T \bar{\xi} \right] \quad (5.29)$$

$$e_y = C e_x' = C e_{mx} + C B_2^{1*} \Lambda^* a_1^1 \left[\tilde{\Omega}^T \bar{\xi} \right] \quad (5.30)$$

where $B_2^{0*} = a_1^1 A B_2^{1*} + a_1^0 B_2^{1*}$. It can be shown that relative degree two our adaptive controller can still stabilize the plant model and achieve bounded command tracking, as stated in the following corollary, whose proof can be found in Appendix D.

Corollary 5.1. *For the plant model (5.26) that follows the notation and the assumptions of (5.4), the relative degree two adaptive controller (5.5), (5.6), (5.7), (5.9), and (5.25) guarantees that $e_y(t)$ is bounded as $t \rightarrow \infty$.*

5.4 Applications to VFA

In Section 4.3, we applied an adaptive controller on VFA models around a single trim while ignoring all actuator dynamics. This section implements an adaptive controller for the 3-wing VFA model with first-order actuator dynamics. One control challenge is that maneuvers of VFA requires navigation through multiple trims, which necessitates additional gain scheduling design. The goal is to use center elevators δ_e and outer ailerons δ_a to track A_z command and regulate η in the meantime. The nonlinear model as described in (2.11) is linearized around each of 25 trim points defined by $V_0 = 30$ ft/sec, $\alpha_0 = 0$ deg, $\theta_0 = 0$ deg, $q = 0$ deg/sec, $\eta_0 \in [10, 12]$ deg with a step of 0.5, and $\dot{\eta}_0 \in [-0.2, 0.2]$ deg/sec with a step of 0.1. Exemplary numerical values of

the linearized model for $\eta_0 = 10$ deg and $\dot{\eta}_0 = 0$ deg/sec is shown as

$$\begin{aligned}
 \begin{bmatrix} V \\ \dot{\alpha} \\ \dot{\theta} \\ \dot{q} \\ \dot{\eta} \\ \ddot{\eta} \\ \dot{\delta}_e \\ \dot{\delta}_a \\ \dot{w}_\eta \\ \dot{w}_{A_z} \end{bmatrix} &= \underbrace{\begin{bmatrix} -0.279 & 3.476 & -32.2 & -0.015 & 0.514 & 0.525 & -2.57 & -6.47 & 0 & 0 \\ -0.070 & -4.104 & 0 & 1.013 & 0.193 & 0.100 & -0.795 & -0.079 & 0 & 0 \\ 0 & 0 & 0 & 1 & 0 & 0 & 0 & 0 & 0 & 0 \\ 0 & -54.04 & 0 & 0.255 & 1.845 & 21.41 & 5.991 & -6.363 & 0 & 0 \\ 0 & 0 & 0 & 0 & 0 & 1 & 0 & 0 & 0 & 0 \\ 0.002 & 0.044 & 0 & 0.819 & -0.075 & -6.518 & 0.195 & -0.034 & 0 & 0 \\ 0 & 0 & 0 & 0 & 0 & 0 & -1 & 0 & 0 & 0 \\ 0 & 0 & 0 & 0 & 0 & 0 & 0 & -1 & 0 & 0 \\ 0 & 0 & 0 & 1 & 0 & 0 & 0 & 0 & 0 & 0 \\ 0 & -123.12 & 0 & 0 & 0 & 0 & -23.84 & -2.376 & 0 & 0 \end{bmatrix}}_{A} \begin{bmatrix} V \\ \alpha \\ \theta \\ q \\ \eta \\ \dot{\eta} \\ \delta_e \\ \delta_a \\ w_\eta \\ w_{A_z} \end{bmatrix} \\
 &+ \underbrace{\begin{bmatrix} 0 & 0 \\ 0 & 0 \\ 0 & 0 \\ 0 & 0 \\ 0 & 0 \\ 0 & 0 \\ 0 & 0 \\ 1 & 0 \\ 0 & 1 \\ 0 & 0 \end{bmatrix}}_{B_2} \underbrace{\begin{bmatrix} u_e \\ u_a \\ u \end{bmatrix}}_{B_z} - \underbrace{\begin{bmatrix} 0 & 0 \\ 0 & 0 \\ 0 & 0 \\ 0 & 0 \\ 0 & 0 \\ 0 & 0 \\ 0 & 0 \\ 0 & 0 \\ 1 & 0 \\ 0 & 1 \end{bmatrix}}_{B_z} \underbrace{\begin{bmatrix} z_q \\ z_{A_z} \\ z_{cmd} \end{bmatrix}}_{C} \\
 y &= \begin{bmatrix} q \\ w_\eta \\ w_{A_z} \end{bmatrix} = \underbrace{\begin{bmatrix} 0 & 0 & 0 & 1 & 0 & 0 & 0 & 0 & 0 & 0 \\ 0 & 0 & 0 & 0 & 0 & 0 & 0 & 0 & 1 & 0 \\ 0 & 0 & 0 & 0 & 0 & 0 & 0 & 0 & 0 & 1 \end{bmatrix}}_C x,
 \end{aligned} \tag{5.31}$$

which includes first-order actuator dynamics with nominal time constant of 1 sec. u_e are elevator commands and u_a are aileron commands to the actuators. It is verified that plant model in Eq.(2.10) holds for all trims with (A, B, C) shown in (5.31). For example, the linearized model for the trim at $\eta_0 = 10$ deg and $\dot{\eta}_0 = 0.2$ deg/sec can be approximated using

$$\Theta_p^* = \begin{bmatrix} 0.06 & -4.52 & 0 & 0.05 & 0.041 & 1.47 \\ 0.01 & 1.83 & 0 & -0.02 & -0.035 & -0.59 \end{bmatrix}, \quad \Lambda^* = \begin{bmatrix} 0.91 & 0.53 \\ 0.52 & 0.79 \end{bmatrix}$$

which only generates an error of 2.6% of the actual $\|A_p\|$ and 1.8% of the actual $\|B_p\|$, respectively. The pitch mode of the VFA when $\eta \geq 11^\circ$ is unstable.

For control design, first we designed control parameters for each trim. For example, L and S_2 for the linearized model (5.31) are found using $a_1^1 = 0.2$, $a_1^0 = 1$, $\varepsilon = 100$, $\Lambda_{max} = 2$ and $\Psi_{max} = 30$:

$$L = \begin{bmatrix} -34.23 & 64.10 & 49.35 \\ -11.54 & 55.96 & 2.23 \\ -5.46 & 31.86 & -2.82 \\ 60.32 & -11.47 & -33.51 \\ -49.09 & 286.3 & -25.20 \\ -0.118 & 20.27 & -2.26 \\ 30.12 & -716 & 21.78 \\ 45.32 & 138.9 & -72.34 \\ -4.88 & 28.50 & -2.51 \\ -50.70 & -45.95 & 218 \end{bmatrix}, \quad S_2 = \begin{bmatrix} -0.817 & 0 & -0.585 \\ 0.585 & 0 & -0.811 \end{bmatrix}. \tag{5.32}$$

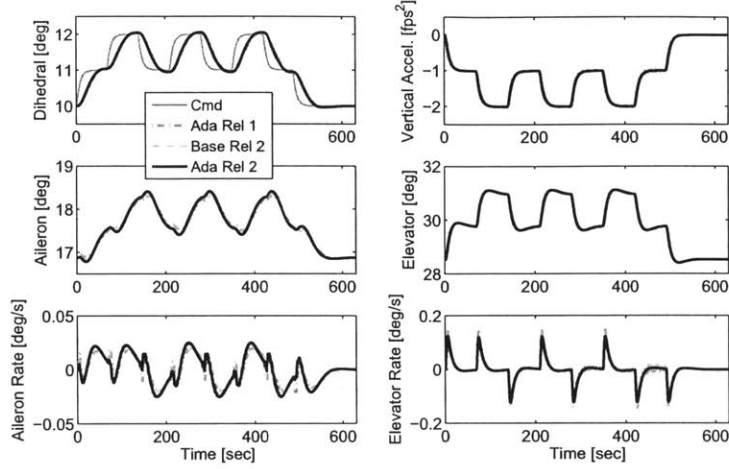
The L design for this particular trim generate adequate stability margin in the baseline controller in the absence of uncertainties, as shown in Figure 5-3 (see legend “nom”). The following relation holds as $a_1^1/a_1^0 \rightarrow 0$ and $\varepsilon \rightarrow \infty$:

$$\overline{B}_2^1 \rightarrow \overline{B}_2, \quad L \rightarrow \overline{B}_2 R^{-1}(\varepsilon) S \rightarrow \infty. \quad (5.33)$$

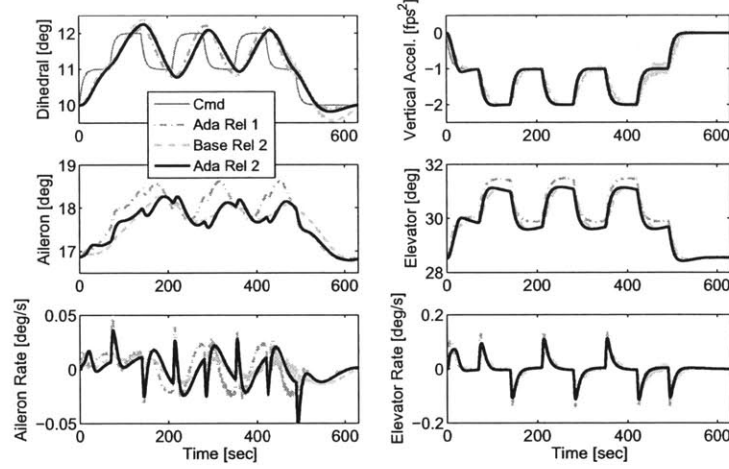
which implies loop transfer recovery (see Lemma 4.6). We schedule the control parameters [32] using real-time η measurements. The total number of integrators used in our adaptive controller is shown in Table 6.1. For the baseline controller without adaptation, the resulting controller is an observer-based gain scheduling linear controller (referred as the baseline controller).

The time domain simulation results with the nonlinear VFA model are shown in Figure 5-1. Three actuators were simulated, one with a nominal time constant of 1 sec, one with a time constant of 2 sec, and the other 4 sec. Besides the baseline controller, two adaptive controllers were tested: one is relative degree one as developed in Section 4.2, which pretends the actuator dynamics is not present; the other is the relative degree two shown in Section 5.2 based on a nominal actuator model as in (5.31). With a nominal actuator, all three controller were able to achieve stable command tracking with almost identical transient performance. When actuator time constant slows down to 2 sec, both adaptive controllers were able to achieve tracking goals while the baseline controller failed to do so, as shown in Figure 5-1a. When actuators further slow down as shown in Figure 5-1, only relative degree two adaptive controller can achieve stable command tracking, whose parameter trajectories are shown in Figure 5-2. The total number of integrators used in each of the controller is summarized in Table 6.1, which shows that our new design uses significantly less integrators compared with the classical one.

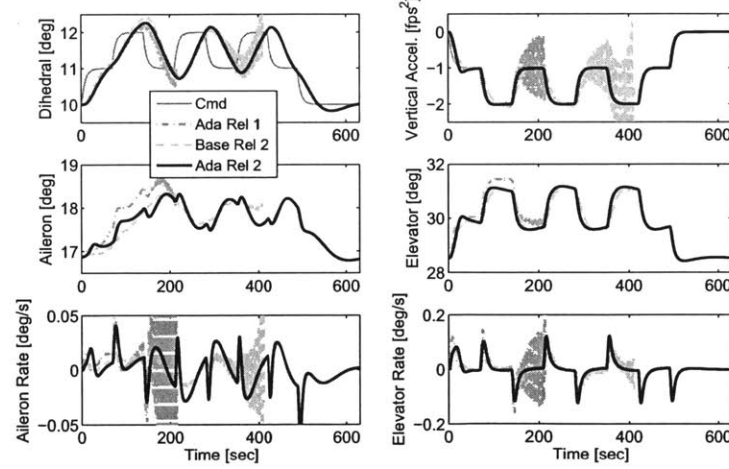
Suppose we freeze the adaptive parameters $\Psi_\Lambda(t)$ and $\Psi_m(t)$ at the end of the simulation, the resulting “snapshot” closed-loop system consists of an uncertain LTI plant and a linear observer-based controllers. The Frequency domain analysis [18, Chapter 5], as illustrated in the Figure 5-3, shows that at $t = 0$ sec the uncertainties reduce the



(a) Actuators with a nominal time constant of 1 sec



(b) Actuators with a time constant of 2 sec



(c) Actuators with a time constant of 4 sec

Figure 5-1: The tracking of η and A_z using the relative degree two adaptive controller for the nonlinear 3-wing VFA model

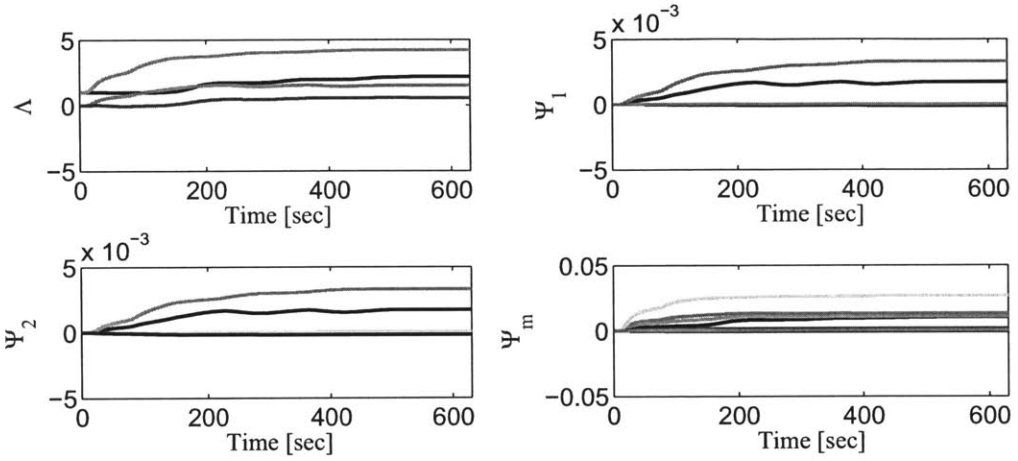


Figure 5-2: The parameter trajectories of the relative degree two adaptive controller in the simulation shown in Figure 5-1b for the nonlinear 3-wing VFA model

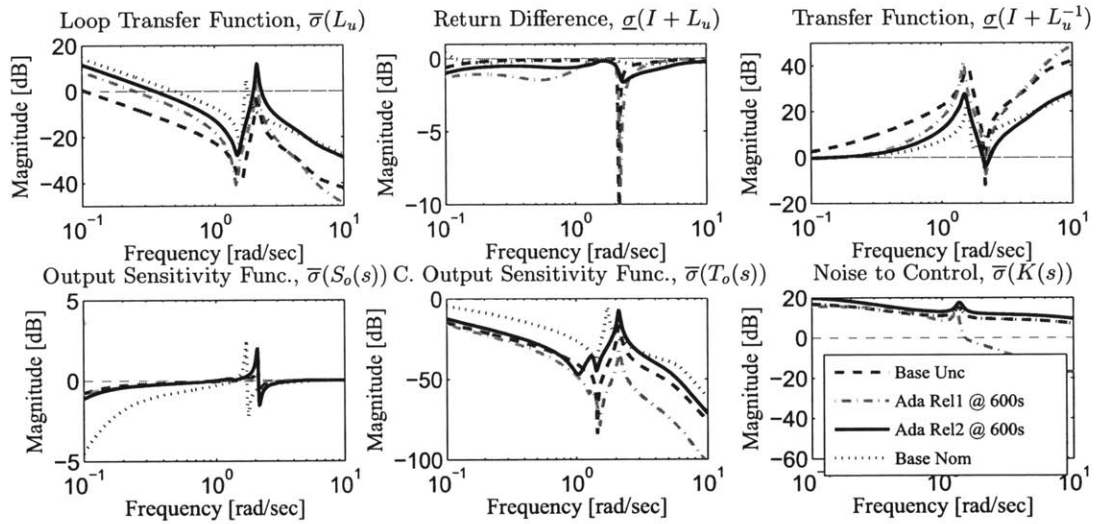


Figure 5-3: The frequency domain analysis of the snapshot closed-loop system shows that adaptation mitigates the effects of model uncertainties on the robustness of the “snapshot” closed-loop systems for the 3-wing VFA model

gain margin from the nominal value (i.e. the baseline controller without uncertainties) of $[-15.7, 27.1]dB$ to $[-2.0, 2.6]dB$, and phase margin from $\pm 57.1^\circ$ to $\pm 14.8^\circ$; The “snapshot” closed-loop systems at $t = 600$ sec recovers them to $[-9.4, 15.3]dB$ and to $\pm 48.9^\circ$, respectively.

Chapter 6

Relative Degree Three Design

This chapter extends the adaptive control design in previous chapters to plant models with relative degree three. In particular, this chapter will address a plant model together with a second-order actuator dynamics. Section 6.1 motivates the control design using a SISO relative degree three transfer function as an example and presents the complete design and stability analysis for this particular case. The main problem we want to address in this thesis is presented in Section 6.2 where a relative degree three MIMO plant model, which is motivated by VFA flight control, is considered. The SISO adaptive control design is then extended in Section 6.3 to address the solution for MIMO plant models. Section 6.4 demonstrates the adaptive controller on a nonlinear VFA model navigating multiple equilibrium flight conditions.

6.1 Relative Degree Three SISO Control Design Example

To show the main concept of the relative degree three control design, this section describes the new adaptive controller when applied on a SISO plant with relative degree three. Section 6.1.1 describes the SISO control problem relevant to flight control. The control design solution is presented in Section 6.1.2 along with error model analysis. Parameter adaptation is discussed in Section 6.1.3 along with stability

proof. In this section, analysis is presented where appropriate to show the design is motivated. For the summary of the design, the readers are referred to Section 6.3.1 where a MIMO case is used.

6.1.1 Relative Degree Three SISO Plant Model

A dynamic behavior of aircraft, such as the response of roll rate x_p to aileron deflection u_p , can be described by a SISO first order model with an unknown pole and gain as

$$\dot{x}_p = (-a_p - \theta_p^*)x_p + b_p \lambda_p^* u_p \quad (6.1)$$

where a_p is a nominal pole location and b_p is a nominal high-frequency gain. θ_p^* is the uncertainty in the aircraft weight and λ_p^* is the uncertainty in the control surface. (See Section 5.1 and 5.2 for the extension to parametric uncertainties with a nonlinear regressor). In this section, the elevator input u_p is driven by a motor, which is modeled as a second-order actuator as

$$\ddot{u}_p + (2\zeta\omega_n + \theta_{\zeta\omega}^*)\dot{u}_p + (\omega_n^2 + \theta_\omega^*)u_p = w_n^2 \lambda_a^* u \quad (6.2)$$

where u is the command to actuators, ζ is the nominal damping ratio and ω_n is the nominal natural frequency, and $\theta_{\zeta\omega}^*$ and θ_ω^* are their corresponding uncertainties. Define $w_u = \lambda_p^* u_p$. Then the overall plant model can be written in the state space

form as

$$\begin{bmatrix} \dot{x}_p \\ \dot{w}_u \\ \ddot{w}_u \end{bmatrix} = \underbrace{\begin{bmatrix} -a_p & b_p & 0 \\ 0 & 0 & I \\ 0 & -\omega_n^2 & -2\zeta\omega_n \end{bmatrix}}_A \underbrace{\begin{bmatrix} x_p \\ w_u \\ \dot{w}_u \end{bmatrix}}_x + \underbrace{\begin{bmatrix} b_p \\ 0 \\ 0 \end{bmatrix}}_{b_1} \underbrace{\begin{bmatrix} -\theta_p^* & 0 & 0 \end{bmatrix}}_{\psi_1^{*T}} x \\ + \underbrace{\begin{bmatrix} 0 \\ 0 \\ \omega_n^2 \end{bmatrix}}_{b_3} \underbrace{\begin{bmatrix} 0 & -\theta_\omega & -\theta_{\zeta\omega}^* \end{bmatrix}}_{\psi_3^{*T}} x + \underbrace{\begin{bmatrix} 0 \\ 0 \\ \omega_n^2 \end{bmatrix}}_{b_3} \underbrace{\lambda_p^* \lambda_a^* u}_{\lambda^*} \\ y = \underbrace{\begin{bmatrix} 1 & 0 & 0 \end{bmatrix}}_{c^T} x \quad (6.3)$$

which can be rewritten concisely as

$$\begin{aligned} \dot{x} &= (A + b_1 \psi_1^{*T} + b_3 \psi_3^{*T}) x + b_3 \lambda^* u \\ y &= c^T x \end{aligned} \quad (6.4)$$

where A , b_1 , b_3 and c are fully known, while ψ_1^{*T} , ψ_3^{*T} and λ^* contains the unknowns.

Define

$$A^* = A + b_1 \psi_1^{*T} + b_3 \psi_3^{*T} \quad (6.5)$$

and note that

$$\begin{aligned} c^T (sI - A^*)^{-1} b_3 &= \frac{b_p \omega_n^2}{p_3^*(s)} \\ p_3^*(s) &:= [s + (a_p + \theta_p^*)] [s^2 + (2\zeta\omega_n + \theta_{\zeta\omega}^*)s + (\omega_n^2 + \theta_\omega^*)] \end{aligned} \quad (6.6)$$

The control goal is then to design u such that y will track a reference trajectory y_m which will be prescribed by a reference model. From (6.3), it is noted that $\psi_1^{*T} b_3 = \psi_1^{*T} A^* b_3 = 0$, since ψ_1^{*T} only affects the pole in the original plant pole location. By Definition 3.5, b_3 is a relative degree three input path with $c^T b_3 = c^T A^* b_3 = 0$ and $c^T A^{*2} b_3 = b_p \omega_n^2 \neq 0$. b_1 is a relative degree one input path with $c^T b_1 = b_p$. The following Proposition specifies the relation between b_1 and b_3 , whose proof can be

found in the Appendix E.

Proposition 6.1. *For plant model (6.3), b_1 can be linearly spanned in the space $(b_3, A^*b_3, A^{*2}b_3)$.*

Proposition 6.1 is a result of the fact that

$$c^T(sI - A^*)^{-1}b_1 = \frac{b_p\omega_n^2}{s + (a_p + \theta_p^*)}. \quad (6.7)$$

6.1.2 Control Design and Error Model Analysis

First a CRM is designed as

$$\begin{aligned} \dot{x}_m &= A_m x_m + l(y - y_m) + f_l(e_y; s) - f_{x_m}(e_y; s) \\ y_m &= c^T x_m \end{aligned} \quad (6.8)$$

where y_m is a reference output trajectory y needs to track, $e_y = y - y_m$ is the output error, and $A_m = A - b_3 k^T$ is designed using LQR techniques and therefore is Hurwitz. Control parameters l , along with $f_l(e_y)$ and $f_{x_m}(e_y)$, will be designed later in Section 6.1.2 and 6.1.2. The error model $e_x = x - x_m$ then is found to be

$$\begin{aligned} \dot{e}_x &= (A^* - lc^T) e_x - f_l(e_y) + b_1 \psi_1^{*T} x_m + b_3 \psi_3'^{*T} x_m + b_3 \lambda^* u + f_{x_m}(e_y) \\ e_y &= c^T e_x \end{aligned} \quad (6.9)$$

where $\psi_3'^{*T} = \psi_3^{*T} + k^T$. The goal of this section is to transform (6.9) into a SPR error model, which is defined as follows.

Definition 6.1. A SPR error model is defined as

$$e_y(t) = W_3^{1*}(s) \tilde{\psi}^T(t) \omega(t) \quad (6.10)$$

where $\tilde{\psi}^T(t) = \psi(t) - \psi^*$ is the parameter error between adjustable parameter $\psi(t)$ and the actual uncertain parameter ψ^* , $\omega(t)$ is a known regressor, and $W_3^{1*}(s)$ is a SPR transfer function.

$W_3^{1*}(s)$ being SPR implies that $W_3^{1*}(s)$ is relative degree one, which in turn implies that we need to add two transmission zeros in both the CRM and u . Zeros addition in CRM, along with l and $f_l(e_y)$, will be addressed in Section 6.1.2. Zeros addition in u , along with $f_{x_m}(e_y)$, will be addressed in Section 6.1.2. In both sections, we will use Lemma 3.3 and Remark 3.3 extensively to design u and CRM that do not require differentiating input signals, and use its equivalent realization with zero addition for error model analysis.

Add Zeros in CRM: Design l and $f_l(e_y)$

Zero addition in CRM can be realized by utilizing Lemma 3.3, which uses different state coordinates and b matrices as

$$\begin{aligned} b_3^{1*} &= A^{*2}b_3 + A^*b_3 \cdot 2 + b_3 \\ b_3^{2*} &= A^*b_3 + b_3 \cdot 2 \end{aligned} \tag{6.11}$$

These b_3^{i*} yield zeros in the error model analysis (6.9) as

$$\begin{aligned} c^T(sI - A^*)^{-1}b_3^{1*} &= \frac{b_p\omega_n^2}{p_3^*(s)}(s^2 + 2s + 1) \\ c^T(sI - A^*)^{-1}b_3^{2*} &= \frac{b_p\omega_n^2}{p_3^*(s)}(s + 2) \end{aligned} \tag{6.12}$$

where $p_3^*(s)$ is defined in (6.6). As a result, b_3^{i*} is an input path with relative degree i . Without loss of generality, we chosen coefficients of (6.11) in such a way that in (6.12) two identical zeros as in $(s+1)^2$ are generated. It is noted that $c^T(sI - A^*)^{-1}b_3^{1*}$ has relative degree one and $c^T(sI - A^*)^{-1}b_3^{2*}$ has relative degree two. The following Lemma states that there exists a l^* such that an underlying SPR property can be guaranteed in the error model, whose proof can be found in Lemma 4.3 and Lemma 4.5.

Lemma 6.1. *For the plant model (6.3), there exists a l^* as*

$$l^* = \varepsilon b_3^{1*} b_p w_n^2, \tag{6.13}$$

and a scalar constant $0 < \varepsilon^* = \varepsilon^*(A^*, b_3^{1*}, c^T, \lambda_{max}, \psi_{max}) < \infty$ such that for $\forall \varepsilon > \varepsilon^*$, the transfer function

$$W_3^{1*}(s) = c^T(sI - A^* + l^*c^T)^{-1}b_3^{1*} = \frac{b_p\omega_n^2(s+1)^2}{p_3^*(s) + \varepsilon(b_p\omega_n^2)^2(s+1)^2} \quad (6.14)$$

where $p_3^*(s)$ is defined in (6.6), is SPR.

Numerical examples will show l^* has a reasonable magnitude. It is noted that l^* uses unknown b_3^{i*} , and therefore in CRM (6.8) we choose to use l , a known relative of l^* , as

$$l = \varepsilon b_3^1 b_p w_n^2 \quad (6.15)$$

where b_3^i is a known version of b_3^{i*} as

$$\begin{aligned} b_3^1 &= A^2 b_3 + A b_3 \cdot 2 + b_3 \\ b_3^2 &= A b_3 + b_3 \cdot 2 \end{aligned} \quad (6.16)$$

It is noted that ε^* (see Lemma 4.3 for a explicit equation) includes (A^*, b_3^{1*}) and therefore is unknown. A known upbound of ε^* can be derived using $\bar{\varepsilon} = \bar{\varepsilon}(A, b_3^1, c^T, \lambda_{max}, \psi_{max})$ with $\lambda_{max} \geq |\lambda^*|$ and $\psi_{max} \geq \|\psi_i\|$, and guarantees $\bar{\varepsilon} > \varepsilon^*$, for which the reader is directed to Section 6.3 for a detail equation. Then if we choose $\varepsilon > \bar{\varepsilon}$, the SPR property in Lemma 6.1 can be guaranteed. The difference between b_3^i and b_3^{i*} still needs to be addressed, as shown in the following Lemma, whose proof can be found in the Appendix.

Lemma 6.2. [Recursive Properties of b_3^i] For the plant model (6.3), b_3^i as in (6.16) and b_3^{i*} as in (6.11) satisfy

$$b_3^{1*} - b_3^1 = b_3^{2*} \psi_3^{1*} + b_3 \psi_3^{2*} \quad (6.17)$$

$$b_3^{2*} - b_3^2 = b_3 \psi_3^{1*} \quad (6.18)$$

where $\psi_3^{1*} = -\theta_{\zeta\omega}^*$, $\psi_3^{2*} = \theta_{\omega}^* + 2\zeta\omega_n\theta_{\zeta\omega}^*$ are elements of ψ_3^* .

It is noted that the $(b_3^{i*} - b_3^i)$ lies in the range of $b_3^{[i+1]*}$ (with $b_3^3 = b_3$) and hence

the name of ‘‘recursive’’. Using (6.15) and (6.17), one can rewrite (6.9) as

$$\begin{aligned}\dot{e}_x &= (A^* - l^* c^T) e_x + b_3^{2*} \psi_3^{1*} e_{sy} + b_3 \psi_3^{2*} e_{sy} - f_l(e_y) \\ &\quad + b_1 \psi_1^{*T} x_m + b_3 \psi_3'^{*T} x_m + b_3 \lambda^* u + f_{x_m}(e_y) \\ e_y &= c^T e_x\end{aligned}\tag{6.19}$$

where $e_{sy} = \varepsilon b_p w_n^2 e_y$. Using (6.12) and (6.14), (6.19) can be rewritten as

$$\begin{aligned}e_y(t) &= W_3^*(s) [(s+2)\psi_3^{1*} e_{sy} + \psi_3^{2*} e_{sy}] + W_{3b}^*(s) [-f_l(e_y)] \\ &\quad + W_{3b}^*(s) [b_1 \psi_1^{*T} x_m + b_3 \psi_3'^{*T} x_m] + W_{3b}^*(s) [b_3 \lambda^* u + f_{x_m}(e_y)]\end{aligned}\tag{6.20}$$

where $W_{3b}^*(s) = c^T(sI - A_{l^*}^*)^{-1}$, $A_{l^*}^* = A^* - l^* c^T$ and $p_{3,cl}^*(s) := p_3^*(s) + \varepsilon(b_p \omega_n^2)^2(s+1)^2$ is its corresponding pole polynomial, i.e.

$$W_3^*(s) = \frac{b_p \omega_n^2}{p_{3,cl}^*(s)} = c^T(sI - A_{l^*}^*)^{-1} b_3 = W_{3b}^*(s) b_3.\tag{6.21}$$

The goal is to have all parameter terms coming through $(s+1)^2$ so that $W_3^*(s)(s+1)^2 = W_3^{1*}(s)$ as in (6.14) becomes SPR. Define filters as

$$\bar{e}_{\psi y}^{[1]} = \frac{s+2}{s^2+2s+1} e_{sy}, \quad \bar{e}_{\psi y}^{[2]} = \frac{1}{s^2+2s+1} e_{sy}\tag{6.22}$$

where the superscript $(\cdot)^{[i]}$ indicates that up to i th derivative is available for control, which transforms (6.20) into

$$\begin{aligned}e_y(t) &= W_3^*(s) [(s+1)^2 (\psi_3^{1*} \bar{e}_{\psi y}^{[1]} + \psi_3^{2*} \bar{e}_{\psi y}^{[2]})] + c^T(sI - A_{l^*}^*)^{-1} [-f_l(e_y)] \\ &\quad + W_{3b}^*(s) [b_1 \psi_1^{*T} x_m + b_3 \psi_3'^{*T} x_m] + W_{3b}^*(s) [b_3 \lambda^* u + f_{x_m}(e_y)]\end{aligned}\tag{6.23}$$

Now it is clear that $f_l(e_y)$ deals with the uncertainties in ψ_3^{i*} , and u and $f_{x_m}(e_y)$ deal with the uncertainties in ψ_1^{*T} and $\psi_3'^{*T}$. In this subsection, we address the design of

$f_l(e_y)$ first as

$$\begin{aligned} f_l(e_y) &= f_3^2(\psi_3^1, \bar{e}_{\psi y}^{[1]}) + f_3(\psi_3^2, \bar{e}_{\psi y}^{[2]}) \\ f_3^2(\psi_3^1, \bar{e}_{\psi y}^{[1]}) &= (b_3^2 \cdot s + b_3) \left[\psi_3^{1T}(t) \bar{e}_{\psi y}^{[1]} \right] + b_3(s+1)^2 \left[\psi_3^{1T}(t) \bar{e}_{\psi y}^{[1][2]} \right] \\ f_3(\psi_3^2, \bar{e}_{\psi y}^{[2]}) &= b_3(s+1)^2 \left[\psi_3^{2T}(t) \bar{e}_{\psi y}^{[2]} \right] \end{aligned} \quad (6.24)$$

where

$$\bar{e}_{\psi y}^{[1][2]} := \frac{1}{s^2 + 2s + 1} \cdot s \left[\psi_3^1(t) \bar{e}_{\psi y}^{[1]} \right] \quad (6.25)$$

with $\bar{e}_{\psi y}^{[1]}$ generated in (6.22), and $\psi_3^1(t)$ and $\psi_3^2(t)$ are estimates of ψ_3^{1*} and ψ_3^{2*} , respectively. In (6.24), we assume that up to the second derivative of $\psi_3^i(t)$ and $\psi_i(t)$ are available for control, which will be realized in Section 6.1.3 using a high order tuner. It is noted that $\dot{\bar{e}}_{\psi y}^{[1][2]}$ is available for control and hence the index $()^{[2]}$. $f_3(\psi_3^2, \bar{e}_{\psi y}^{[2]})$ is designed following Proposition 3.2 and is used to deal with $\psi_3^{2*} \bar{e}_{\psi y}^{[2]}$ in (6.23). $f_3^2(\psi_3^1, \bar{e}_{\psi y}^{[1]})$ is used to deal with $\psi_3^{1*} \bar{e}_{\psi y}^{[1]}$, as stated in the following Lemma, whose proof can be found in the Appendix E.

Lemma 6.3. [Recursive Adaptation] For plant model (6.3), $f_3^2(\psi_3^1, \bar{e}_{\psi y}^{[1]})$ as in (6.24) yields a SPR error model in (6.23) as

$$c^T(sI - A_{l^*}^*)^{-1} \left[b_3(s+1)^2 \psi_3^{1*} \bar{e}_{\psi y}^{[1]} - f_3^2(\psi_3^1, \bar{e}_{\psi y}^{[1]}) \right] = W_3^{1*}(s) \left[-\tilde{\psi}_3^1(t) \left(\bar{e}_{\psi y}^{[1]} + \bar{e}_{\psi y}^{[1][2]} \right) \right], \quad (6.26)$$

where $\tilde{\psi}_3^1(t) = \psi_3^1(t) - \psi_3^{1*}$ is parameter error.

It is noted that $f_3^2(\psi_3^1, e_y)$ only used $\dot{\bar{e}}_{\psi y}^{[1]}$ and was able to produce $(s+1)^2 \left[\psi_3^1(t) \bar{e}_{\psi y}^{[1]} \right]$ in the error model analysis (at the cost of using $\bar{e}_{\psi y}^{[1][2]}$) and hence the name “recursive adaptation”. Lemma 6.3 transforms (6.23) into

$$\begin{aligned} e_y(t) &= W_3^{1*}(s) \left[-\tilde{\psi}_3^1(t) \bar{e}_{\psi y}^{[1]} - \tilde{\psi}_3^1(t) \bar{e}_{\psi y}^{[1][2]} - \tilde{\psi}_3^2 \bar{e}_{\psi y}^{[2]} \right] \\ &\quad + W_{3b}^*(s) \left[b_1 \psi_1^{*T} x_m + b_3 \psi_3'^{*T} x_m \right] + W_{3b}^*(s) [b_3 \lambda^* u + f_{x_m}(e_y)] \end{aligned} \quad (6.27)$$

We will address $b_1 \psi_1^{*T} + b_3 \psi_3'^{*T}$ using u in the following section.

Add Zeros in u : Design u and $f_{x_m}(e_y)$

Section 6.1.2 used recursive adaptation to address the uncertainties $b_3^{2*}\psi_3^{1*}$ that comes from l^* . The remaining uncertainties $b_1\psi_1^{*T} + b_3\psi_3'^{*T}$ in (6.27) can be reparameterized in b_3^{i*} as stated in the following proposition 6.2. For the proof, the reader is direct to the proof of Lemma 6.3 in the MIMO case.

Proposition 6.2. *For plant model (6.3), there exists $\bar{\psi}_1^*$, $\bar{\psi}_1^*$ and $\bar{\psi}_3^*$ such that*

$$b_1\psi_1^{*T} + b_3\psi_3'^{*T} = b_3^{1*}\lambda^*\bar{\psi}_1^{*T} + b_3^{2*}\lambda^*\bar{\psi}_2^{*T} + b_3\lambda^*\bar{\psi}_3^{*T}, \quad (6.28)$$

where b_3^{i*} is defined in (6.11) and $\bar{\psi}_1^{*T} = [\times \ 0 \ 0]$.

Proposition 6.2 transforms the error model (6.27) into

$$\begin{aligned} e_y(t) &= W_3^{1*}(s) \left[-\tilde{\psi}_3^1(t)\bar{e}_{\psi y}^{[1]} - \tilde{\psi}_3^1(t)\bar{e}_{\psi y}^{[1][2]} - \tilde{\psi}_3^2\bar{e}_{\psi y}^{[2]} \right] \\ &\quad + W_3^*(s)\lambda^*(s+1)^2 \left[\bar{\psi}_1^{*T}x_m + \bar{\psi}_2^{*T}\bar{x}_m^{[1]} + \bar{\psi}_3^{*T}\bar{x}_m^{[2]} \right] \\ &\quad + W_{3b}^*(s)[b_3\lambda^*u + f_{x_m}(e_y)] \end{aligned} \quad (6.29)$$

where we have used (6.12) and the filter design as

$$\bar{x}_m^{[1]} = \frac{s+2}{s^2+2s+1}x_m, \quad \bar{x}_m^{[2]} = \frac{1}{s^2+2s+1}x_m. \quad (6.30)$$

The error model (6.29) implies that $u = (s+1)^2[\psi_1^T(t)x_m]$, which is not implementable since \ddot{x}_m is not accessible (see x_m design in CRM (6.8)). Alternatively, we design u as

$$\begin{aligned} u &= u_1 + u_2 \\ u_1 &= -(s+1)^2[\psi_2^T(t)\bar{x}_m^{[1]} + \psi_3^T(t)\bar{x}_m^{[2]}] \end{aligned} \quad (6.31)$$

$$u_2 = -((s+2)\cdot s \cdot [\psi_1^T(t)])e_{y_1^0} - (s+1)^2[\psi_1^T(t)v_m] \quad (6.32)$$

where $\psi_1(t)$, $\psi_2(t)$, $\psi_3(t)$ are estimates of $\bar{\psi}_1^*(t)$, $\bar{\psi}_2^*(t)$, $\bar{\psi}_3^*(t)$, respectively, whose derivatives will be realized in Section 6.1.3 using a high order tuner. u_1 deals with

the $\bar{\psi}_2^*(t)$ and $\bar{\psi}_3^*(t)$ terms in (6.27) using Proposition 3.2. u_2 deal with $\bar{\psi}_1^*(t)$ terms in (6.27), where $\psi_1^T(t)$ adopted a similar structure of $\psi_1^{*T} = \begin{bmatrix} \times & 0 & 0 \end{bmatrix}$ as

$$\psi_1^T(t) = \begin{bmatrix} \times & 0 & 0 \end{bmatrix}. \quad (6.33)$$

$v_m(t)$ is an artificial signal with artificial derivatives as

$$\begin{aligned} (s^2 \cdot v_m) &:= A^2 x_m - A l e_y \\ (s^1 \cdot v_m) &:= A x_m, \quad (s^0 \cdot v_m) := x_m \end{aligned} \quad (6.34)$$

which are accessible parts of \ddot{x}_m and \dot{x}_m . The inaccessible parts of \ddot{x}_m are dealt with using $e_{y_1^0}$, which defined as

$$e_{y_1^0} := \int_0^t l e_y(\tau) d\tau, \quad (6.35)$$

and $f_{x_m}(e_y)$, which is designed using recursive adaptation in Lemma 6.3 as

$$f_{x_m}(e_y) = f_3^2(\lambda, \bar{e}_{\Psi_1 y_1^0}^{[1]}) = (b_3^2 \cdot s + b_3) \left[\lambda(t) \bar{e}_{\Psi_1 y_1^0}^{[1]} \right] + b_3(s+1)^2 \left[\psi_3^1(t) \bar{e}_{\Psi_1 y_1^0}^{[1][2]} \right] \quad (6.36)$$

since $\ddot{\bar{e}}_{\Psi_1 y_1^0}^{[1]}$ is required in error model analysis but only $\dot{\bar{e}}_{\Psi_1 y_1^0}^{[1]}$ is available for control:

$$\begin{aligned} \bar{e}_{\Psi_1 y_1^0}^{[1]} &= \frac{s+2}{s^2+2s+1} \cdot s \cdot \left[\psi_1^T(t) e_{y_1^0} \right] \\ \bar{e}_{\Psi_1 y_1^0}^{[1][2]} &= \frac{1}{s^2+2s+1} \cdot s \cdot \left[\lambda(t) \bar{e}_{\Psi_1 y_1^0}^{[1]} \right]. \end{aligned} \quad (6.37)$$

$\lambda(t)$ is an estimate of λ^* . The following Lemma, which uses the results of Lemma 6.3, shows that u_2 and $f_{x_m}(e_y)$ produces a SPR transfer function in (6.27), whose proof can be found in the Appendix E.

Lemma 6.4. *For plant model (6.3) and CRM (6.8), u_2 as in (6.32) and $f_{x_m}(e_y)$ as in (6.36) produces a SPR error model as*

$$\begin{aligned} c^T (sI - A_{l^*}^*)^{-1} &\left\{ b_3 \lambda^* \left[(s+1)^2 \left[\bar{\psi}_1^{*T} x_m \right] + u_2 \right] + f_{x_m}(e_y) \right\} \\ &= W_3^{1*}(s) \left[-\tilde{\psi}_1^{*T} x_m + \tilde{\lambda} \bar{e}_{\Psi_1 y_1^0}^{[1]} + \tilde{\psi}_3^1 \bar{e}_{\Psi_1 y_1^0}^{[1][2]} \right] \end{aligned} \quad (6.38)$$

where $\tilde{\psi}_1(t) = \psi_1(t) - \psi_1^*$ and $\tilde{\lambda}(t) = \lambda(t) - \lambda^*$ are parameter errors.

Plugging u (6.32) and the results of Lemma 6.4 into (6.27) yields

$$\begin{aligned} e_y(s) &= W_3^{1*}(s) \left[\tilde{\psi}_3^1 \left(\bar{e}_{\Psi_1 y_1^0}^{[1][2]} - \bar{e}_{\psi y}^{[1]} - \bar{e}_{\psi y}^{[1][2]} \right) - \tilde{\psi}_3^2 \bar{e}_{\psi y}^{[2]} + \tilde{\lambda} \bar{e}_{\Psi_1 y_1^0}^{[1]} \right] \\ &\quad - W_3^{1*}(s) \lambda^* \left[\tilde{\psi}_1^{*T} x_m + \tilde{\psi}_2^{*T} \bar{x}_m^{[1]} + \tilde{\psi}_3^{*T} \bar{x}_m^{[2]} \right]. \end{aligned} \quad (6.39)$$

At this point, we have achieved a SPR error model as in (6.39). The minimal realization of (6.39) can be written as in the following Lemma, whose proof has already been presented in this section.

Lemma 6.5. *For the plant model (6.3), CRM design (6.8) with $f_l(e_y)$ in (6.24), $f_{x_m}(e_y)$ in (6.36) and u in (6.32), the error model*

$$\begin{aligned} \dot{e}_{mx} &= A_l^* e_{mx} + b_3^{1*} \lambda^* \left[\tilde{\psi}_1^T(t) x_m + \dots \right] \\ e_y &= c^T e_{mx} \end{aligned} \quad (6.40)$$

where $c^T(sI - A_l^*)^{-1} b_3^{1*} = W_3^{1*}(s)$ is a SPR error model.

Some extra terms similar to $\tilde{\psi}_1^T(t) x_m$ in (6.40) are omitted without loss of generality. The expression for e_{mx} can be found using Lemma 3.3, of which the details can be found in Lemma 6.8, its counterpart in MIMO cases. Without loss of generality, we will proceed using the error model in (6.40) for our following stability analysis.

6.1.3 High Order Tuner and Stability Proof

In the previous sections, we have assumed that up to the second derivatives of $\psi_1(t)$ (and $\psi_i(t)$ and $\psi_3^i(t)$, etc.) are accessible. In this section, we will realize $\dot{\psi}_1(t)$ and $\ddot{\psi}_1(t)$ through a high-order tuner [51] as

$$\begin{aligned} \dot{x}_h &= (A_h x_h + b_h \psi_1'^T(t)) g(x_m) \\ g(x_m) &= (1 + \mu x_m^T x_m), \quad \dot{\psi}_1'(t) = -x_m e_y \\ \psi_1^T(t) &= c_h^T x_h, \quad \dot{\psi}_1^T(t) = c_{h,1}^T x_h, \quad \ddot{\psi}_1^T(t) = c_{h,2}^T x_h \end{aligned} \quad (6.41)$$

where

$$A_h = \begin{bmatrix} 0 & 1 \\ -1 & -2 \end{bmatrix}, \quad b_h = \begin{bmatrix} 0 \\ 1 \end{bmatrix} \quad (6.42)$$

$$c_h^T = [1 \ 0], \quad c_{h,1}^T = [0 \ 1], \quad c_{h,2}^T = [-1 \ -2].$$

(6.41) consists of

$$c_h^T(sI - A_h)^{-1}b_h = \frac{1}{s^2 + 2s + 1}, \quad (6.43)$$

and a varying input gain $g(x_m)$. The following theorem guarantees the overall stability of the closed-loop system, whose proof can be found in the Appendix E.

Theorem 6.1. *For plant model (6.3) and the CRM (6.8), u is designed as in (6.32) with its parameter adjusted as in (6.41), such that i) the closed-loop system has a bounded solution and, ii) $e_y(t) \rightarrow 0$ as $t \rightarrow \infty$.*

As $e_y(t) \rightarrow 0$, $f_l(e_y) \rightarrow 0$ and $f_{x_m}(e_y) \rightarrow 0$ as $t \rightarrow \infty$, and therefore CRM (6.8) recovers its open-loop reference model form as $t \rightarrow \infty$. As a result, the tracking goal is achieved. The formal proof of tracking results is presented in Theorem 6.2 where a MIMO case is used.

6.2 Relative Degree Three MIMO Problem Statement

This section describes a class of MIMO plant model that we want to address in this thesis: a plant model with relative degree three as motivated by VFA control challenges. Our starting point is a linearized model derived in Section 2.2 around a single equilibrium flight condition, which has the form as in (2.10). In the plant model, $x_p \in \mathbb{R}^{n_p}$ are states, $u_p \in \mathbb{R}^m$ are control inputs, $y_p = C_p x_p \in \mathbb{R}^{p_p}$ are measurement outputs and $z \in \mathbb{R}^d$ are tracking outputs. We also define tracking outputs

$$z = C_{pz}x_p + D_z\Theta_p^{*T}x_p + D_z\Lambda^*u_p \quad (6.44)$$

where $C_{pz} \in \mathbb{R}^{d \times n_p}$ and $D_z \in \mathbb{R}^{d \times m}$ are known. The number of inputs and number of outputs are assumed to satisfy $p_p + d > m$. Λ^* is unknown actuator anomalies, and Θ_p^* is unknown state-dependent flexible effects with x_p being linear regressors (see Section 4.1 and Section 4.2 for relaxation to nonlinear regressors). It is assumed that $C_p B_p$ is full rank and therefore the plant model has relative degree one (see Section 4.1 for justification). For mechanical plant models, the relative degree one assumption requires that the plant has velocity measurements available for control and ignores actuator dynamics all together. Adaptive control design for relative degree one plants has been developed in Section in Chapter 4 and is able to achieve asymptotic tracking. While relative degree one assumption is relaxed in Chapter 5 to allow a first order actuator, this chapter focuses on a class of relative degree three or higher plant models.

The problem we want to address in this chapter is a relative degree three plant model that includes uncertain second order actuator dynamics as

$$\ddot{u}_p + (D_{\zeta\omega} + \Theta_{\zeta\omega}^{*T}) \dot{u}_p + (D_\omega + \Theta_\omega^{*T}) u_p = D_\omega u \quad (6.45)$$

where $D_{\zeta\omega}$ and D_ω are diagonal matrices with nominal damping ratios and natural frequencies for each actuator, respectively, and $\Theta_{\zeta\omega}^{*T} \in \mathbb{R}^{m \times m}$ and $\Theta_\omega^{*T} \in \mathbb{R}^{m \times m}$ are their uncertainties. For command tracking we define integral error states $e_{pz} = z - z_{cmd}$ and $w_z := \int e_{pz} dt$. Define $w_u := \Lambda^* u_p$. Including w_z and w_u as states, the augmented plant model can be written as

$$\begin{bmatrix} \dot{x}_p \\ \dot{w}_u \\ \ddot{w}_u \\ \dot{w}_z \end{bmatrix} = \underbrace{\begin{bmatrix} A_p & B_p & 0 & 0 \\ 0 & 0 & I & 0 \\ 0 & -D_\omega & -D_{\zeta\omega} & 0 \\ C_{pz} & D_z & 0 & 0 \end{bmatrix}}_A \underbrace{\begin{bmatrix} x_p \\ w_u \\ \dot{w}_u \\ w_z \end{bmatrix}}_x + \underbrace{\begin{bmatrix} B_p \\ 0 \\ 0 \\ D_z \end{bmatrix}}_{B_1} \Theta_p^{*T} x_p$$

$$- \underbrace{\begin{bmatrix} 0 \\ 0 \\ I \\ 0 \end{bmatrix}}_{B_3} \begin{bmatrix} \Theta_\omega^{*T} & \Theta_{\zeta\omega}^{*T} \end{bmatrix} \begin{bmatrix} w_u \\ \dot{w}_u \end{bmatrix} + \underbrace{\begin{bmatrix} 0 \\ 0 \\ D_\omega \\ 0 \end{bmatrix}}_{B_z} \Lambda^* u + \underbrace{\begin{bmatrix} 0 \\ 0 \\ 0 \\ -I \end{bmatrix}}_{B_z} z_{cmd}$$

$$y = \underbrace{\begin{bmatrix} C_p & 0 & 0 & 0 \\ 0 & 0 & 0 & I \end{bmatrix}}_C x, \quad z = \underbrace{\begin{bmatrix} C_{pz} & D_z & 0 & 0 \end{bmatrix}}_{C_z} x + D_z \Theta_p^{*T} x_p,$$
(6.46)

which can be rewritten in a compact form as

$$\begin{aligned}
\dot{x} &= (A + B_1 \Psi_1^{*T} + B_3 \Psi_3^{*T}) x + B_3 \Lambda^* u + B_z z_{cmd} \\
y &= C x, \quad z = C_z x + D_z \Psi_1^{*T} x
\end{aligned}$$
(6.47)

where $x \in \mathbb{R}^n$ are augmented states, $u \in \mathbb{R}^m$ are new control inputs, $y \in \mathbb{R}^p$ are augmented measurement outputs. The plant model is nonsquare ($p = p_p + d > m$). It is noted that (6.46) and (6.47) are the extension of (6.3) and (6.4), respectively. There exists another class of relative degree three plant models that include relative degree one plant dynamics, first order actuators and first order sensors, which can also be written as (6.47) (with some slight modifications, see Appendix E). Matrices $A \in \mathbb{R}^{n \times n}$, $B_1, B_3 \in \mathbb{R}^{n \times m}$, $C \in \mathbb{R}^{m \times n}$, $B_z = \mathbb{R}^{n \times d}$, $C_z \in \mathbb{R}^{d \times n}$ and $D_z \in \mathbb{R}^{d \times m}$ are known. $\Lambda^* \in \mathbb{R}^{m \times m}$, $\Psi_1^{*T} = \begin{bmatrix} \Theta_p^{*T} & 0 & 0 & 0 \end{bmatrix} \in \mathbb{R}^{m \times n}$ and $\Psi_3^{*T} = (D_\omega)^{-1} \begin{bmatrix} 0 & \Theta_\omega^{*T} & \Theta_{\zeta\omega}^{*T} & 0 \end{bmatrix} \in \mathbb{R}^{m \times n}$ are unknown. $B_1 \Psi_1^{*T} x$ are the uncertainties from the original plant model, and $B_3 \Psi_3^{*T} x$ are the uncertainties in the actuator dynamics. (See Section 5.1 and 5.2 for the extension to parametric uncertainties with a nonlinear

regressor). The MIMO plant model (6.47) is a generalized version of the SISO plant (6.4) presented in Section 6.1.1.

The control goal is to design u such that z tracks a trajectory z_m from a reference model despite the presence of uncertainties. The adaptive controller that we will present requires the following assumptions regarding the plant model (7.1):

Assumption 6.1. (A, B_3, C) is a minimal realization;

Assumption 6.2. $\{A, B_3, C\}$ has stable transmission zeros;

Assumption 6.3. $\{A, B_3, C\}$ has uniform relative degree 3;

Assumption 6.4. B_1 can be spanned by a linear combination of $\{B_3, AB_3, A^2B_3\}$;

Assumption 6.5. Ψ_1^* satisfies $\Psi_1^{*T} \begin{bmatrix} B_3 & AB_3 \end{bmatrix} = \begin{bmatrix} 0 & 0 \end{bmatrix}$;

Assumption 6.6. $\|\Psi_i^*\|$ are bounded by a known value, respectively, i.e. $\|\Psi_i^*\| < \Psi_{i,\max}^*$ for $i = 1, 2$;

Assumption 6.7. Λ^* is diagonal and $\|\Lambda^*\|$ is bounded by a known value, $\|\Lambda^*\| < \Lambda_{\max}$ and $\text{sign}(\Lambda^*)$ is known.

It can be shown that the relative degree three plant model (6.46) and (6.4) satisfy all these assumptions, with $r = 3$. Assumption 6.4 is always satisfied if the plant model has the structure as in (6.46), i.e.

$$B_1 = D_\omega^{-1} A^2 B_3 + D_{\zeta\omega} D_\omega^{-1} A B_3 + B_3 \quad (6.48)$$

(see Proposition 6.1 for derivations). Assumption 6.1 is standard. Assumption 6.2 is ubiquitous for adaptive control. It is noted that plant models with stable transmission zeros do not require zeros of each individual transfer functions to be stable as shown in Example 3.1. For nominal MIMO plant models satisfying Assumptions 6.1 and 6.2, a baseline observer-based controller (such as LQG/LTR [9]) can be designed to achieve a satisfactory tracking performance with adequate stability margins. For adaptive control, additional assumptions on the plant model are needed. Assumption 6.3 implies $\begin{bmatrix} (C_p B_p)^T & D_z^T \end{bmatrix}$ is full rank. Assumption 6.7 implies that actuator

anomalies are physically bounded and independent from each other. Assumption 6.6 is commonly satisfied for aerial platforms with physical constraints on the maximum amount of flexible deformation and deformation rate [52].

6.3 Relative Degree Three MIMO Adaptive Control Design

This section extends the adaptive controller presented in Section 6.1 to the relative degree three MIMO plant model (6.46). A complete adaptive control design is presented in Section 6.3.1. An error model is derived with guaranteed SPR properties in Section 6.3.2. Stability proof, along with a high order tuner, is derived in Section 6.3.3. For simplicity, we first design controller assuming $p = m$, i.e. (6.47) is square. Extension to nonsquare plant models is discussed in Section 6.3.4. A step-wise design procedure is summarized in Section 6.3.5.

6.3.1 Control Design

The control design will extend the design in Section 4.2 to relative degree three plant models by adding two transmission zeros as

$$\begin{aligned}\pi_2^0(s) &= a_2^2, \quad \pi_2^1(s) = a_2^2 s + a_2^1, \\ \pi_2^2(s) &= a_2^2 s^2 + a_2^1 s + a_2^0,\end{aligned}\tag{6.49}$$

to the error model without explicitly differentiating given signals. The coefficients a_2^i , without loss of generality, are chosen as the polynomial expansion coefficients of $(as + 1)^2 = a_2^2 s^2 + a_2^1 s^1 + a_2^0$ for some $a > 0$. We choose the control input u as

$$u = u_{bl} + u_{ad}\tag{6.50}$$

where u_{bl} is determined using a baseline observer-based controller and u_{ad} by an adaptive controller. The baseline portion u_{bl} is chosen as

$$u_{bl} = -K^T x_m \quad (6.51)$$

where $K^T \in \mathbb{R}^{m \times n}$ is designed by the linear quadratic regulator (LQR) technique. x_m are the states of a modified closed-loop reference model (CRM, based on Ref. [19–21]) as

$$\begin{aligned} \dot{x}_m &= Ax_m + B_3 u_{bl} + B_z z_{cmd} + L(y - y_m) + F_L(e_y) - F_{x_m}(e_y) \\ y_m &= Cx_m, \quad z_m = C_z x_m \end{aligned} \quad (6.52)$$

where L is designed as

$$S = (CB_3^1)^T, \quad \bar{C} := SC, \quad (6.53)$$

$$\begin{aligned} R^{-1}(\epsilon) &= (\bar{C}B_3^1)^{-1} [\bar{C}AB_3^1 \\ &\quad + (\bar{C}AB_3^1)^T] (\bar{C}B_3^1)^{-1} + \epsilon I \end{aligned} \quad (6.54)$$

$$L = B_3^1 R^{-1}(\epsilon) S. \quad (6.55)$$

$\epsilon > 0$ is chosen to be large enough as

$$\begin{aligned} \epsilon &> \bar{\epsilon}, \quad \bar{\epsilon} = \max[\epsilon_1, \epsilon_2] \\ \epsilon_1 &= \lambda_{\max} \left\{ -(\bar{C}B_3^1)^{-1} [\bar{C}AB_3^1 + (\bar{C}AB_3^1)^T] (\bar{C}B_3^1)^{-1} \right\} \\ \epsilon_2 &= \lambda_{\max} \left\{ (\bar{C}B_3^1)^{-2} \left[2 \|\bar{C}B_3^1\|^2 (\bar{\Psi}_{\max} + R_{\max}) + H_{\max}^2 \right] \right\} \\ H_{\max} &= (1 + 2\bar{\Psi}_{\max} \|P_I\|) \|P_I\| \cdot \left(\|N^1 AB_3^1\| + a_2^2 \bar{\Psi}_{\max}^2 R_{\max} + a_2^1 \bar{\Psi}_{\max} R_{\max} \right) \\ &\quad + \|\bar{C}AM\| + \|CB_3^1\| \bar{\Psi}_{\max} \end{aligned} \quad (6.56)$$

where $N^1 = (M^T M)^{-1} M^T [I - B_3^1 (\bar{C}B_3^1)^{-1} \bar{C}]$, M is the null space of C , P_I is a solution of $P_I N^1 A M + (N^1 A M)^T P_I = -I$ (see Lemma 3.1 for its existence), $\bar{\Psi}_{\max} = \Psi_{\max} \left\| \begin{bmatrix} \mathfrak{B} & \mathfrak{M} \end{bmatrix} \right\|$, and $R_{\max} = \|(\mathfrak{C}\mathfrak{B})^{-1} \mathfrak{C}A^2 B\|$, where $\mathfrak{C}^T = \begin{bmatrix} C^T & (CA)^T & (CA^2)^T \end{bmatrix}^T$, $\mathfrak{B} = \begin{bmatrix} B_3 & AB_3 & A^2 B_3 \end{bmatrix}$ and \mathfrak{M} is the null space of \mathfrak{C} (see Lemma 3.1). ϵ is so chosen that an underlying SPR condition is guaranteed in Section 6.3.2. Numerical examples

will show L has a reasonable magnitude. $F_L(e_y)$ and $F_\Psi(e_y)$ are designed as

$$F_L(e_y) = F_3^2(\psi_3^{1T}(t)\bar{e}_{\psi y}^{[1]}) + F_3^3(\psi_3^{1T}(t)\bar{e}_{\psi y}^{[1][2]}) + F_3^3(\psi_3^{2T}(t)\bar{e}_{\psi y}^{[2]}) \quad (6.57)$$

$$F_{x_m}(e_y) = F_3^2(\Lambda^T(t)\bar{e}_{\Psi_1 y_1^0}^{[1]}) + F_3^3(\psi_3^{1T}(t)\bar{e}_{\Psi_1 y_1^0}^{[1][2]}) \quad (6.58)$$

$F_3^i(w)$ for $i = 2, 3$ and some $w(t) \in \mathbb{R}^m$ are defined as

$$\begin{aligned} F_3^2(x) &= (B_3^2 s + B_3 a_2^0)[w] \\ F_3^3(w) &= B_3 \pi_2^2(s)[w] \end{aligned} \quad (6.59)$$

where B_3^i is defined as

$$\begin{aligned} B_3^1 &= A^2 B_3 a_2^2 + A B_3 a_2^1 + B_3 a_2^0 \\ B_3^2 &= A B_3 a_2^2 + B_3 a_2^1, \quad B_3^3 = B_3 a_2^0 \end{aligned} \quad (6.60)$$

which are relative degree i th input paths through $\{A, B_3^i, C\}$. $\psi_3^{1T}(t) \in \mathbb{R}^{m \times m}$ and $\psi_3^{2T}(t) \in \mathbb{R}^{m \times m}$ are estimates of $\psi_3^{1*T}(t) \in \mathbb{R}^{m \times m}$ and $\psi_3^{2*T}(t) \in \mathbb{R}^{m \times m}$, which are elements of Ψ_3^* and will be defined in Section 6.3.2. $\Lambda(t)$ is the estimate of Λ^* . We have assumed that $\ddot{\Lambda}(t)$, $\ddot{\psi}_3^1(t)$ and $\ddot{\psi}_3^2(t)$ are accessible, which will be realized using a high-order tuner in Section 6.3.3. Signals $\bar{e}_{\psi y}^{[i][j]}$ are outputs of a series of filters as

$$\begin{aligned} e_{sy} &:= R^{-1} S e_y, \quad \text{where } e_y := y - y_m \\ \bar{e}_{\psi y}^{[1]} &= \frac{\pi_2^1(s)}{\pi_2^2(s)} e_{sy}, \quad \bar{e}_{\psi y}^{[2]} = \frac{\pi_2^0(s)}{\pi_2^2(s)} e_{sy} \\ \bar{e}_{\psi y}^{[1][2]} &= \frac{\pi_2^0(s)}{\pi_2^2(s)} s \left[\psi_3^{1T} \bar{e}_{\psi y}^{[1]} \right], \end{aligned} \quad (6.61)$$

where R and S is designed as in (6.53) and (6.54), respectively. It is noted that j th derivative of $\bar{e}_{\psi y}^{[i][j]}$ are available for control. Signals $\bar{e}_{\Psi_1 y_1^0}^{[i][j]}$ are outputs of a series of filters as

$$\begin{aligned} e_{y_1^0} &:= \int_0^t L e_y(\tau) d\tau \\ \bar{e}_{\Psi_1 y_1^0}^{[1]} &= \frac{\pi_2^1(s)}{\pi_2^2(s)} \cdot s \left[\Psi_1^T(t) e_{y_1^0} \right] \\ \bar{e}_{\Psi_1 y_1^0}^{[1][2]} &= \frac{\pi_2^0(s)}{\pi_2^2(s)} \cdot s \left[\Lambda^T(t) \bar{e}_{\Psi_1 y_1^0}^{[1]} \right]. \end{aligned} \quad (6.62)$$

It is noted that the j th derivative of $\bar{e}_{\Psi_1 y_1^0}^{[i][j]}$ are available for control.

The F_L term in CRM deals with the uncertainties introduced when using a known L as in (6.55) to guarantee an underlying unknown SPR model (see Section 6.3.2). The F_{x_m} term will be used to deal with the inaccessibility of \ddot{x}_m (see CRM (6.52)), which is used to address the uncertainty $B_1 \Psi_1^{*T} x$ in the plant model. We have put the equivalent realization of the inaccessible parts of \ddot{x}_m in F_{x_m} (using Lemma 3.3) and putting the rest accessible parts of \ddot{x}_m in u_{ad} as

$$u_{ad} = -u_{bl} + \pi_2^2(s) \left[\Lambda^T(t) \bar{u}_{bl}^{[2]} - \Psi_1^T(t) v_m - \Psi_2^T(t) \bar{x}_m^{[1]} - \Psi_3^T(t) \bar{x}_m^{[2]} \right] \\ - \sum_{i=1}^2 a_2^i d_i^i \Psi_1^{(i+1)T}(t) e_{y_1^0} \quad (6.63)$$

where v_m are artificial signals with artificial derivatives defined as

$$s^2 \cdot v_m = A^2 x_m + AB_z z_{cmd} + B_z \dot{z}_{cmd} - AL e_y \\ s \cdot v_m = Ax_m + B_z z_{cmd} \\ v_m = x_m \quad (6.64)$$

It is noted that $s^i \cdot v_m$ are parts of $x_m^{(i)}$. The adjustable parameters $\Lambda^T(t)$ and $\Psi_i^T(t)$ are estimates of Λ^{*-1} and $\bar{\Psi}_i^{*T}$, respectively, which will be defined in Section 6.3.3. The derivatives $\ddot{\Lambda}(t)$ and $\ddot{\Psi}_i(t)$ will be realized using high-order tuner in Section 6.3.2. In particular, we design $\Psi_1(t)$ as

$$\Psi_1^T(t) = \begin{bmatrix} \times & 0 & 0 & 0 \end{bmatrix} \quad (6.65)$$

which matches the structure of Ψ_1^{*T} as Assumption 6.5 holds. Signal $\overline{(\cdot)}$ is a filtered version of signal (\cdot) as

$$\bar{u}_{bl}^{[2]} = \frac{1}{\pi_2^2(s)} u_{bl}, \quad \bar{x}_m^{[1]} = \frac{\pi_2^1(s)}{\pi_2^2(s)} x_m, \quad \bar{x}_m^{[2]} = \frac{\pi_2^0(s)}{\pi_2^2(s)} x_m \quad (6.66)$$

It is noted that up to i th derivatives of $\overline{(\cdot)}^{[i]}$ are available for control.

6.3.2 Error Model Analysis

The following paragraphs show that the control design in the previous section yields an underlying SPR error model. The error model is derived by subtracting the CRM (6.52) from the plant model (6.47), which yields

$$\begin{aligned}\dot{e}_x = & (A^* - LC)e_x - F_L(e_y; s) + F_{x_m}(e_y; s) \\ & + B_1\Psi_1^{*T}x_m + B_2\Psi_2^{*T}x_m + B_3\Psi_3^{*T}x_m \\ & + B_3\Lambda^*(u_{bl} + u_{ad}) - B_3u_{bl}.\end{aligned}\quad (6.67)$$

where

$$A^* = A + B_1\Psi_1^{*T} + B_3\Psi_3^{*T}. \quad (6.68)$$

The input path of relative degree i corresponding to A are B_3^i , for $i = 1, 2, 3$, as defined in (6.60) and they are known; the input path of relative degree i corresponding to A^* are B_3^{i*} , which are defined as

$$\begin{aligned}B_3^{1*} &= A^{*2}B_3a_2^2 + A^*B_3a_2^1 + B_3a_2^0 \\ B_3^{2*} &= A^*B_3a_2^2 + B_3a_2^1, \quad B_3^{3*} = B_3a_2^2,\end{aligned}\quad (6.69)$$

and they are unknown. Define

$$A_L^* = A^* - LC. \quad (6.70)$$

B_3^{i*} are also the relative degree i system input paths for $\{A_L^*, B_3^{i*}, C\}$, i.e. B_3^{i*} are invariant for any $L \in \mathbb{R}^{n \times m}$.

The following error model analysis will be a direct extension of its counterpart in the SISO case in Section 6.1.2, and therefore only a few important Lemma will be provided for the MIMO case while some intermediate steps are omitted. The following Lemma guarantees a SPR transfer function, which is an extension of Lemma 6.10, whose proof can be found in the Appendix E.

Lemma 6.6. *With $R(\epsilon)$ as in (6.55) and ϵ as in (6.56), $\overline{W}_3^{1*}(s) = SC(sI - A^* + L^*C)^{-1}B_3^{1*}$ is SPR, where $L^* = B_3^{1*}R^{-1}(\epsilon)S$.*

The goal of this Section is to formulate the SPR error model as in Definition 6.1. To realize L^* in $\overline{W}_3^{1*}(s)$ while using L in CRM, we need to address the difference between B_3^i and B_3^{i*} , which can be parametrized using the following Lemma (an extension of Lemma 6.2). The proof can be found in the Appendix E.

Lemma 6.7. *[Recursive Properties of B_3^i] For plant model $\{A, B_3, C\}$ satisfying Assumptions 6.3 and 6.5, B_3^i as in (6.60) and B_3^{i*} (6.69) satisfies*

$$\begin{aligned} B_3^{1*} - B_3^1 &= B_3^{2*}\psi_3^{1*T} + B_3^{3*}\psi_3^{2*T} \\ B_3^{2*} - B_3^2 &= B_3^{3*}\psi_3^{1*T}, \quad B_3^{3*} - B_3^3 = 0 \end{aligned} \tag{6.71}$$

for $i = 1, 2, 3$ where uncertain terms ψ_3^{i*} are elements of Ψ_3^* .

The difference between B_3^i and B_3^{i*} can be written in terms of $B_3^{\{i+1\}*}$ and hence the name ‘‘recursive’’. $F_L(e_y)$ as in (6.57) deals with L^*C , while $F_{x_m}(e_y)$ as in (6.58), together with u_{ad} , deals with $B_i\Psi_i^{*T}x_m$ for $i = 1, 3$. First $B_i\Psi_i^{*T}x_m$ can be written in terms of B_3^{i*} using the following Proposition (an extension of Proposition 6.2), whose proof can be found in the Appendix.

Proposition 6.3. *For plant model $\{A, B_3, C\}$ satisfying Assumptions 6.3 and 6.4, there exists $\overline{\Psi}_1^*$, $\overline{\Psi}_1^*$ and $\overline{\Psi}_3^*$ such that*

$$B_1\Psi_1^{*T} + B_3\Psi_3^{*T} = B_3^{1*}\Lambda^*\overline{\Psi}_1^{*T} + B_3^{2*}\Lambda^*\overline{\Psi}_2^{*T} + B_3\Lambda^*\overline{\Psi}_3^{*T}, \tag{6.72}$$

where B_3^{i*} is defined in (6.71) and $\overline{\Psi}_1^{*T} = \begin{bmatrix} \times & 0 & 0 \end{bmatrix}$

Then all uncertainties in the error model lie in the range of B_3^{i*} . Both of $F_L(e_y)$ and $F_{x_m}(e_y)$ use an equivalent realization of zero addition (see Lemma 3.3) to generate zeros in error model analysis, as summarized in the following Lemma (an extension of Lemma 6.3), whose proof is shown in the Appendix E.

Lemma 6.8. [Recursive Adaptation] Suppose an error model

$$\begin{aligned}\dot{e}_x &= A_L^* e_x + B_3^{2*} \phi^{*T} \omega(t) - F(t) \\ e_y &= C e_x\end{aligned}\tag{6.73}$$

where $A_L^* = A^* - LC$ with any $L \in \mathbb{R}^{n \times m}$, B_3^{2*} defined in (6.69), $\{A, B_3, C\}$ satisfies Assumptions 6.3 to 6.5, ϕ^* is unknown constant parameters, $\omega(t)$ is a known regressor with $\dot{\omega}(t)$ inaccessible, and $F(t)$ is free to choose, then $F(t)$ can be chosen as

$$F(t) = F_3^2(\phi^T(t)\bar{\omega}^{[1]}(t)) + F_3^3(\psi_3^{1T}(t)\bar{\omega}^{[1][2]}(t))\tag{6.74}$$

where F_3^i is defined in (6.59), $\phi(t)$ is an estimate of ϕ^* with $\ddot{\phi}(t)$ accessible, $\psi_3^1(t)$ is an estimate of ψ_3^{1*} as in (6.71) with $\ddot{\psi}_3^1(t)$ accessible, and $\bar{\omega}^{[i]}(t)$ for $i = 1, 2$ is a filtered version of $\omega(t)$ as

$$\bar{\omega}^{[1]}(t) = \frac{\pi_2^1(s)}{\pi_2^2(s)}\omega(t), \quad \bar{\omega}^{[1][2]}(t) = \frac{\pi_2^0(s)}{\pi_2^2(s)} \cdot s [\phi^T(t)\bar{\omega}^{[1]}(t)],\tag{6.75}$$

such that the error model can be transformed into

$$\begin{aligned}\dot{e}'_x &= A^* e'_x - B_3^{1*} \tilde{\phi}^T(t)\bar{\omega}^{[1]}(t) - B_3^{1*} \tilde{\psi}_3^{1T} \bar{\omega}^{[1][2]}(t) \\ e_y &= C e'_x\end{aligned}\tag{6.76}$$

where $\tilde{\phi}(t) = \phi(t) - \phi^*$, $\tilde{\psi}_3^1 = \psi_3^1(t) - \psi_3^{1*}$ and

$$\begin{aligned}e'_x &= e_x + B_3^{3*} \phi^{*T} \omega(t) - B_3^{3*} \phi^T(t) \omega(t) \\ &\quad + [B_3^{2*} + B_3^{3*} s] \tilde{\phi}^T(t)\bar{\omega}^{[1]}(t) + [B_3^{2*} + B_3^{3*} s] \tilde{\psi}_3^{1T} \bar{\omega}^{[1][2]}(t)\end{aligned}\tag{6.77}$$

Remark 6.1. If $\Psi_3^* = 0$, then $\bar{\Psi}_3^* = 0$ and therefore $\psi_3^{1*} = 0$; as a result, we can choose $\psi_3^1(t) \equiv 0$ and all terms with $\bar{\omega}^{[1][2]}$ will be zero in $F(t)$.

Lemma 6.8 is used in deriving the SPR error model shown in the following Lemma (an extension of Lemma 6.5), whose proof can be found in the Appendix E.

Lemma 6.9. For the plant model (6.47) satisfying Assumptions 6.1 to 6.7, with the

CRM as in (6.52) and u as in (6.50)(6.51)(6.63), the error model $e_x = x - x_m$ is a SPR error model as

$$\dot{e}_{mx} = A_{L^*}^* e_{mx} + B_3^{1*} \tilde{\Phi}^T \bar{\nu} + B_3^{1*} \Lambda^* \tilde{\Omega}^T \bar{\xi} \quad (6.78)$$

$$Se_y = SC e_{mx}$$

where $A_{L^*}^* = A^* - L^*C$, B_3^{1*} defined in (6.69) and

$$\begin{aligned} \bar{\xi} &= \begin{bmatrix} \bar{u}_{bl}^{[2]} \\ -x_m \\ -\bar{x}_m^{[1]} \\ -\bar{x}_m^{[2]} \end{bmatrix}, \quad \bar{\nu} = \begin{bmatrix} -\bar{e}_{\psi y}^{[1]} - \bar{e}_{\psi y}^{[1][2]} + \bar{e}_{\Psi_1 y_1^0}^{[1][2]} \\ -\bar{e}_{\psi y}^{[2]} \\ \bar{e}_{\Psi_1 y_1^0}^{[1]} \end{bmatrix} \\ \Omega^{*T} &= \begin{bmatrix} \Lambda^{*-1} & \Psi_1^{*T} & \Psi_2^{*T} & \Psi_3^{*T} \end{bmatrix} \\ \Omega^T &= \begin{bmatrix} \Lambda^T & \Psi_1^T & \Psi_2^T & \Psi_3^T \end{bmatrix} \\ \tilde{\Omega}^T &= \begin{bmatrix} \tilde{\Lambda}^T & \tilde{\Psi}_1^T & \tilde{\Psi}_2^T & \tilde{\Psi}_3^T \end{bmatrix} \\ \Phi^{*T} &= \begin{bmatrix} \psi_3^{1*T} & \psi_3^{2*T} & \Lambda^* \end{bmatrix} \\ \Phi^T &= \begin{bmatrix} \psi_3^{1T} & \psi_3^{2T} & \Lambda^T \end{bmatrix} \\ \tilde{\Phi}^T &= \begin{bmatrix} \tilde{\psi}_3^{1T} & \tilde{\psi}_3^{2T} & \tilde{\Lambda}^T \end{bmatrix}. \end{aligned} \quad (6.79)$$

where $\bar{\xi} \in \mathbb{R}^{(m+3n) \times 1}$ and $\bar{\nu} \in \mathbb{R}^{3m \times 1}$.

At this point, we have generated a SPR error model.

6.3.3 High Order Tuner and Stability Proof

In this section, a high order tuner adaptive law [51] is used to generate $\ddot{\Omega}(t)$ and $\ddot{\Phi}(t)$ so that the control (6.63) and the CRM (6.52) is realizable. The design is very similar to (6.41) in SISO case and therefore only key equations are presented below. The adjustable parameters $\Omega^T(t) \in \mathbb{R}^{m \times (m+3n)}$ and $\Phi^T(t) \in \mathbb{R}^{m \times 3m}$ are outputs of tuners as

$$\begin{aligned} \dot{X}_\Omega &= (A_H X_\Omega + B_H \Omega'^T) g(\bar{\xi}; \mu_\xi), \quad \Omega^T(t) = C_H X_\Omega \\ \dot{X}_\Phi &= (A_H X_\Phi + B_H \Phi'^T) g(\bar{\nu}; \mu_\nu), \quad \Phi^T(t) = C_H X_\Phi \end{aligned} \quad (6.80)$$

where $X_\Omega \in \mathbb{R}^{2m \times (m+3n)}$ and $X_\Phi \in \mathbb{R}^{2m \times 3m}$ are augmented matrices with columns being the states of the tuner. $A_H \in \mathbb{R}^{2m \times 2m}$, $B_H \in \mathbb{R}^{2m \times m}$ and $C_H \in \mathbb{R}^{m \times 2m}$ are block diagonal matrices with A_h , b_h and c_h as their diagonal elements, respectively. $\{A_h, b_h, c_h\}$ chosen as

$$A_h = \begin{bmatrix} 0 & 1 \\ -a_2^0/a_2^2 & -a_2^1/a_2^2 \end{bmatrix}, \quad b_h = \begin{bmatrix} 0 \\ a_2^0/a_2^2 \end{bmatrix}, \quad c_h = \begin{bmatrix} 1 & 0 \end{bmatrix} \quad (6.81)$$

i.e. $c_h(sI - A_h)^{-1}b_h = \frac{\pi_2^2(0)}{\pi_2^2(s)}$. Then the derivatives of adjustable parameters can be obtained by

$$\begin{aligned} \dot{\Omega}^T(t) &= C_H^1 X_\Omega, \quad \ddot{\Omega}^T(t) = C_H^2 X_\Omega \\ \dot{\Phi}^T(t) &= C_H^1 X_\Phi, \quad \ddot{\Phi}^T(t) = C_H^2 X_\Phi \end{aligned} \quad (6.82)$$

where $C_H^1 \in \mathbb{R}^{m \times 2m}$ and $C_H^2 \in \mathbb{R}^{m \times 2m}$ are block diagonal matrices with $c_h^1 = \begin{bmatrix} 0 & 1 \end{bmatrix}$ and $c_h^2 = \frac{-1}{a_2^2} \begin{bmatrix} a_2^0 & a_2^1 \end{bmatrix}$ as their diagonal elements, respectively. The varying gain function $g(x; \mu)$ is defined as

$$g(x; \mu) := 1 + \mu x^T x \quad (6.83)$$

where μ for each equation of (6.80) chosen to be

$$\begin{aligned} \delta_\xi &= \frac{\|C_H\|\Lambda_{max}}{\gamma \|P_H A_H^{-1} B_H\|}, \quad \mu_\xi = \frac{4(m+3n)\|SC\|^2 \|C_H\|^2}{n \lambda_Q \delta_\xi} \\ \delta_\nu &= \frac{\|C_H\|}{\gamma \|P_H A_H^{-1} B_H\|}, \quad \mu_\nu = \frac{4 \cdot 3m \|SC\|^2 \|C_H\|^2}{n \lambda_Q \delta_\nu} \end{aligned} \quad (6.84)$$

P_H is a solution matrix for the equation $P_H A_H + A_H^T P_H = -I$ and λ_Q is the smallest eigenvalues of Q , which is defined as

$$Q = -N^{1T} H (\bar{C} B_3^{1*})^{-1} \bar{C} - \bar{C}^T (\bar{C} B_3^1)^{-1} H^T N^{1T} + \varepsilon \bar{C}^T \bar{C} + N^{1T} N^1 \quad (6.85)$$

where $H = M^T A^T \bar{C}^T + P_I N^1 A B_3^1$ and ε is defined in (6.56). The input to the tuner are adjusted using

$$\begin{aligned}\dot{\Omega}'(t) &= -\Gamma \bar{\xi} e_y^T S^T \text{sign}(\Lambda^*) \\ \dot{\Phi}'(t) &= -\Gamma \bar{\nu} e_y^T S^T\end{aligned}\tag{6.86}$$

where $\Gamma = \gamma I > 0$ are adaptation gains. The following theorem guarantees the global stability and asymptotic tracking of the adaptive system, whose proof can be found in the Appendix E. Define $e_z(t) = z - z_m$ as tracking errors.

Theorem 6.2. *For the plant model (6.47) that satisfies Assumptions 6.1 to 6.7, and for any $z_{cmd}(t)$ that is piecewise continuous, the adaptive controller (6.50), (6.51), (6.63), (6.52), and (6.86), with L and S designed in (6.55)(6.53), guarantees that i) the closed-loop system has bounded solutions, ii) $e_y(t) \rightarrow 0$ as $t \rightarrow \infty$, and iii) $e_z(t) \rightarrow 0$ as $t \rightarrow \infty$.*

6.3.4 Extension to Nonsquare Plant Models

This section extends the control design in 6.3 to a plant model whose number of outputs exceeds that of inputs, i.e. $p > m$. Define n_z as the number of transmission zeros in the plant model (6.47). The overall method integrates a squaring-up procedure (see Section 5.2 for details), which requires an additional assumption on the plant model (6.47).

Assumption 6.8. *Dimensions of $B_3 \in \mathbb{R}^{n \times m}$ and $C \in \mathbb{R}^{p \times n}$ satisfy $(n - n_z - 3m) \geq (p - m)$.*

All the equations for design in 6.3.1 are still valid except that the design of L needs to be modified as

$$\begin{aligned}L &= \bar{B}_3^1 R^{-1}(\varepsilon) S, \quad S = (C \bar{B}_3^1)^T \\ \bar{B}_3^1 &= A^2 \bar{B}_3 a_2^2 + A \bar{B}_3 a_2^1 + \bar{B}_3 a_2^0 \\ \varepsilon &> \bar{\varepsilon}, \quad \bar{\varepsilon} = \bar{\varepsilon}(A, \bar{B}_3, C, \Lambda_{max}, \Psi_{max})\end{aligned}\tag{6.87}$$

where $\bar{B}_3 \in \mathbb{R}^{n \times p}$ is a squared-up B_3 as defined in the following Lemma, whose proof is very similar to the proof of Lemma 5.1 and therefore is omitted here.

Lemma 6.10. *For plant models satisfying Assumptions 6.1 to 6.3 and 6.8, there exists a $B_{s1} \in \mathbb{R}^{n \times m_s}$ such that $\{A, \bar{B}_3, C\}$, where $\bar{B}_3 = [B_3, B_{s1}]$, has stable transmission zeros and nonuniform input relative degree as $r_i = 3$ for $i = 1, 2, \dots, m$ and $r_i = 1$ for $i = m+1, m+2, \dots, p$.*

Then L as in (6.87) guarantees the SPR property of $\{A_{L^*}^*, \bar{B}_3^{1*}, SC\}$ where $\bar{B}_3^{1*} = A^{*2}\bar{B}_3a_2^2 + A^*\bar{B}_3a_2^1 + \bar{B}_3a_2^0$. Partition of S as

$$S^T = [S_3^T, S_1^T] \quad (6.88)$$

with $S_3 \in \mathbb{R}^{m \times p}$, guarantees the SPR properties $\{A_{L^*}^*, B_3^{1*}, S_3C\}$ (using KYP Lemma). As a result, Lemma 6.6 holds. Also, Lemma 6.7 holds with B_3^1 and B_3^{1*} as well as \bar{B}_3^1 and \bar{B}_3^{1*} . Since L is designed using \bar{B}_3^1 , $F_L(e_y)$ is designed using \bar{B}_3 . Control signal u still goes into plant through B_3 and therefore F_{x_m} is designed using B_3 . The rest of design and analysis follows exactly Section 6.3.2 and Section 6.3.3. It is noted \bar{B}_3 is only used in CRM.

6.3.5 Design Procedure

The overall control design in this section can be summarized into the following step-wise procedure:

Step 6.1. *Given a plant model (A, B, C, C_z, D_z) , check Assumptions 6.1 to 6.7;*

Step 6.2. *Add integral error states to the plant model using (6.46);*

Step 6.3. *Design a baseline observer-based controller (6.51)(6.52) (without adaptive terms) and choose K and an observer parameter using the LQR and the LTR techniques, respectively;*

Step 6.4. *(For nonsquare plant models only). Pick a B_{s1} using Lemma 6.10 and produce a squared-up \bar{B}_3 ;*

Step 6.5. Design a ε using (6.56), then design a SPR pair L using Eq.(6.55) and S_1 using Eq.(6.53), and replace the observer gain in the baseline controller (6.52) with L ;

Step 6.6. Design high order tuners as in (6.80) and prescribe parameter adaptation; (6.86)

Step 6.7. Add the adaptive portion (6.63) to the baseline control (6.50) and add adaptive portion (6.57) and (6.58) to the CRM.

Step 6.1 to Step 6.3 are conventional observer-based controller designs. Step 6.5 to Step 6.7 are for the adaptive component addition, which completes our adaptive control design. It is noted that for both the baseline controller and the adaptive controller, the L design is independent from the K design. We can generally consider that K is designed for performance, and L is designed for stability. The overall controller structure diagram is shown in Figure 4-1.

6.4 Applications to VFA

This section applies the relative degree three adaptive controller on the nonlinear 3-wing VFA model as shown in Section 2.2.1. The nonlinear model is linearized around each of 25 trim points defined by $V_0 = 30$ ft/sec, $\alpha_0 = 0$ deg, $\theta_0 = 0$ deg, $q = 0$ deg/sec, $\eta_0 \in [10, 12]$ deg with a step of 0.5, and $\dot{\eta}_0 \in [-0.2, 0.2]$ deg/sec with a step

of 0.1. Exemplary numerical values of the linearized model is shown below as

$$\begin{bmatrix} V \\ \dot{\alpha} \\ \dot{\theta} \\ \dot{q} \\ \dot{\eta} \\ \ddot{\eta} \\ \dot{\delta}_e \\ \dot{\delta}_a \\ \dot{\delta}_e \\ \dot{\delta}_a \\ \dot{w}_\eta \\ \dot{w}_{A_z} \end{bmatrix} = \underbrace{\begin{bmatrix} -0.279 & 3.476 & -32.2 & -0.015 & 0.514 & 0.525 & 0 & 0 & -2.57 & -6.47 & 0 & 0 \\ -0.070 & -4.104 & 0 & 1.013 & 0.193 & 0.100 & 0 & 0 & -0.795 & -0.079 & 0 & 0 \\ 0 & 0 & 0 & 1 & 0 & 0 & 0 & 0 & 0 & 0 & 0 & 0 \\ 0 & -54.04 & 0 & 0.255 & 1.845 & 21.41 & 0 & 0 & 5.991 & -6.363 & 0 & 0 \\ 0 & 0 & 0 & 0 & 0 & 1 & 0 & 0 & 0 & 0 & 0 & 0 \\ 0.002 & 0.044 & 0 & 0.819 & -0.075 & -6.518 & 0 & 0 & 0.195 & -0.034 & 0 & 0 \\ 0 & 0 & 0 & 0 & 0 & 0 & 1 & 0 & 0 & 0 & 0 & 0 \\ 0 & 0 & 0 & 0 & 0 & 0 & 0 & 1 & 0 & 0 & 0 & 0 \\ 0 & 0 & 0 & 0 & 0 & 0 & -1 & 0 & -1.4 & 0 & 0 & 0 \\ 0 & 0 & 0 & 0 & 0 & 0 & 0 & -1 & 0 & -1.4 & 0 & 0 \\ 0 & 0 & 0 & 1 & 0 & 0 & 0 & 0 & 0 & 0 & 0 & 0 \\ 0 & -123.12 & 0 & 0 & 0 & 0 & 0 & 0 & -23.84 & -2.376 & 0 & 0 \end{bmatrix}}_{x} \begin{bmatrix} V \\ \alpha \\ \theta \\ q \\ \eta \\ \dot{\eta} \\ \delta_e \\ \delta_a \\ \dot{\delta}_e \\ \dot{\delta}_a \\ w_\eta \\ w_{A_z} \end{bmatrix}$$

$$+ \underbrace{\begin{bmatrix} 0 & 0 \\ 0 & 0 \\ 0 & 0 \\ 0 & 0 \\ 0 & 0 \\ 0 & 0 \\ u_e \\ u_a \\ u \\ 1 & 0 \\ 0 & 1 \\ 0 & 0 \\ 0 & 0 \end{bmatrix}}_{B_2} - \underbrace{\begin{bmatrix} 0 & 0 \\ 0 & 0 \\ 0 & 0 \\ 0 & 0 \\ 0 & 0 \\ 0 & 0 \\ z_q \\ z_{A_z} \\ z_{cmd} \\ 0 & 0 \\ 1 & 0 \\ 0 & 1 \end{bmatrix}}_{B_z} \underbrace{\begin{bmatrix} q \\ w_\eta \\ w_{A_z} \end{bmatrix}}_{y} = \underbrace{\begin{bmatrix} 0 & 0 & 0 & 1 & 0 & 0 & 0 & 0 & 0 & 0 & 0 & 0 \\ 0 & 0 & 0 & 0 & 0 & 0 & 0 & 0 & 0 & 0 & 1 & 0 \\ 0 & 0 & 0 & 0 & 0 & 0 & 0 & 0 & 0 & 0 & 0 & 1 \end{bmatrix}}_{C} x$$
(6.89)

for $\eta_0 = 10$ deg and $\dot{\eta}_0 = 0$ deg/sec, where we have included 2nd-order actuator dynamics with nominal natural frequency $\omega_n = 1\text{Hz}$ and nominal damping ratio $\zeta = 0.7$. u_e are elevator commands and u_a are aileron commands to the actuators. It is verified that Eq.(2.10) holds for all trims in the range $\eta_0 \in [10, 12]$ deg. For example, the linearized model for $\eta_0 = 10$ deg and $\dot{\eta}_0 = 0.2$ deg/sec can be approximated using

$$\Theta_p^* = \begin{bmatrix} 0.06 & -4.52 & 0 & 0.05 & 0.041 & 1.47 \\ 0.01 & 1.83 & 0 & -0.02 & -0.035 & -0.59 \end{bmatrix}, \quad \Lambda^* = \begin{bmatrix} 0.91 & 0.53 \\ 0.52 & 0.79 \end{bmatrix}$$

within an error of 2.6% $\|A_p\|$ and 1.8% $\|B_p\|$, respectively. The pitch mode of the VFA when $\eta \geq 11^\circ$ is unstable.

For control design, we designed control parameters for the trim of (6.89). L and

S_3 are found using $a_2^2 = 1$, $a_2^1 = 2$, $a_2^0 = 1$, $\varepsilon = 10$, $\Lambda_{max} = 2$ and $\Psi_{max} = 30$:

$$L = \begin{bmatrix} -44.83 & -123.56 & 64.29 \\ 1.416 & 3.290 & 8.712 \\ -0.339 & -0.194 & -0.007 \\ 529.9 & 985.3 & -21.85 \\ 14.99 & 8.600 & 0.329 \\ -93.98 & -8.302 & -2.089 \\ -10.93 & -105.4 & -4.762 \\ 5.970 & 51.85 & -4.127 \\ 15.32 & 147.5 & 6.667 \\ -10.82 & -74.00 & 5.72 \\ -3.151 & -1.806 & -0.069 \\ -20.56 & 62.48 & 260.0 \end{bmatrix}, \quad S_3 = \begin{bmatrix} -0.045 & -0.888 & -0.457 \\ 0.084 & 0.453 & -0.887 \end{bmatrix}. \quad (6.90)$$

For the baseline controller without adaptation, the resulting controller is an observer-based linear controller (referred as the baseline controller). The L design for this particular trim generate adequate stability margin in the baseline controller in the absence of uncertainties, as shown in Figure 6-5 (see legend “nom”). The following relation holds as $a_2^2/a_2^0 \rightarrow 0$, $a_2^1/a_2^0 \rightarrow 0$ and $\varepsilon \rightarrow \infty$:

$$\bar{B}_3^1 \rightarrow \bar{B}_3, \quad L \rightarrow \bar{B}_3 R^{-1}(\varepsilon) S \rightarrow \infty. \quad (6.91)$$

which implies loop transfer recovery (see Lemma 4.6) for the loop gain at the input, as shown in Figure 6-5 (see the legend “nom”).

We schedule the control parameters [32] using real-time η measurements. The time domain simulation results with the nonlinear VFA model are shown in Figure 6-1. Three actuator models were simulated, including a nominal one with $\omega_n = 1\text{Hz}$ and $\zeta = 0.7$, a bumpy one with $\omega_n = 2\text{Hz}$ and $\zeta = 0.5$, and a slow one with $\omega_n = 0.5\text{Hz}$ and $\zeta = 2$. Besides the baseline controller, two adaptive controllers were tested: one is relative degree one as developed in Ref. [25], which pretends the actuator dynamics is not present; the other is the relative degree three shown in Section 6.3 based on a nominal actuator model as in (6.89). The number of integrators required for each controller are listed in Table 6.1, which shows that the number of integrators used in the adaptive relative degree three controller is an order of magnitude smaller than that of the classical one [14].

With nominal actuators, all three controllers almost has the same ideal perfor-

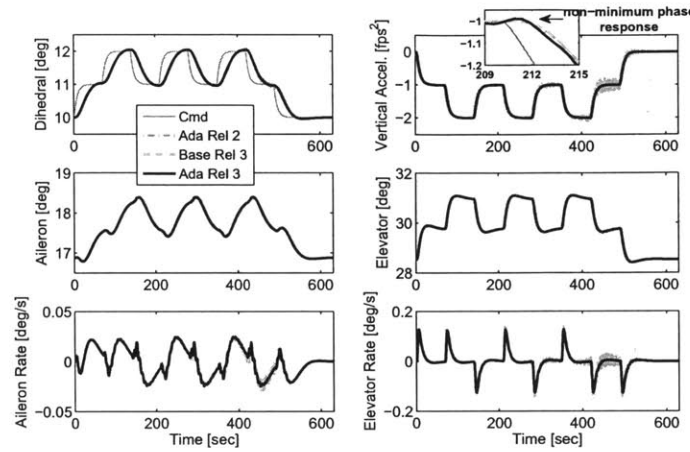
	Baseline observer-based controller	Adaptive relative degree one (Section 4.2)	Adaptive relative degree two (Section 5.2)	Adaptive relative degree three (Section 6.3)	Classical adaptive controller [14]
3-Wing VFA (6 states)	6	18	48	169	1328
Vulture VFA (122 states)	122	366	412	2162	68,238

Table 6.1: Total number of integrators required for each controller

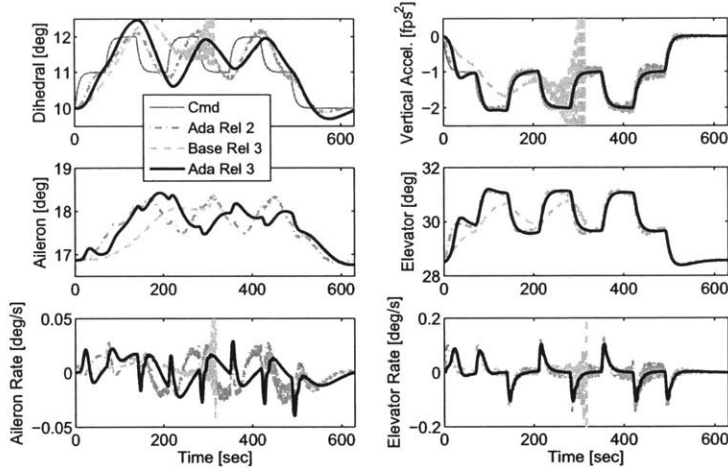
mance, as shown in Figure 6-1a. Notice that the VFA navigates through $\eta = 11, 12$ deg where the pitch mode is unstable. It is also noted that the individual transfer function from δ_e to A_z has unstable zeros, which still can be accommodated by our design since Assumption 6.2 only asks for stable transmission zeros. With fast actuators, both adaptive controllers were able to achieve tracking goals while the baseline controller failed to do so, as shown in Figure 6-1b. When actuator dynamics was slow as shown in Figure 6-1c, only relative degree two adaptive controller can achieve stable command tracking, whose parameter trajectories are shown in Figure 6-2.

The spectrum of the aileron δ_a trajectories, as shown in Figure 6-3, illustrates that the adaptive relative degree three controller requires more effort from actuator in low frequency range, less than 5Hz, compared with the adaptive relative degree two controller. The additional effort can be realized by an ordinary motor, whose bandwidth is usually around 30Hz.

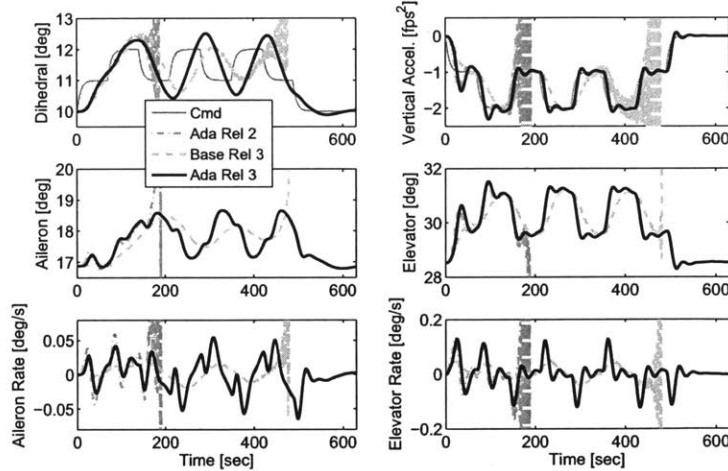
Suppose we freeze all the adaptive parameters $\Psi_i(t)$, $\psi_3^i(t)$ and $\Lambda(t)$ at the end of the simulation, the resulting “snapshot” closed-loop system consists of an uncertain LTI plant and a linear observer-based controllers. Figure 6-4 shows the frequency response of the snapshot closed-loop system for the relative degree three adaptive controller at the end of the simulation, and the effects of the initial conditions of $\Psi_i(0)$, $\psi_3^i(0)$ and $\Lambda(0)$. All trajectories tend to converge to the nominal closed-loop system (without uncertainties), except when initial conditions are large (too far away from Ψ_i^*).



(a) Nominal actuators with $\omega_n = 1\text{Hz}$ and $\zeta = 0.7$



(b) Bumpy actuators with $\omega_n = 2\text{Hz}$ and $\zeta = 0.5$



(c) Slow actuators with $\omega_n = 0.5\text{Hz}$ and $\zeta = 2$

Figure 6-1: The tracking of η and A_z using the relative degree three adaptive controller on the nonlinear VFA model

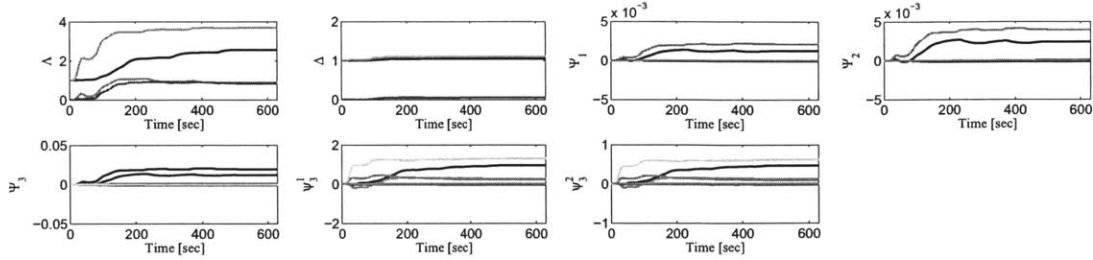


Figure 6-2: The parameter trajectories of the relative degree three adaptive controller in the simulation shown in Figure 6-1b for the nonlinear 3-wing VFA model

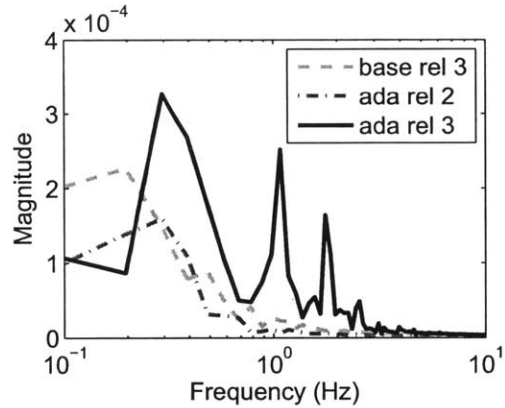


Figure 6-3: The spectrum of the aileron δ_a response in the simulation shown in Figure 6-1b for the nonlinear 3-wing VFA model

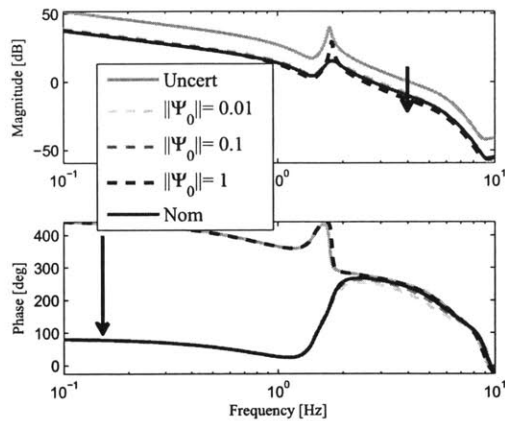


Figure 6-4: The frequency response of the snapshot closed-loop system with the relative degree three adaptive controller, from δ_e to V_z , and the effects of $\Psi_i(0)$ for the 3-wing VFA model

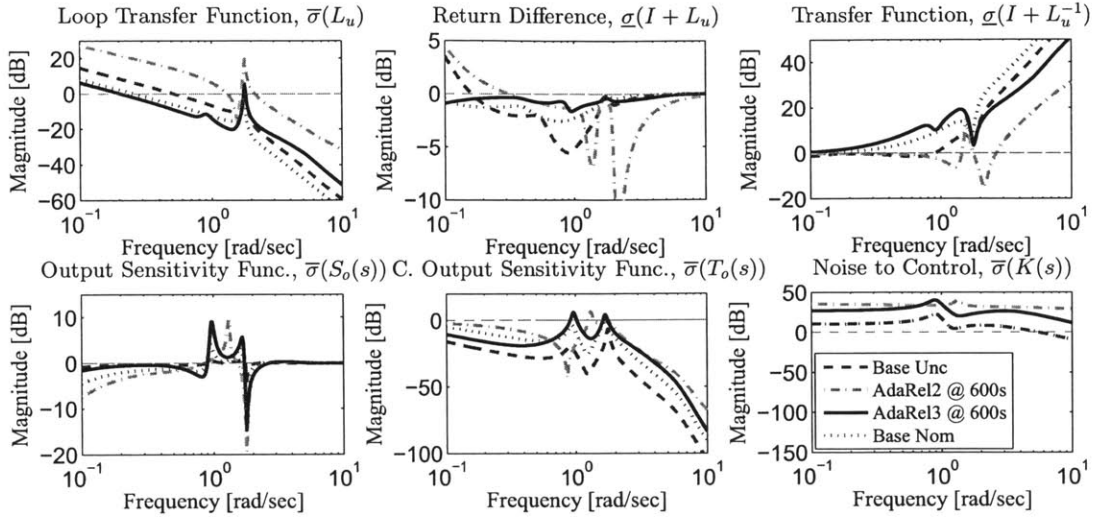


Figure 6-5: The frequency domain analysis of the snapshot closed-loop system shows that adaptation mitigates the effects of model uncertainties on robustness for the 3-wing VFA model

The gang-of-six frequency domain analysis [18, Chapter 5], as illustrated in the Figure 6-5, shows that at $t = 0$ sec the uncertainties reduce the gain margin from the nominal value (i.e. the baseline controller without uncertainties) of $[-14.8, 13.2]dB$ to $[-2.2, 1.8]dB$, and phase margin from $\pm 47.9^\circ$ to $\pm 9.6^\circ$; The “snapshot” closed-loop systems at $t = 600$ sec recovers them to $[-24, 14.2]dB$ and to $\pm 55.0^\circ$, respectively.

The trade off is that the output sensitivity of the “snapshot” system increases to 9.1dB after adaptation is complete, which increases the sensitivities to the measurement noise. Loop transfer function also has a spike at around 1.5 rad/sec at the end of adaptation, which implies sensitivities to input disturbance. To examine the robustness of the adaptive system over disturbance/noise, we introduce sinusoidal disturbance/noise of magnitude 0.2 with frequency ranging from 0.1 to 4 rad/sec in all input channels and all output channels for the simulation of bumpy actuators as in Figure 6-1b. Three exemplary time domain responses of η and δ_a are plotted in Figure 6-6a for disturbance/noise at three different frequencies, i.e. 0.3, 2 and 3 rad/sec, and show that disturbance/noise is amplified at 2 rad/sec. The mean of the moving window standard deviation, with a window size of 10, of η and δ_a is calculated and plotted against the frequencies of disturbance/noise in Figure 6-7 and shows that the

largest amplification occurs around 1.5 rad/sec, which is consistent to our gang-of-six analysis in Figure 6-5. To mitigate the effects of disturbance/noise, a σ modification is used in place of the adaptation law (6.86) as

$$\begin{aligned}\dot{\Omega}'(t) &= -\Gamma \bar{\xi} e_y^T S^T \text{sign}(\Lambda^*) - \sigma \Omega'(t) \\ \dot{\Phi}'(t) &= -\Gamma \bar{\nu} e_y^T S^T - \sigma \Phi'(t)\end{aligned}\tag{6.92}$$

with $\sigma = 0.001$. The stability proof will be very similar to the proof of Theorem 6.2 and therefore is omitted here. The same simulation was carried out with the σ modification and the three exemplary time domain responses of η and δ_a all show improvement in their magnitude oscillations, as presented in Figure 6-6b. The mitigation of oscillations across the frequency range of 0.1 to 4 rad/sec is shown in Figure 6-7. The trade-off is that since parameter adaptation with σ modifications will not converge to steady state values, the tracking performance is compromised, as shown in Figure 6-6b.

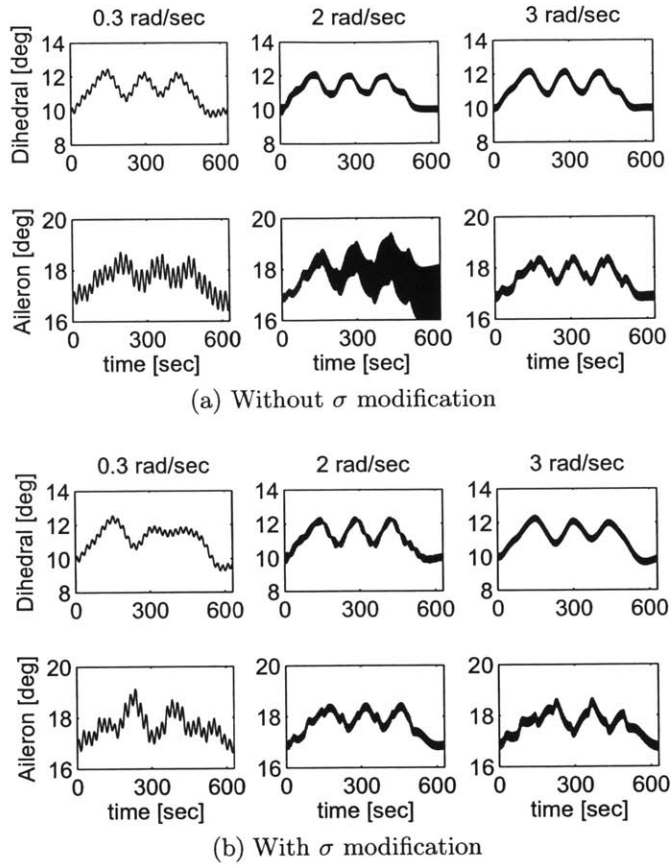


Figure 6-6: The time domain response of η and δ_a when subject to sinusoidal disturbance/noise of magnitude 0.2 and frequencies 0.3, 2, 3 rad/sec for the nonlinear 3-wing VFA model

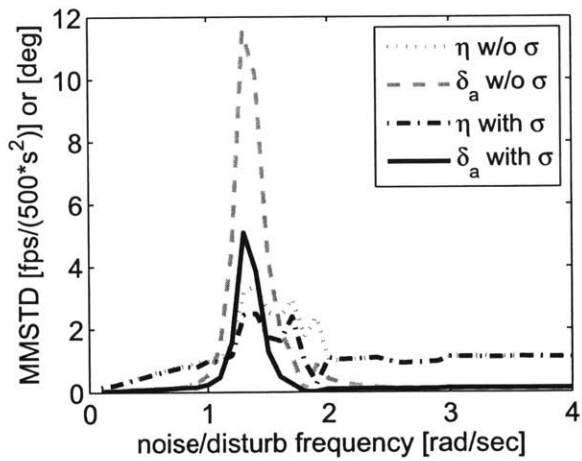


Figure 6-7: The mean of the moving window standard deviation (MMSTD) of η tracking and δ_a control when subject to sinusoidal disturbance/noise of various frequencies for the nonlinear 3-wing VFA model

Chapter 7

Arbitrary Relative Degree Design

This section extends the MIMO design in Section 6.3 to plant models with arbitrary relative degree r . The control problem motivated by VFA includes high order actuator dynamics or sensor dynamics, and is presented in Section 7.1. Key steps of design and Lemma for stability analysis, which are direct extensions of its counterpart in Chapter 6, are presented in Section 7.2.

7.1 Arbitrary Relative Degree Problem Statement

This section focuses on the main problem we want to address in this thesis: a class of MIMO plant model with uniform input relative degree $r \in \mathbb{N}^+$ as motivated by VFA control problem. The class of plant models we want to address is plant models with higher order actuator dynamics or additional sensor dynamics, which has a similar structure of (6.46) and can be written as

$$\begin{aligned}\dot{x} &= \left(A + \sum_{k=1}^r B_k \Psi_k^{*T} \right) x + B_r \Lambda^* u + B_z z_{cmd} \\ y &= Cx\end{aligned}\tag{7.1}$$

where r is its input relative degree. The plant model (7.1) is a generalized version of the MIMO plant (6.47) and (6.4), in which $r = 3$. Linear parametric uncertainties $B_k \Psi_k^{*T} x$ are considered in this section, and the reader is referred to Section 4.1 and 4.2 for the extension to parametric uncertainties with a nonlinear regressor.

The control goal is to design u such that z tracks a trajectory z_m from a reference model despite the presence of uncertainties. The adaptive controller that we will present requires the following assumptions regarding the plant model (7.1):

Assumption 7.1. (A, B_r, C) is a minimal realization;

Assumption 7.2. $\{A, B_r, C\}$ has stable transmission zeros;

Assumption 7.3. $\{A, B_i, C\}$ has uniform relative degree i , for $i = 1, 2, \dots, r$;

Assumption 7.4. $CA^{i-1}B_i$ has full rank, B_i can be spanned by a linear combination of $\{B_r, AB_r, \dots, A^{(r-i)}B_r\}$ for $i = 1, 2, \dots, (r-1)$;

Assumption 7.5. Ψ_i^* satisfies $\Psi_i^{*T} \begin{bmatrix} B_r & AB_r & \dots & A^{r-2}B_r \end{bmatrix} = \begin{bmatrix} 0 & 0 & \dots & 0 \end{bmatrix}$ for $i = 1, 2, \dots, (r-1)$;

Assumption 7.6. $\|\Psi_i^*\|$ are bounded by a known value, respectively, i.e. $\|\Psi_i^*\| < \Psi_{i,\max}^*$ for $i = 1, 2, \dots, r$;

Assumption 7.7. Λ^* is diagonal and $\|\Lambda^*\|$ is bounded by a known value, $\|\Lambda^*\| < \Lambda_{\max}$ and $\text{sign}(\Lambda^*)$ is known.

It can be shown that the relative degree three plant model (6.46) satisfy all these assumptions, with $r = 3$. The reader is directed to Section 6.2 for the justifications of these assumptions.

7.2 Extension of Control Design to Arbitrary Relative Degree

Since the control design for relative degree r plant model is a direct extension of the design in Section 6.3, only key design steps and Lemma for analysis are presented in this section, as well as the final equations for the control and CRM.

The design of L and S in (6.55), as well as u , can be extended while guaranteeing the SPR property of $\{A_{L^*}^*, B_r^{1*}, SC\}$ with

$$B_r^i = \sum_{j=0}^{r-i} a_{r-1}^{r-1-j} A^{\{r-i-j\}} B_r, \quad i = 1, 2, \dots, r. \quad (7.2)$$

The design of F_L and F_{x_m} in CRM, on the other hand, requires two key Lemma, Lemma 6.7 and Lemma 6.8, to be extended to relative degree r . Define $A^* = A + \sum_{k=1}^r B_k \Psi_k^{*T}$. We will first show the difference between B_r^i and

$$B_r^{i*} = \sum_{j=0}^{r-i} a_{r-1}^{r-1-j} A^{*\{r-i-j\}} B_r, \quad i = 1, 2, \dots, r, \quad (7.3)$$

the true input path to a relative degree system $\{A^*, B_r^{i*}, C\}$, in the following Lemma, whose proof is omitted here due to its high similarity of Lemma 6.7.

Lemma 7.1. [Recursive Properties of B_r^i] For plant model $\{A, B_r, C\}$ satisfying Assumptions 6.3 and 6.5, B_r^i as in (7.2) and B_r^{i*} (7.3) satisfy

$$B_r^{i*} - B_r^i = B_r^{[i+1]*} \psi_r^{1*T} + \dots + B_r^{r*} \psi_r^{[r-i]*T} \quad (7.4)$$

for $i = 1, 2, \dots, r$ with uncertain terms ψ_r^{i*} being elements of Ψ_r^* .

Lemma 7.1 is the extension of Lemma 6.7. In (6.71), terms with index $[i+1] > r$ and $[r-i] < 1$ are zeros. Define

$$\pi_{r-1}^i(s) = \sum_{j=0}^i a_{r-1}^{r-1-j} s^{r-1-j}, \quad \underline{\pi}_{r-1}^i(s) = \sum_{j=0}^i a_{r-1}^j s^j \quad (7.5)$$

such that the recursive property (3.2) holds as $\pi_{r-1}^i(s) \cdot s^{r-i-1} + \underline{\pi}_{r-1}^{r-i-1}(s) = \pi_{r-1}^{r-1}(s)$, and

$$F_r^i(x) = B_r^i s^{i-1}[x] + B_r \underline{\pi}_{r-1}^{i-2}[x] \quad (7.6)$$

Then we will show the extension of Lemma 6.8 as follows, whose proof can be found in Appendix F.

Lemma 7.2. [Recursive Adaptation] Suppose an error model

$$\begin{aligned} \dot{e}_x &= A_L^* e_x + B_r^{i*} \phi^{*T} \omega(t) - F(t) \\ e_y &= C e_x \end{aligned} \quad (7.7)$$

for $i = 1, 2, \dots, r$, where $A_L^* = A^* - LC$ with any $L \in \mathbb{R}^{n \times m}$, B_3^{2*} defined in (6.69),

$\{A, B_3, C\}$ satisfies Assumptions 6.3 to 6.5, ϕ^* is unknown constant parameters, $\omega(t)$ is a known regressor with $\dot{\omega}(t)$ inaccessible, and $F(t)$ is free to choose, then $F(t)$ can be chosen as

$$\begin{aligned} F(t) &= F_r^i(\phi^T(t)\bar{\omega}^{[i-1]}(t)) \\ &+ \sum_{j=1}^{r-1-i} [F_r^{i+j}(\psi_r^{jT}(t)\bar{\omega}^{[i-1][i-1+j]}(t)) \\ &+ \sum_{k=1}^{r-i-j} F_r^{i+j+k}(\psi_r^{kT}(t)\bar{\omega}^{[i-1][i-1+j][i-1+j+k]}(t)) + \dots] \end{aligned} \quad (7.8)$$

where the sequence stops when the last index of $\bar{\omega}^l$ reaches $[r-1]$; F_r^i is defined as in (7.6), $\bar{\omega}^{[i]}(t)$ for $i = 0, 1, \dots, (r-1)$ is a filtered version of $\omega(t)$ as

$$\bar{\omega}^{[i]}(t) = \frac{\pi_{r-1}^{r-1-i}(s)}{\pi_{r-1}^{r-1}(s)}\omega(t), \quad (7.9)$$

and $\bar{\omega}^{[i]\dots[j][k]}(t)$ for $(j+1) \leq k \leq (r-1)$ is a filtered version of $\bar{\omega}^{[i]\dots[j]}(t)$ as

$$\bar{\omega}^{[i]\dots[j][k]}(t) = \frac{\pi_{r-1}^{r-1-k}(s)}{\pi_{r-1}^{r-1}(s)} \cdot s^{\{j\}} [\phi^T(t)\bar{\omega}^{[i]\dots[j]}(t)], \quad (7.10)$$

such that the error model can be transformed into

$$\begin{aligned} \dot{e}_x' &= A_L^* e_x' + B_r^{1*} \tilde{\phi}^T(t)\bar{\omega}^{[i-1]}(t) \\ &+ B_r^{1*} \sum_{j=1}^{r-1-i} [\tilde{\psi}_r^{jT}\bar{\omega}^{[i-1][i-1+j]}(t) \\ &+ \sum_{k=1}^{r-i-j} \psi_r^{kT}(t)\bar{\omega}^{[i-1][i-1+j][i-1+j+k]}(t) + \dots] \\ e_y &= Ce_x' \end{aligned} \quad (7.11)$$

where the sequence stops when the last index of $\bar{\omega}^l$ reaches $[r-1]$.

Detail expression of e_x' can be found using Lemma 3.3. Following Lemma 7.2,

$F_L(e_y)$ and $F_{x_m}(e_y)$ are designed as

$$F_L(e_y) = \sum_{i=2}^r \left\{ F_r^i(\psi_r^{[i-1]T} \bar{e}_{\psi_y}^{[i-1]}) + \sum_{j=1}^{r-1-i} \left[F_r^{[i+j]}(\psi_r^{[j]T} \bar{e}_{\psi_y}^{[i-1][i-1+j]}(t)) + \dots \right] \right\} \quad (7.12)$$

$$F_{x_m}(e_y) = \sum_{i=2}^{r-1} \sum_{l=0}^{i-1} \left\{ F_r^i(\Lambda^T \bar{e}_{\Psi_l y_{i-1-l}}^{[i-1]}) + \sum_{j=1}^{r-1-i} \left[F_r^{[i+j]}(\psi_r^{[j]T} \bar{e}_{\Psi_l y_{i-1-l}}^{[i-1][i-1+j]}(t)) + \dots \right] \right\} \quad (7.13)$$

where $\bar{e}_{\psi_y}^{[i]\dots[j]}$ and $\bar{e}_{\Psi_l y_{i-1-l}}^{[i-1][i-1+j]}$ are defined similarly in (6.62) and (7.10), and u_{ad} is designed as

$$\begin{aligned} u_{ad} = & -u_{bl} + \pi_{r-1}^{r-1}(s) \left[\Lambda^T(t) \bar{u}_{bl}^{[3]} - \Psi_3^T(t) \bar{x}_m^{[2]} - \Psi_4^T(t) \bar{x}_m^{[3]} \right] \\ & - \sum_{i=1}^{r-2} \sum_{j=1}^{r-1} a_{r-1}^j \sum_{k=1}^j d_j^k \Psi_i^{(k)T}(t) [v_m^{[j-k]} - \underline{v}_m^{[i-1][j-k]}] \\ & - \sum_{k=1}^{r-2} \sum_{l=1}^{r-1-k} \sum_{i=1}^{r-l} \sum_{j=i-3+l}^i a_{r-1}^i d_i^j \Psi_k^{(j)T}(t) e_{y_l^{l-k}} \end{aligned} \quad (7.14)$$

where

$$v_m^{[i]} = A^i x_m - A^{i-1} L e_y \quad (7.15)$$

$$\underline{v}_m^{[i][j]} = \frac{\pi_3^{i-1}(s)}{\pi_3^3(s)} s^{j-1} \cdot x_m \quad (7.16)$$

$$e_{y_i^j} = s^{\{-i\}} \cdot A^j L e_y(t) \quad (7.17)$$

(terms are zero if index $(i-1)$ is negative) are artificial signals available for control. The rest follows the error model derivations in Section 6.1.2 and Section 6.3.2 where recursive adaptation is used to address uncertainties that lies in the range of B_r^{i*} and generate a SPR error model. Stability analysis is highly similar to Lemma 6.2 and therefore is also omitted here due to space limitations. The reader is also referred to

Section 6.3 for the extension to nonsquare plant models.

Chapter 8

Conclusions

This thesis develops a new adaptive output feedback controller for a class of nonsquare MIMO plant models with parametric uncertainties and arbitrary relative degree. The new design includes a baseline controller based on observers and parameter adaptation based on a closed-loop reference model, and therefore uses significantly less number of integrators compared with classical adaptive approaches. Conditions are delineated under which global stability and asymptotic tracking is guaranteed. The overall design is validated using simulation results on high-fidelity VFA model with high-order actuators.

8.1 Future Work

Although simulation results in all sections show the smoothness of the transient performance, the \mathcal{L}_1 , \mathcal{L}_2 or \mathcal{L}_∞ bound on the tracking error should be derived and should show their dependence on the control parameters or adaptation gains, which could provide the guidance of parameter design.

Although simulation study has been conducted on the robustness of the new adaptive controller over input disturbance and measurement noise, theoretical results should be provided to guarantee the stability of the overall closed-loop system in the presence of these adversities, which are commonly seen in real applications.

Applications to large dimension VFA models with high order actuator dynamics

should also be provided to show the numerical viability of the parameter design. The dependency of the magnitude of L on the locations of added transmission zeros should be further investigated.

Bibliography

- [1] J. Langford, *The Daedalus Project - A Summary of Lessons Learned*, 1989, pp. 10.2514/6.1989–2048.
- [2] R. Gadiant, K. Wise, and E. Lavretsky, “Very Flexible Aircraft Control Challenge Problem,” in *AIAA, Guidance, Navigation, and Control Conferences*, 2012, pp. 10.2514/6.2012–4973.
- [3] C. Shearer and C. Cesnik, “Nonlinear Flight Dynamics of Very Flexible Aircraft,” *AIAA Journal of Aircraft*, vol. 44, pp. 1528–1545, 2005.
- [4] W. Su and C. E. C. S., “Dynamic Response of Highly Flexible Flying Wings,” *AIAA Journal*, vol. 49, no. 2, pp. 324–339, 2011.
- [5] T. Gibson, A. Annaswamy, and E. Lavretsky, “Modeling for Control of Very Flexible Aircraft,” in *AIAA, Guidance, Navigation, and Control Conferences*, 2011.
- [6] T. E. Noll, J. M. Brown, M. E. Perez-Davis, S. D. Ishmael, G. C. Tiffany, and M. Gaier, “Investigation of the Helios Prototype Aircraft Mishap Volume I: Mishap Report,” *NASA*, 2004.
- [7] C. Shearer and C. Cesnik, “Trajectory Control of Very Flexible Aircraft,” *AIAA Guidance, Navigation, and Control Conference and Exhibit*, 2006.
- [8] W. Su, “Coupled nonlinear aeroelasticity and flight dynamics of fully flexible aircraft,” Ph.D, University of Michigan, Ann Arbor, 2008.
- [9] J. Doyle and G. Stein, “Multivariable feedback design: Concepts for a classical/modern synthesis,” *Automatic Control, IEEE Transactions on*, vol. 26, no. 1, pp. 4–16, 1981.
- [10] E. Rynaski, “Flight control synthesis using robust output observers,” in *AIAA, Guidance, Navigation, and Control Conferences*, 1982, pp. 10.2514/6.1982–1575.
- [11] C. Thompson, E. Coleman, and J. Blight, “Integral LQG controller design for a fighter aircraft,” in *AIAA, Guidance, Navigation, and Control Conferences*, 1987, pp. 10.2514/6.1987–2452.

- [12] K. Wise and E. Lavretsky, "Asymptotic Properties of LQG/LTR Controllers in Flight Control Problems," *AIAA Guidance, Navigation, and Control Conference*, pp. 10.2514/6.2012–4889, 2012.
- [13] J. M. Maciejowski, *Multivariable feedback design*. Wokingham, England; Reading, Mass.: Addison-Wesley, 1989.
- [14] K. S. Narendra and A. M. Annaswamy, *Stable adaptive systems*. Dover Publications, 2004.
- [15] G. Tao, *Adaptive control design and analysis*. Hoboken, N.J.: Wiley-Interscience, 2003.
- [16] A. S. Morse, "Parameterizations for multivariable adaptive control," in *Proceedings of the 20th IEEE Conference on Decision and Control including the Symposium on Adaptive Processes*. New York, NY, USA: IEEE, 1981, pp. 970–972.
- [17] R. P. Singh and K. S. Narendra, "Prior information in the design of multivariable adaptive controllers," *IEEE Transactions on Automatic Control*, vol. AC-29, no. 12, p. 1108, 1984.
- [18] E. Lavretsky and K. A. Wise, *Robust and adaptive control: with aerospace applications*. London ; New York: Springer, 2013.
- [19] T. Gibson, A. Annaswamy, and E. Lavretsky, "Improved Transient Response in Adaptive Control Using Projection Algorithms and Closed Loop Reference Models," in *AIAA, Guidance, Navigation, and Control Conferences*, 2012, pp. 10.2514/6.2012–4775.
- [20] T. E. Gibson, A. M. Annaswamy, and E. Lavretsky, "Closed-Loop Reference Models in Adaptive Control: Stability, Robustness and Performance," in *ArXiv: 1201.4897*, 2012.
- [21] T. E. Gibson, A. M. Annaswamy, E., and Lavretsky, "Closed-loop Reference Models for Output-Feedback Adaptive Systems," in *European Control Conference*, 2013, pp. 365–370.
- [22] Z. Qu, E. Lavretsky, and A. M. Annaswamy, "An Adaptive Controller for Very Flexible Aircraft," in *AIAA, Guidance, Navigation, and Control Conferences*, 2013, pp. 10.2514/6.2013–4854.
- [23] T. E. Gibson, Z. Qu, A. M. Annaswamy, and E. Lavretsky, "Adaptive Output Feedback Based on Closed-Loop Reference Models," *IEEE Transactions Automatic Control*, vol. 60, no. 10, pp. 2728 – 2733, 2015.
- [24] D. P. Wiese, A. M. Annaswamy, J. A. Muse, M. A. Bolender, and E. Lavretsky, "Adaptive Output Feedback Based on Closed-Loop Reference Models for Hypersonic Vehicles," in *AIAA Guidance, Navigation, and Control Conference (To Appear)*, 2015, pp. 10.2514/6.2015–1755.

- [25] Z. Qu and A. M. Annaswamy, “Adaptive Output-Feedback Control with Closed-Loop Reference Models for Very Flexible Aircraft,” *AIAA, Journal of Guidance, Control, and Dynamics*, 2015.
- [26] H. Weiss, Q. Wang, and J. L. Speyer, “System characterization of positive real conditions,” *IEEE Transactions on Automatic Control*, vol. 39, no. 3, pp. 540–544, 1994.
- [27] P. Misra, “A computational algorithm for squaring-up. I. Zero input-output matrix,” in *Proceedings of 1992 31st IEEE Conference on Decision and Control*. New York, NY, USA: IEEE, 1992, pp. 149–150.
- [28] ——, “Numerical algorithms for squaring-up non-square systems part II: general case,” in *Proceedings of the 1993 American Control Conference Part 3 (of 3)*, June 2, 1993 - June 4, 1993, pp. 1573–1577.
- [29] B. Kouvaritakis and A. G. J. MacFarlane, “Geometric approach to analysis and synthesis of system zeros. I. Square systems,” *International Journal of Control*, vol. 23, no. 2, pp. 149–156, 1976.
- [30] M. Mueller, “Output feedback control and robustness in the gap metric,” Ph.D Dissertation, Universitätsverlag Ilmenau, 2009.
- [31] Z. T. Dydek, A. M. Annaswamy, and E. Lavretsky, “Adaptive Control of Quadrotor UAVs: A design Trade Study with Flight Evaluations,” *IEEE Transactions on Control Systems Technology*, vol. 21, no. 4, 2013.
- [32] W. J. Rugh and J. S. Shamma, “Research on gain scheduling,” *Automatica*, vol. 36, no. 10, pp. 1401–1425, 2000.
- [33] A. G. J. MacFarlane and N. Karcanias, “Poles and zeros of linear multivariable systems : a survey of the algebraic, geometric and complex-variable theory,” *International Journal of Control*, vol. 24, no. 1, pp. 33–74, 1976.
- [34] B. Kouvaritakis and A. G. J. MacFarlane, “Geometric approach to analysis and synthesis of system zeros. II. Non-square systems,” *International Journal of Control*, vol. 23, no. 2, pp. 167–181, 1976.
- [35] M. Mueller, “Normal form for linear systems with respect to its vector relative degree,” *Linear Algebra and Its Applications*, vol. 430, no. 4, pp. 1292–1312, 2009.
- [36] C. H. Huang, P. A. Ioannou, J. Maroulas, and M. G. Safonov, “Design of strictly positive real systems using constant output feedback,” *Automatic Control, IEEE Transactions on*, vol. 44, no. 3, pp. 569–573, 1999.
- [37] K. S. Narendra and J. H. Taylor, *Frequency domain criteria for absolute stability*. New York: Academic Press, 1973.

- [38] J. T. Wen, "Time domain and frequency domain conditions for strict positive realness," *Automatic Control, IEEE Transactions on*, vol. 33, no. 10, pp. 988–992, 1988.
- [39] T. E. Gibson, A. M. Annaswamy, and E. Lavretsky, "On Adaptive Control With Closed-Loop Reference Models: Transients, Oscillations, and Peaking," *Access, IEEE*, vol. 1, pp. 703–717, 2013.
- [40] J.-t. Yu, M.-L. Chiang, and L.-C. Fu, "Synthesis of static output feedback SPR systems via LQR weighting matrix design," in *Decision and Control (CDC), 2010 49th IEEE Conference on*, 2010, pp. 4990–4995.
- [41] Z. Qu, D. Wiese, E. Lavretsky, and A. M. Annaswamy, "Squaring-Up Method In the Presence of Transmission Zeros," in *19th World Congress, The International Federation of Automatic Control*, 2014, pp. 4164–4169.
- [42] W. Durham, *Aircraft Dynamics and Control*. New York, NY, USA: Wiley, 2013.
- [43] L. Vandenberghe and S. Boyd, "Semidefinite programming," *SIAM Review*, vol. 38, no. 1, pp. 49–95, 1996.
- [44] P. A. Parrilo, "Structured semidefinite programs and semialgebraic geometry methods in robustness and optimization," 2000. [Online]. Available: <http://www.cds.caltech.edu/{~}pablo/>.
- [45] J. Lofberg, "YALMIP : a toolbox for modeling and optimization in MATLAB," in *Computer Aided Control Systems Design, 2004 IEEE International Symposium on*, 2004, pp. 284–289.
- [46] B. Moore, "Principal component analysis in linear systems: Controllability, observability, and model reduction," *IEEE Trans. Automat. Contr. IEEE Transactions on Automatic Control*, vol. 26, no. 1, pp. 17–32, 1981.
- [47] K. J. Astrom and R. M. Murray, *Feedback systems : an introduction for scientists and engineers*. Princeton: Princeton University Press, 2008.
- [48] E. Lavretsky and T. E. Gibson, "Projection Operator in Adaptive Systems," *arXiv:1112.4232*.
- [49] H. S. Hussain, M. Matsutani, A. M. Annaswamy, and E. Lavretsky, "Robust Adaptive Control in the Presence of Unmodeled Dynamics: A Counter to Rohrs's Counterexample," in *AIAA Guidance, Navigation, and Control (GNC) Conference*, 2013. [Online]. Available: <http://dx.doi.org/10.2514/6.2013-4753>
- [50] Z. Qu, A. M. Annaswamy, and E. Lavretsky, "Adaptive Output-Feedback Control for Relative Degree Two Systems Based on Closed-Loop Reference Models," in *IEEE 54th Conference on Decision and Control*, Osaka, Japan, 2015.

- [51] S. Evesque, A. M. Annaswamy, S. Niculescu, and A. P. Dowling, "Adaptive Control of a Class of Time-Delay Systems," *Journal of Dynamic Systems, Measurement, and Control*, vol. 125, no. 2, pp. 186–193, jun 2003. [Online]. Available: <http://dx.doi.org/10.1115/1.1567755>
- [52] Z. Qu, A. M. Annaswamy, and E. Lavretsky, "Adaptive Output-Feedback Control for A Class of Multi-Input-Multi-Output Plants with Applications to Very Flexible Aircraft," in *IEEE, 2016 American Control Conference (to appear)*, 2016.
- [53] N. Truhar, "The perturbation bound for the solution of the Lyapunov equation," *Mathematical Communications*, vol. 12, pp. 83–94, 2007.

Appendix A

Proof for Results in Chapter 2

Proof of Lemma 2.1

Proof: Define $(\cdot)_{/\cdot|_0} = \frac{\partial(\cdot)}{\partial[\cdot]}|_{\cdot|_0}$ as partial differential variables. Linearizing (2.5) around a trim point $[\ddot{\epsilon}_0, \dot{\epsilon}_0, \epsilon_0, \dot{\beta}_0, \beta_0, \lambda_0, u_0]^T$ yields

$$\begin{aligned}
 & \left(\underbrace{\begin{bmatrix} I & 0 & 0 \\ 0 & (M_{FF})_{\epsilon_0} & (M_{FB})_{\epsilon_0} \\ 0 & (M_{BF})_{\epsilon_0} & (M_{BB})_{\epsilon_0} \end{bmatrix}}_{\bar{Q}_1(0,0,\epsilon_0,0,\beta_0)} + \underbrace{\begin{bmatrix} 0 & 0 & 0 \\ 0 & \Delta M_{FF} & \Delta M_{FB} \\ 0 & \Delta M_{BF} & \Delta M_{BB} \end{bmatrix}}_{\Delta Q_1^*(\ddot{\epsilon}_0, \dot{\epsilon}_0, \dot{\beta}_0)} \right) \begin{bmatrix} \dot{\epsilon} \\ \ddot{\epsilon} \\ \dot{\beta} \end{bmatrix} \\
 &= \underbrace{\begin{bmatrix} 0 & I & 0 \\ -(K_{FF})_{\epsilon_0} + (J_{he}^T)_{\epsilon_0} F_{/\epsilon_0}^{load} & -C_e & (J_{he}^T)_{\epsilon_0} F_{/\beta_0}^{load} \\ 0 & 0 & -C_{RB} + (J_{hb}^T)_{\epsilon_0} F_{/\beta_0}^{load} \end{bmatrix}}_{\bar{Q}_2(0,0,\epsilon_0,0,\beta_0)} \\
 &+ \underbrace{\begin{bmatrix} 0 & 0 & 0 \\ \Delta K_{FF} & \Delta C_{FF} & \Delta C_{FB} \\ \Delta K_{BF} & \Delta C_{BF} & \Delta C_{BB} \end{bmatrix}}_{\Delta Q_2^*(\ddot{\epsilon}_0, \dot{\epsilon}_0, \dot{\beta}_0)} \begin{bmatrix} \epsilon \\ \dot{\epsilon} \\ \beta \end{bmatrix} + \underbrace{\begin{bmatrix} 0 \\ B_{F/u_0} \\ B_{B/u_0} \end{bmatrix}}_{Q_3} u_p \quad (\text{A.1})
 \end{aligned}$$

where, following the definition of terms in (2.6), the unknown deviation terms are

$$\begin{aligned}
\Delta M_{FF} &= -(J_{h\epsilon}^T)_{\epsilon_0} F_{/\ddot{\epsilon}_0}^{load} & \Delta M_{FB} &= -(J_{h\epsilon}^T)_{\epsilon_0} F_{/\dot{\beta}_0}^{load} \\
\Delta M_{BF} &= -(J_{hb}^T)_{\epsilon_0} F_{/\ddot{\epsilon}_0}^{load} & \Delta M_{BB} &= -(J_{hb}^T)_{\epsilon_0} F_{/\dot{\beta}_0}^{load} \\
\Delta B_{F/\lambda_0} &= (J_{h\epsilon}^T)_{\epsilon_0} F_{/\lambda_0}^{load} & \Delta B_{B/\lambda_0} &= (J_{hb}^T)_{\epsilon_0} F_{/\lambda_0}^{load} \\
\Delta K_{FF} &= M_{FF/\epsilon_0} \ddot{\epsilon}_0 + M_{FB/\epsilon_0} \dot{\beta}_0 \\
\Delta K_{BF} &= M_{BF/\epsilon_0} \ddot{\epsilon}_0 + M_{BB/\epsilon_0} \dot{\beta}_0 \\
\Delta C_{FF} &= -(C_{FF})_{x_0} - C_{FF/\dot{\epsilon}_0} \dot{\epsilon}_0 - C_{FB/\dot{\epsilon}_0} \beta_0 + (J_{h\epsilon}^T)_{\epsilon_0} F_{/\dot{\epsilon}_0}^{load} \\
\Delta C_{BF} &= -(C_{BF})_{x_0} - C_{BF/\dot{\epsilon}_0} \dot{\epsilon}_0 - C_{BB/\dot{\epsilon}_0} \beta_0 + (J_{hb}^T)_{\epsilon_0} F_{/\dot{\epsilon}_0}^{load} \\
\Delta C_{FB} &= -(C_{FB})_{x_0} - C_{FF/\beta_0} \dot{\epsilon}_0 - C_{FB/\beta_0} \beta_0 \\
\Delta C_{BB} &= -(C_{BB})_{x_0} - C_{BF/\beta_0} \dot{\epsilon}_0 - C_{BB/\beta_0} \beta_0
\end{aligned} \tag{A.2}$$

$B_{F/u_0} = (J_{h\epsilon}^T)_{\epsilon_0} F_{/u_0}^{load}$ and $B_{B/u_0} = (J_{hb}^T)_{\epsilon_0} F_{/u_0}^{load}$, which also have $J_{(\cdot)}$ as their leading factors as Assumption 2.2 holds. Without loss of generality, we scale each input so that $F_{/u_0}^{load} = I$. In realistic application, only $[\epsilon_0, \beta_0, u_0]^T$ can be measured accurately and therefore variables that depend on them can be well calculated. $[\dot{\epsilon}_0, \ddot{\epsilon}_0, \dot{\beta}_0, \lambda_0]^T$ cannot be measured accurately and therefore variables that depends on them are generally unknown. As a result, \bar{Q}_1 , \bar{Q}_2 and Q_3 are known but ΔQ_1^* and ΔQ_2^* are unknown. Examination on (A.2) using (2.6) shows that

$$\Delta Q_1^* = \left[\begin{array}{c} 0 \\ J_{h\epsilon}^T \\ J_{hb}^T \\ 0 \end{array} \right]_{\epsilon_0} \underbrace{\left[\begin{array}{cccc} 0 & F_{/\ddot{\epsilon}_0}^{load} & F_{/\dot{\beta}_0}^{load} & 0 \end{array} \right]}_{\Theta_{q1}^{*T}} = Q_3 \Theta_{q1}^{*T} \tag{A.3}$$

and

$$\begin{aligned}\Delta Q_2^* &= \begin{bmatrix} 0 \\ J_{h\epsilon}^T \\ J_{hb}^T \end{bmatrix}_{\epsilon_0} \underbrace{\begin{bmatrix} M_e \left(\frac{\partial J_{h\epsilon}}{\partial \epsilon} \ddot{\epsilon} + \frac{\partial J_{hb}}{\partial \epsilon} \beta \right) & M_e \left(\dot{J}_{h\epsilon} + \frac{\partial J_{h\epsilon}}{\partial \epsilon} \dot{\epsilon} + \frac{\partial J_{hb}}{\partial \epsilon} \beta \right) \\ M_e \left(\dot{J}_{hb} + \frac{\partial J_{h\epsilon}}{\partial \beta} \dot{\epsilon} + \frac{\partial J_{hb}}{\partial \beta} \beta \right) \end{bmatrix}_{x_0}}_{\Theta_{q_2}^{*T}} \\ &= Q_3 \Theta_{q_2}^{*T}\end{aligned}\quad (\text{A.4})$$

which is used to rewritten (A.1) as

$$(\bar{Q}_1 + Q_3 \Theta_{q_1}^{*T}) \dot{x}_p = (\bar{Q}_2 + Q_3 \Theta_{q_2}^{*T}) x_p + Q_3 u_p. \quad (\text{A.5})$$

Assume that \bar{Q}_1 , $(\bar{Q}_1 + Q_3 \Theta_{q_1}^{*T})$ and $(I + \Theta_{q_2}^{*T} \bar{Q}_1^{-1} Q_3)$ are invertible around the equilibrium. Taking inverse on both sides, and noting

$$(\bar{Q}_1 + Q_3 \Theta_{q_1}^{*T})^{-1} = \bar{Q}_1^{-1} - \bar{Q}_1^{-1} Q_3 \underbrace{(I + \Theta_{q_1}^{*T} \bar{Q}_1^{-1} Q_3)^{-1} \Theta_{q_1}^{*T} \bar{Q}_1^{-1}}_{\bar{\Theta}_{q_1}^{*T}} \quad (\text{A.6})$$

yields

$$\begin{aligned}\dot{x}_p &= \left(\bar{Q}_1^{-1} - \bar{Q}_1^{-1} Q_3 \bar{\Theta}_{q_1}^{*T} \bar{Q}_1^{-1} \right) (\bar{Q}_2 + Q_3 \Theta_{q_2}^{*T}) x_p \\ &\quad + \left(\bar{Q}_1^{-1} - \bar{Q}_1^{-1} Q_3 \bar{\Theta}_{q_1}^{*T} \bar{Q}_1^{-1} \right) Q_3 u_p\end{aligned}\quad (\text{A.7})$$

$$\begin{aligned}&= \left[\bar{Q}_1^{-1} \bar{Q}_2 + \bar{Q}_1^{-1} Q_3 \left(\Theta_{q_2}^{*T} - \bar{\Theta}_{q_1}^{*T} \bar{Q}_1^{-1} \bar{Q}_2 - \bar{\Theta}_{q_1}^{*T} \bar{Q}_1^{-1} Q_3 \Theta_{q_2}^{*T} \right) \right] x_p \\ &\quad + \bar{Q}_1^{-1} Q_3 \left(I - \bar{\Theta}_{q_1}^{*T} \bar{Q}_1^{-1} Q_3 \right) u_p\end{aligned}\quad (\text{A.8})$$

$$= \left[A_p + B_p \underbrace{\left(\Theta_{q_2}^{*T} - \bar{\Theta}_{q_1}^{*T} A_p - \bar{\Theta}_{q_1}^{*T} B_p \Theta_{q_2}^{*T} \right)}_{\Theta_p^{*T}} \right] x_p + B_p \underbrace{\left(I - \bar{\Theta}_{q_1}^{*T} B_p \right)}_{\Lambda_p^*} u_p \quad (\text{A.9})$$

with $A_p = \bar{Q}_1^{-1} \bar{Q}_2$, $B_p = \bar{Q}_1^{-1} Q_3$. C_p as in $y_p = C_p x_p$ is the selection matrix that picks out measurable states from x_p . ■

Appendix B

Proof for Results in Chapter 3

Proof of Lemma 3.3

Proof: It is noted from the definition of B_r^i in (3.17) that $B_r^r = Ba_{r-1}^{r-1}$ and

$$B_r^i = AB_r^{i+1} + B_ra_{r-1}^{i-1}. \quad (\text{B.1})$$

Then substituting (3.18) and applying Eq.(B.1) converts the system (3.15) to (3.16). The reverse is also true. Since $\{A, B, C\}$ has uniform relative degree r , $CA^jB = 0$ for $j = 0, 1, \dots, r-2$ and therefore $CB_r^j = 0$ for $j = i-1, i, \dots, r$, which leads to $y = Cx = Cx'$. ■

Proof of Proposition 3.1

Proof: The proof follows Definition 3.4. It is noted that the second column of

$$R(s) = \begin{bmatrix} zI - A & \left(\sum_{j=0}^{r-i} A^{r-i-j} Ba_{r-1}^{r-1-j}\right) \\ C & 0 \end{bmatrix} \quad (\text{B.2})$$

can be replaced by multiplying the first column with $\sum_{j=0}^{r-i} A^{r-1-j-1} B a_{r-1}^{r-1-j}$ and using the fact that $C A^{r-1-j-1} B = 0$, i.e.

$$\begin{aligned} \text{rank} \left[\begin{array}{cc} zI - A & \left(\sum_{j=0}^{r-i} A^{r-i-j} B a_{r-1}^{r-1-j} \right) \\ C & 0 \end{array} \right] = \\ \text{rank} \left[\begin{array}{cc} zI - A & \left(\sum_{j=0}^{r-i} A^{r-i-j-1} B a_{r-1}^{r-1-j} z \right) \\ C & 0 \end{array} \right] \end{aligned} \quad (\text{B.3})$$

Keep repeating this process yields

$$\begin{aligned} \text{rank} \left[\begin{array}{cc} zI - A & \left(\sum_{j=0}^{r-i} A^{r-i-j-1} B a_{r-1}^{r-1-j} z \right) \\ C & 0 \end{array} \right] = \\ \text{rank} \left[\begin{array}{cc} zI - A & \left(\sum_{j=0}^{r-i} A^{r-i-j-1} B a_{r-1}^{r-1-j} z \right) + B a_{r-1}^{i-1} z \\ C & 0 \end{array} \right] = \\ \text{rank} \left[\begin{array}{cc} zI - A & \left(\sum_{j=0}^{r-i} B a_{r-1}^{r-1-j} z^{r-i-j} \right) \\ C & 0 \end{array} \right] \end{aligned} \quad (\text{B.4})$$

then the results follows. ■

Proof of Corollary 3.3

Proof: We will prove the SPR properties using Lemma 3.6. Since $\{A, B, C\}$ is SPR, by Lemma 3.4 there exists a $P = P^T > 0$ and a $Q = Q^T > 0$ such that

$$PA + A^T P = -Q < 0 \quad (\text{B.5})$$

$$PB = C^T \quad (\text{B.6})$$

Taking $K = \sqrt{2aCB}$ satisfies

$$K^T K = aCB + a(CB)^T = 2aCB \quad (\text{B.7})$$

since $CB = (CB)^T > 0$. Then taking $W^T = aPAB(CB)^{-\frac{1}{2}}$ satisfies

$$PB_a^0 = aPAB + PB = aPAB(2aCB)^{-\frac{1}{2}}(2aCB)^{\frac{1}{2}} + PB = W^T K + C^T \quad (\text{B.8})$$

Then taking

$$\alpha^* < \frac{2 \|Q\|}{\lambda_{min}^{-1}(CB) \|PAB\|^2} \quad (\text{B.9})$$

yields that $\forall a < \alpha^*$,

$$PA + A^T P = -Q < -\frac{a}{2} PAB(2aCB)^{-1} B^T A^T P = -W^T W \quad (\text{B.10})$$

Then the results follows. ■

Appendix C

Proof for Results in Chapter 4

Proof of Lemma 4.1

Proof: The goal is to show $e_x(t) \rightarrow 0$ as $t \rightarrow \infty$. Since we have designed an SPR pair of L and S_1 such that $\{(A - LC), B, S_1C\}$ is SPR, there exists a $P = P^T > 0$ such that Eq.(4.13) and Eq.(4.14) hold for a $Q > 0$. We propose a Lyapunov function candidate using the P as

$$V = e_x^T P e_x + Tr(\tilde{\Lambda}^T \Gamma_{\lambda}^{-1} \tilde{\Lambda} |\Lambda^*|) + Tr(\tilde{\Theta}^T \Gamma_{\theta}^{-1} \tilde{\Theta} |\Lambda^*|) > 0 \quad (\text{C.1})$$

where Tr stands for the trace of a matrix. Using Eq.(4.10), V has a derivative as

$$\begin{aligned} \dot{V} &= e_x^T ((A - L_\rho C)^T P + P(A - L_\rho C)) e_x + 2e_x^T P B \Lambda^* \Theta^{*T} [\Phi(x_p) - \Phi(x_{mp})] \\ &\quad + 2e_x^T P B \Lambda^* \tilde{\Lambda}^T u_{bl} - 2e_x^T P B \Lambda^* \tilde{\Theta}^T \Phi(x_{mp}) + 2Tr(\tilde{\Lambda}^T \Gamma_{\lambda}^{-1} \dot{\tilde{\Lambda}} |\Lambda|) + 2Tr(\tilde{\Theta}^T \Gamma_{\theta}^{-1} \dot{\tilde{\Theta}} |\Lambda|) \end{aligned} \quad (\text{C.2})$$

$$\begin{aligned} &= e_x^T ((A - L_\rho C)^T P + P(A - L_\rho C)) e_x + 2e_x^T P B \Lambda^* \Theta^{*T} [\Phi(x_p) - \Phi(x_{mp})] \\ &\quad + 2e_x^T [PB - C^T S_1^T] \Lambda^* \tilde{\Lambda}^T u_{bl} - 2e_x^T [PB - C^T S_1^T] \Lambda^* \tilde{\Theta}^T \Phi(x_{mp}). \end{aligned} \quad (\text{C.3})$$

To achieve (C.3), we used the property of trace and adaptation law (4.11). By far, the derivation is general for $\Theta^* \neq 0$. For the special case $\Theta^* = 0$, we choose $\Theta(t) \equiv 0$, then $\tilde{\Theta}(t) \equiv 0$. Also, $L = L_\rho$. As a result, the error model (4.10) has a form of (4.12).

Then the derivative of Lyapunov function (C.3) becomes

$$\dot{V} = e_x^T((A - LC)^T P + P(A - LC))e_x + 2e_x^T[PB - C^T S_1^T]\Lambda^* \tilde{\Lambda}^T u_{bl}. \quad (\text{C.4})$$

Using Eq.(4.13) and Eq.(4.14) turns (C.4) into

$$\dot{V} = -e_x^T Q e_x \leq 0. \quad (\text{C.5})$$

As a result, e_x , $\tilde{\Lambda}$ and $\tilde{\Theta}$ are bounded. Moreover, \ddot{V} exists and is bounded and Barbalat's Lemma implies $e_x(t) \rightarrow 0$ as $t \rightarrow \infty$, which proves ii). Consequently, the $L_\rho(y - y_m)$ term in (4.8) approaches to zero as $t \rightarrow \infty$ and the observer/CRM (4.8) approaches to a open loop reference model (as it becomes standalone without feedback of y). It follows that when $t \rightarrow \infty$ reference states x_m are bounded (by the design of K). This in turn implies x is bounded. It then can be concluded that all signals in the system are bounded, which proves i). ■

Proof of Lemma 4.2

Proof: We will prove by construction. Definition 3.4 states that the transmission zeros depend on $R(s)$, the Rosenbrock matrix. $R(s)$ of the given plant model $\{A, B, C\}$ can be written in the observer canonical form $\tilde{R}(s)$ as

$$R(s) \xrightarrow{T} \tilde{R}(s) = \left[\begin{array}{cc|c} sI_p - A_{11} & -A_{12} & B_{11} \\ -A_{21} & sI_{n-p} - A_{22} & B_{21} \\ \hline I_p & 0 & 0 \end{array} \right] \quad (\text{C.6})$$

where $T^{-1} = [C^{-R} \ C^\perp]$ is an invertible coordinate transformation matrix satisfying $CC^{-R} = I_p$ and $CC^\perp = 0_{p \times (n-p)}$. Since transmission zeros are invariant under coordinate transformation, $Z[R(s)]$ coincide $Z[\tilde{R}(s)]$. The goal then is to design $\hat{B}_{12} \in \mathbb{R}^{p \times (p-m)}$, $\hat{B}_{22} \in \mathbb{R}^{(n-p) \times (p-m)}$ and $\hat{D}_2 \in \mathbb{R}^{p \times (p-m)}$ such that the squared-up

plant model $\hat{R}(s)$ as

$$\bar{R}(s) = \left[\begin{array}{cc|cc} sI_p - A_{11} & -A_{12} & B_{11} & \hat{B}_{12} \\ -A_{21} & sI_{n-p} - A_{22} & B_{21} & \hat{B}_{22} \\ \hline I_p & 0 & 0 & \hat{D}_2 \end{array} \right] \quad (\text{C.7})$$

satisfies two conditions: *i*) $\bar{R}(s)$ only loses rank at a set of finite s that lie in the open left half of the complex plane, and *ii*) Eq.s(3.6) and (3.7) holds for some $\bar{\tau} = [r_1, r_2, \dots, r_m, \dots, r_p]^T$. The use of \hat{D}_2 depends on the choice of $\bar{\tau}$, which will be discussed separately in the following discussion. Define $Z[\cdot]$ as the set of transmission zeros.

Case I: this case introduces new inputs with relative degree zero, which requires $\hat{D}_2 \neq 0$. This case does not solve the problem in Lemma 4.2, and therefore only introduced here as a reference for the use in higher relative degree cases. Since B has rank m , with some permutations we can put all independent rows of B in B_{11} and perform row elimination on (C.7) as

$$\bar{R}_1(s) = \left[\begin{array}{cc|cc} sI_m - A_{11} & -A_{12} & B_{11} & \hat{B}_{12} \\ \times & sI_{n-m} - \tilde{A}_{22} & 0 & \tilde{B}_{22} \\ \hline I_m & 0 & 0 & 0 \\ 0 & C_{22} & 0 & \hat{D}_{22} \end{array} \right] \quad (\text{C.8})$$

where $\hat{D}_2 = \begin{bmatrix} \hat{D}_{21} \\ \hat{D}_{22} \end{bmatrix}$, $\hat{D}_{21} = 0$, and $\begin{bmatrix} I_p & 0 \end{bmatrix} = \begin{bmatrix} I_m & 0 \\ 0 & C_{22} \end{bmatrix}$ where $C_{22} = \begin{bmatrix} I_{p-m} & 0 \end{bmatrix}$; $\tilde{A}_{22} = A_{22} - B_{21}B_{11}^{-1}A_{12}$ and $\tilde{B}_{22} = \hat{B}_{22} - B_{21}B_{11}^{-1}$. It is noted that this mode only requires $\text{rank}[C] = m < p$. It follows that $Z[\bar{R}(s)] = Z[\bar{R}_1(s)] = Z[\bar{R}_1^s(s)]$ where

$$\bar{R}_1^s(s) = \left[\begin{array}{c|c} sI_{n-p} - \tilde{A}_{22} & \tilde{B}_{22} \\ \hline C_{22} & \hat{D}_{22} \end{array} \right]. \quad (\text{C.9})$$

is a submatrix of $\bar{R}_1(s)$. With an invertible \hat{D}_{22} , the transmission zeros of $\bar{R}_1^s(s)$ is the eigenvalues of $\tilde{A}_{22} - \tilde{B}_{22}\hat{D}_{22}^{-1}C_{22}$. It can be shown that (\tilde{A}_{22}, C_{22}) must be a

detectable pair and its unobservable mode is the pre-existing transmission zeros of $R(s)$ (following Ref. [41]). The complete procedure of squaring-up for Case I is as follows:

$$\text{pick any } \hat{B}_{12} \in \mathbb{R}^{p \times (p-m)} \quad (\text{C.10})$$

$$\text{pick } \hat{D}_{22} \text{ s.t. } \text{rank} \begin{bmatrix} B_{11} & \begin{bmatrix} 0 \\ \hat{D}_{22} \end{bmatrix} \end{bmatrix} = p \quad (\text{C.11})$$

$$\tilde{A}_{22} = A_{22} - B_{21}B_{11}^{-1}A_{12} \quad (\text{C.12})$$

$$W^T = \text{lqr}(\tilde{A}_{22}^T, C_{22}^T) \quad (\text{C.13})$$

$$\tilde{B}_{22} = W\hat{D}_{22} \quad (\text{C.14})$$

$$\hat{B}_{22} = \tilde{B}_{22} + B_{21}B_{11}^{-1} \quad (\text{C.15})$$

It is noted that (C.12)-(C.15) are used to satisfy Condition *i*), while (C.11) guarantees Condition *ii*) with $r = [1, 1, 1, \dots, 0, 0, 0]$, where r includes $m+r$ relative degree one.

Case II: this case introduces new inputs with relative degree one, which requires $\hat{D}_2 = 0$ and then is used prove Lemma 4.2. The dual form of this case has been solved in the Ref. [27, 41] and is adopted here by performing a transpose. With $\hat{D}_2 = 0$ and some row elimination, $Z[\bar{R}(s)] = Z[\bar{R}_1(s)]$ where

$$\hat{R}_1(s) = \left[\begin{array}{cc|cc} sI_p - A_{11} & -A_{12} & B_{11} & \hat{B}_{12} \\ \times & sI_{n-p} - \tilde{A}_{22} & 0 & 0 \\ \hline I_p & 0 & 0 & 0 \end{array} \right] \quad (\text{C.16})$$

and $\tilde{A}_{22} = A_{22} - B_2B_1^{-1}A_{12}$, $B_2 = [B_{21} \ \hat{B}_{22}]$, and $B_1 = [B_{11} \ \hat{B}_{12}]$. B_1 is invertible since $\hat{B}_{12} = (\text{null}(B_{11}))^T$ where $\text{null}(\cdot)$ stands for the null space of (\cdot) . Then it is clear that $Z[\bar{R}_1(s)]$ are the eigenvalues of \tilde{A}_{22} . As a result, the complete

procedure for Mode 1 is as follows:

$$\hat{B}_{12} = (\text{null}(B_{11}))^T \text{ s.t. } B_1 = \begin{bmatrix} B_{11} & \hat{B}_{12} \end{bmatrix} \text{ is invertible} \quad (\text{C.17})$$

$$\tilde{A}_{22}^* = A_{22} - \begin{bmatrix} B_{21} & 0 \end{bmatrix} B_1^{-1} A_{12} \quad (\text{C.18})$$

$$\begin{bmatrix} \times \\ E^* \end{bmatrix} = B_1^{-1} A_{12}, \quad E^* \in \mathbb{R}^{(p-m) \times (n-p)} \quad (\text{C.19})$$

$$\hat{B}_{22}^T = \text{lqr}(\tilde{A}_{22}^{*T}, E^{*T}) \quad (\text{C.20})$$

It is noted that (\tilde{A}_{22}^*, E^*) must be a detectable pair and its unobservable mode is the pre-existing transmission zeros of $R(s)$ (see [41] for a proof). (C.17) guarantees that Condition *i*) is satisfied with $\tau = 1$, and (C.18)-(C.20) guarantees that Condition *ii*) is satisfied. Let $\hat{B}_{s1} = \begin{bmatrix} \hat{B}_{12} \\ \hat{B}_{22} \end{bmatrix}$ and transform \hat{B}_{s1} to the original coordinate, which yield B_{s1} . ■

Proof of Lemma 4.3

Proof: The proof follows the idea in Ref. [40], but uses a different approach. First, we will show that $\{(\bar{A} - LC), B, S_1 C\}$ is SPR, where $\bar{A} = A + \mu^* I$. We note that $\{\bar{A}, \bar{B}, \bar{C}\}$ has stable transmission zeros. A weight R^{-1} is chosen in (4.21) and a weight \bar{Q} (different from Ref. [40]) is chosen as

$$\bar{Q} = -N^T H(\bar{C}\bar{B})^{-1}\bar{C} - \bar{C}^T(\bar{C}\bar{B})^{-1}H^TN + \varepsilon\bar{C}^T\bar{C} + N^TQ_I N \quad (\text{C.21})$$

where H is defined in (4.23) and ε is chosen in (4.22). N is the null space of \bar{B} and M is the null space of \bar{C} satisfying and $NM = I$. We will show that the finite constant ε chosen in inequality (4.22) guarantees $R^{-1} > 0$ and $\bar{Q} > 0$. $R^{-1} > 0$ because $\varepsilon > \varepsilon_1$ where ε_1 is defined in (4.22). To show $\bar{Q} > 0$, it is equivalent to show that $T_{\bar{B}}^T \bar{Q} T_{\bar{B}} > 0$, where

$$T_{\bar{B}} = [M, \bar{B}] \quad (\text{C.22})$$

is an invertible matrix. Examination on $T_{\bar{B}}^T Q T_{\bar{B}}$ yields

$$T_{\bar{B}}^T \bar{Q} T_{\bar{B}} = \begin{bmatrix} M^T \bar{Q} M & M^T \bar{Q} \bar{B} \\ \bar{B}^T \bar{Q} M & \bar{B}^T \bar{Q} \bar{B} \end{bmatrix} = \begin{bmatrix} I & -H \\ -H^T & \epsilon(\bar{C}\bar{B}) \bar{C}\bar{B} \end{bmatrix} > 0. \quad (\text{C.23})$$

The inequality is guaranteed to hold using Schur complement and the fact that $\varepsilon > \varepsilon_2$, where ε_2 is defined in (4.22), and therefore $\bar{Q} > 0$ is guaranteed.

Propose a P as

$$P = \bar{C}^T (\bar{C}\bar{B})^{-1} \bar{C} + N^T P_I N \quad (\text{C.24})$$

where $P_I > 0$ is the unique solution to Eq.(4.24) and therefore $P > 0$. We will show because of the L design in (4.20) and S_1 design in (4.16), the P as in (C.24) satisfies

$$(\bar{A} - LC)^T P + P(\bar{A} - LC) = -\bar{Q} - \bar{C}R^{-1}\bar{C} < 0 \quad (\text{C.25})$$

and Eq.(4.14) simultaneously. First, let's show Eq.(C.25) holds. Using L as in (4.28) and the fact $P\bar{B} = \bar{C}^T$, Eq.(C.25) can be rewritten as

$$\{\emptyset\} := (\bar{A} - \bar{B}R^{-1}\bar{C})^T P + P(\bar{A} - \bar{B}R^{-1}\bar{C}) + \bar{C}^T R^{-1}\bar{C} + \bar{Q}. \quad (\text{C.26})$$

To show $\{\emptyset\} = 0$, it is equivalent to show $T_{\bar{B}}^T \{\emptyset\} T_{\bar{B}} = 0$. Examination on the block elements of $T_{\bar{B}}^T \{\emptyset\} T_{\bar{B}}$ reveals

$$T_{\bar{B}}^T \{\emptyset\} T_{\bar{B}} = \begin{bmatrix} M^T \{\emptyset\} M & M^T \{\emptyset\} \bar{B} \\ \bar{B}^T \{\emptyset\} M & \bar{B}^T \{\emptyset\} \bar{B} \end{bmatrix} = 0. \quad (\text{C.27})$$

Eq.(C.27) holds since $\bar{C}M = 0$, $N\bar{B} = 0$, $P\bar{B} = \bar{C}^T$, $PM = N^T P_I$, R^{-1} is chosen in (4.21) and Eq.(4.24) holds. This proves Eq.(C.25). The choice of P as in (C.24) implies $P\bar{B} = \bar{C}^T$. Then proper partition as in Eq.(4.16) and (4.15) allows element-wise equality (4.14). This implies that $\{(\bar{A} - LC), B, S_1 C\}$ is SPR.

Now, we note that for any μ satisfying $0 \leq \mu \leq \mu^*$, $(\mu^* - \mu)P \geq 0$. Following

(C.25), it is clear that

$$(A + \mu I - LC)^T P + P(A + \mu I - LC) = -\bar{Q} - \bar{C}R^{-1}\bar{C} - 2(\mu^* - \mu)P < 0. \quad (\text{C.28})$$

Eq.(C.28) and Eq.(4.14) implies that $\{(A + \mu I - LC), B, S_1 C\}$ is SPR. Because ϵ is finite, L is finite. This completes the proof of Lemma 4.3.

An additional result, $\lambda_{\min}(P) > 1$, will be used later and therefore is proved here. With the proposed solution P in (C.24), it can be shown that

$$T_{\bar{B}}^T \{P - I\} T_{\bar{B}} = \begin{bmatrix} P_I - M^T M & -M^T \bar{B} \\ -\bar{B}^T M & \bar{C} \bar{B} \end{bmatrix}. \quad (\text{C.29})$$

Applying Schur complement shows that since P_I satisfies (4.25), $T_{\bar{B}}^T \{P - I\} T_{\bar{B}} > 0$ and therefore $P > I$. ■

Proof of Lemma 4.4

Proof: Given that we have designed an SPR pair of L_ρ and S_1 for the system $\{(A + \eta I + \frac{1}{\eta} B\Psi^* - L_\rho C), B, S_1 C\}$ with some $\eta > 0$, there exist a $P > 0$ such that

$$(A + \eta I + \frac{1}{\eta} B\Psi^* - L_\rho C)^T P + P(A + \eta I + \frac{1}{\eta} B\Psi^* - L_\rho C) = -Q_\rho < 0 \quad (\text{C.30})$$

and Eq.(4.14) hold simultaneously for a $Q_\rho > 0$. Without loss of generality, we assume $\lambda_{\min}(P) \geq 1$, which can always be satisfied by scaling Q_ρ and S_1 (as we did at the end of proof of Lemma 4.3).

A Lyapunov function V as in (C.1) is proposed using the P in Eq.(C.30)(4.14), and therefore \dot{V} is as in Eq.(C.3). Since $\Theta^* \neq 0$, \dot{e}_x is as in Eq.(4.10) and the second term of the right hand side of Eq.(C.3) is no longer zero. By Assumption 4.6, the

non-zero term can be bounded as

$$\begin{aligned}
e_x^T P B \Lambda^* \Theta^{*T} [\Phi(x_p) - \Phi(x_{mp})] &\leq \|e_x^T P B \Lambda^* \Theta^{*T}\| l_\phi \|e_x\| \\
&\leq \frac{l_\phi}{\sqrt{\eta}} \|e_x^T P B \Lambda^* \Theta^{*T}\| \left\| \sqrt{\eta} P^{\frac{1}{2}} e_x \right\| \\
&\leq \frac{l_\phi^2}{4\eta} e_x^T P B \Lambda^* \Theta^{*T} \Theta^* \Lambda^* B^T P e_x + e_x^T \eta P e_x
\end{aligned} \tag{C.31}$$

Substituting the definition of Ψ^* (4.26) and Eq.(4.14) into Eq.(C.31) yields

$$e_x^T P B \Lambda^* \Theta^{*T} [\Phi(x_p) - \Phi(x_{mp})] \leq e_x^T \frac{1}{\eta} P B \Psi^* e_x + e_x^T \eta P e_x. \tag{C.32}$$

Using inequality (C.32), the derivative of Lyapunov function (C.3) can be bounded as

$$\begin{aligned}
\dot{V} &\leq e_x^T ((A - L_\rho C)^T P + P(A - L_\rho C)) e_x + 2 \left[e_x^T \frac{1}{\eta} P B \Psi^* e_x + e_x^T \eta P e_x \right] \\
&\quad + 2e_x^T [PB - C^T S_1^T] \Lambda^* \tilde{\Lambda}^T u_{bl} - 2e_x^T [PB - C^T S_1^T] \Lambda^* \tilde{\Theta}^T \Phi(x_{mp})
\end{aligned} \tag{C.33}$$

$$\begin{aligned}
&= e_x^T ((A + \eta I + \frac{1}{\eta} B \Psi^* - L_\rho C)^T P + P(A + \eta I + \frac{1}{\eta} B \Psi^* - L_\rho C)) e_x \\
&\quad + 2e_x^T [PB - C^T S_1^T] \Lambda^* \tilde{\Lambda}^T u_{bl} - 2e_x^T [PB - C^T S_1^T] \Lambda^* \tilde{\Theta}^T \Phi(x_{mp})
\end{aligned} \tag{C.34}$$

Substituting Eq.(C.30) and Eq.(4.14) turns Eq.(C.4) into

$$\dot{V} \leq -e_x^T Q_\rho e_x \leq 0. \tag{C.35}$$

Thus, Eq.(C.1) is indeed the Lyapunov function of the system. Following the last part of the proof of Lemma 4.1, it can be concluded that $e_x(t) \rightarrow 0$ as $t \rightarrow \infty$, which proves ii) and $x, e_x, \tilde{\Lambda}$ and $\tilde{\Theta}$ are bounded, which proves i). ■

Proof of Lemma 4.5

Proof: We will show that with the L_ρ design (4.28), the P that guarantees the SPR properties of $\{(A + \mu I - LC), B, S_1 C\}$ also guarantees the SPR properties of

$\{(A + \mu I + \frac{1}{\mu^*} B\Psi - L_\rho C), B, S_1 C\}$ for $\forall \Psi$ that $\|\Psi\| \leq \Psi_{max}^*$ and $\forall \mu$ that $0 \leq \mu \leq \mu^*$.

Since $\{(A + \mu I - LC), B, S_1 C\}$ is SPR by design (see Lemma 4.3), Eq.(C.28) and Eq.(4.14) holds for a $P > 0$ and \tilde{Q} in (4.30). Therefore, the following equation also holds:

$$\begin{aligned} & (A + \mu I + \frac{1}{\mu^*} B\Psi - LC)^T P + P(A + \mu I + \frac{1}{\mu^*} B\Psi - LC) \\ & \leq -\tilde{Q} + \frac{1}{\mu^*} PB\Psi^T + \frac{1}{\mu^*} \Psi B^T P = -\tilde{Q} + \frac{1}{\mu^*} CS_1\Psi^T + \frac{1}{\mu^*} \Psi S_1^T C^T \end{aligned} \quad (\text{C.36})$$

where $\tilde{Q} = \overline{Q} + \overline{C}R^{-1}\overline{C} > 0$. Because of the extra $CS_1\Psi^T$ term, the right hand side of (C.36) may not be negative definite. Adding an extra term $2\rho C^T S^T SC$ on both sides of Eq.(C.36) yields

$$\begin{aligned} & (A + \mu I + \frac{1}{\mu^*} B\Psi - L_\rho C)^T P + P(A + \mu I + \frac{1}{\mu^*} B\Psi - L_\rho C) \\ & \leq -\tilde{Q} + \frac{1}{\mu^*} CS_1\Psi^T + \frac{1}{\mu^*} \Psi S_1^T C^T - 2\rho C^T S^T SC \triangleq Q_\rho \end{aligned} \quad (\text{C.37})$$

with L_ρ defined in Eq.(4.28). We will show that the ρ chosen in (4.29) will always produce a negative definite Q_ρ . Consider the following block matrix

$$M(\rho) = \begin{bmatrix} -2\rho S^T S & \frac{1}{\mu^*} S_1^T \Psi^T \\ \frac{1}{\mu^*} \Psi S_1 & -\tilde{Q} \end{bmatrix}. \quad (\text{C.38})$$

$\tilde{Q} < 0$ since Lemma 4.3 holds for the L and S_1 . Using Schur complement, it can be proved that when ρ is picked using inequality (4.29), $M(\rho) < 0$ for any Ψ bounded by $\|\Psi\| \leq \Psi_{max}^*$. Perform a transformation on $M(\rho)$ using a tall matrix T_C

$$T_C = \begin{bmatrix} C \\ I_{n \times n} \end{bmatrix} \quad (\text{C.39})$$

shows that

$$Q_\rho = T_C^T M(\rho) T_C = \begin{bmatrix} C^T & I \end{bmatrix} \begin{bmatrix} -2\rho S^T S & \frac{1}{\mu^*} S_1^T \Psi^T \\ \frac{1}{\mu^*} \Psi S_1 & -\tilde{Q} \end{bmatrix} \begin{bmatrix} C \\ I \end{bmatrix} < 0. \quad (\text{C.40})$$

The last inequality holds because $M(\rho) < 0$ and T_C does not have a right null space. Combining Eq.(C.37)(C.40) and (4.14) proves that $\{(A + \mu I + \frac{1}{\mu^*} B\Psi - L_\rho C), B, S_1 C\}$ is SPR. Finally, it is noted that Eq.(4.16) ensures the boundedness of S and S_1 . Ψ_{max}^* in (4.27) is finite. μ^* is non-zero. As a result, a finite ρ^* always exists, so does a finite L_ρ . ■

Proof of Theorem 4.1

Proof: Choosing $\mu = \mu^*$ and $\Psi = \Psi^*$ in Lemma 4.5 proves that the L_ρ (4.28) and S_1 (4.16) guarantees the SPR properties of $\{(A + \mu^* I + \frac{1}{\mu^*} B\Psi^* - L_\rho C), B, S_1 C\}$. Therefore, the results of Lemma 4.4 holds: i) all signals in the system, including $\tilde{\Lambda}^T(t) = \Lambda^T(t) - \Lambda^{*-1}$ and $\tilde{\Theta}^T(t) = \Theta^T(t) - \Theta^{*T}$, are bounded and; ii) state error $e_x(t) \rightarrow 0$ as $t \rightarrow \infty$, which implies $e_y(t) \rightarrow 0$ as $t \rightarrow \infty$.

To prove iii), similar to $e_{pz}(t) = z(t) - z_{cmd}$, denote $e_{mz}(t) = z_m(t) - z_{cmd} + L_e C e_x$ where L_e is the corresponding rows of L_ρ . $\int e_{pz}(t) dt$ is a state of x and $\int e_{mz}(t) dt$ is a state of x_m (see Section 4.2.1). As a result, the fact $e_x(t) \rightarrow 0$ as $t \rightarrow \infty$ implies that

$$\left[\int e_{pz}(t) dt - \int e_{mz}(t) dt \right] \rightarrow 0, \quad \text{as } t \rightarrow \infty. \quad (\text{C.41})$$

Substituting the definitions of $e_{pz}(t)$ and $e_{mz}(t)$ transforms (C.41) into

$$\left\{ \int [z(t) - z_{cmd}] dt - \int [z_m(t) - z_{cmd} + L_e C e_x] dt \right\} \rightarrow 0, \quad \text{as } t \rightarrow \infty. \quad (\text{C.42})$$

Since z_{cmd} is piecewise continuous and both $z(t)$ and $z_m(t)$ are integrable, Eq.(C.42) can be simplified as

$$\int e_z(t) dt \rightarrow L_e C \int e_x dt < \infty, \quad \text{as } t \rightarrow \infty. \quad (\text{C.43})$$

where $e_z(t) = z - z_m$. On the other hand, using the definition of z in (4.5) and definition of z_m in (4.8), $e_z(t)$ has the following expression

$$e_z = C_z e_x + D_z \Lambda^* \Theta^{*T} [\Phi(x_p) - \Phi(x_{mp})] + D_z \Lambda^* [\tilde{\Lambda}^T u_{bl} - \tilde{\Theta}^T \Phi(x_{mp})] \quad (\text{C.44})$$

whose derivative is

$$\begin{aligned} \dot{e}_z &= C_z \dot{e}_x + D_z \Lambda^* \Theta^{*T} [\Phi_{x_p} \dot{x}_p - \Phi_{x_{mp}} \dot{x}_{mp}] \\ &\quad + D_z \Lambda^* [\tilde{\Lambda}^T u_{bl} + \tilde{\Lambda}^T \dot{u}_{bl} - \tilde{\Theta}^T \Phi - \tilde{\Theta}^T \Phi_{x_{mp}} \dot{x}_{mp}] \end{aligned} \quad (\text{C.45})$$

where $\Phi_{(\cdot)}$ stands for $\frac{\partial \Phi}{\partial (\cdot)}$. Because all signals in the system are bounded and Φ is globally differentiable, \dot{e}_z is bounded. Applying Barbalat's Lemma shows that $e_z(t) \rightarrow 0$ as $t \rightarrow \infty$, which proves iii). \blacksquare

Proof of Lemma 4.6

Proof: In this proof, the matrix notation $A \rightarrow B$ is defined as $(\underline{\sigma}[A] - \underline{\sigma}[B]) \rightarrow 0$ where $\underline{\sigma}[\cdot]$ denotes the minimum singular value of matrix $[\cdot]$. Define $\phi_p(s) = (sI - A_p)^{-1}$, $\phi(s) = (sI - A)^{-1}$, $\bar{\phi}(s) = (sI - A + BK)^{-1}$ and $\bar{\phi}_L(s) = (sI - A + BK + L_\rho C)^{-1}$. Denote $\bar{R}^{-1} = R^{-1} + \rho I$. As $\epsilon \rightarrow \infty$ or $\rho \rightarrow \infty$, $\bar{R}^{-1} \rightarrow \infty$ and

$$L_\rho = \bar{R}^{-1} S \rightarrow \infty. \quad (\text{C.46})$$

For loop gain at input, we can treat the error integrator (introduced in Section 4.2.1) as a part of the plant. The loop gain at input for a LQR controller is

$$L_u^*(s) = K \phi B \quad (\text{C.47})$$

The loop gain at input for a observer-based controller with a L_ρ and the same K is

$$L_u(s) = K[sI - A + BK + L_\rho C]^{-1} L_\rho C \phi B \quad (\text{C.48})$$

To prove i), define $\bar{K} \in \mathbb{R}^{p \times n}$ as

$$\bar{K} = \begin{bmatrix} K \\ 0_{(p-m) \times n} \end{bmatrix} \quad (\text{C.49})$$

such that $BK = \bar{B}\bar{K}$. The asymptotic relation (C.46) implies

$$\bar{L}_u(s) \triangleq \bar{K}[sI - A + BK + L_\rho C]^{-1}L_\rho C\phi\bar{B} \quad (\text{C.50})$$

$$= \bar{K}[sI - A + \bar{B}\bar{K} + L_\rho C]^{-1}L_\rho C\phi\bar{B} \quad (\text{C.51})$$

$$\rightarrow \bar{K}\phi\bar{B} \quad (\text{C.52})$$

pointwisely for $s \in \mathcal{D}$. Given (C.51), the proof of (C.52) can be found in Ref. [9], which can be applied here because $C\phi(s)\bar{B}$ is square and has stable transmission zeros and therefore $C\phi(s)\bar{B}$ is invertible for all $s \in \mathcal{D}$ (see Definition 3.3 and 3.4). The partition (C.49) and (4.15) shows that element-wise convergence of (C.52) holds, i.e. the submatrix L_u

$$L_u(s) \triangleq K[sI - A + BK + L_\rho C]^{-1}L_\rho C\phi B \rightarrow K\phi B \quad (\text{C.53})$$

pointwisely for $s \in \mathcal{D}$ as $\epsilon \rightarrow \infty$ or $\rho \rightarrow \infty$, which proves i).

For loop gain at output, we have to remove the error integrators from the augmented plant model (4.5) and treat them as a part of our controller. Consider $s \in \mathcal{D}$. Divide $K = [K_p, K_i]$ where $K_p \in \mathbb{R}^{m \times n_p}$ and $K_i \in \mathbb{R}^{m \times d}$. For a LQR controller, the loop gain at output is

$$L_o^*(s) = \left(\begin{bmatrix} I_{n_p} \\ C_{pz} \end{bmatrix} \phi_p(s)B_p + \begin{bmatrix} 0 \\ D_{pz} \end{bmatrix} \right) \begin{bmatrix} K_p & \frac{1}{s} & K_i \end{bmatrix} \quad (\text{C.54})$$

Divide $L_\rho = [L_p, L_i]$ where $L_p \in \mathbb{R}^{n \times p_p}$ and $L_i \in \mathbb{R}^{n \times r}$. Define

$$A_k = \begin{bmatrix} A - BK - L_\rho & L_i \\ 0 & 0 \end{bmatrix}, \quad B_k = \begin{bmatrix} L_p & 0 \\ 0 & I \end{bmatrix}, \quad C_k = \begin{bmatrix} K & 0 \end{bmatrix}. \quad (\text{C.55})$$

For the LQG controller, the transfer function of the controller is $C_k(sI - A_k)^{-1}B_k$ and the loop gain at output is

$$L_o(s) = \left(\begin{bmatrix} C_p \\ C_{pz} \end{bmatrix} \phi_p(s)B_p + \begin{bmatrix} 0 \\ D_{pz} \end{bmatrix} \right) C_k(sI - A_k)^{-1}B_k \quad (\text{C.56})$$

$$= \left(\begin{bmatrix} C_p \\ C_{pz} \end{bmatrix} \phi_p(s)B_p + \begin{bmatrix} 0 \\ D_{pz} \end{bmatrix} \right) K\bar{\phi}_L(s) \begin{bmatrix} L_p & \frac{1}{s} L_i \end{bmatrix}. \quad (\text{C.57})$$

From (C.56) to (C.57), we used the identity

$$(sI - A_k)^{-1} = \begin{bmatrix} \bar{\phi}_L & \bar{\phi}_L L_i \frac{1}{s} \\ 0 & \frac{1}{s} \end{bmatrix}.$$

To prove ii), we need to use an asymptotic relation

$$\bar{\phi}_L L_\rho = [\bar{\phi}^{-1} + L_\rho C]^{-1} L_\rho \quad (\text{C.58})$$

$$= \bar{\phi}[I + L_\rho C\bar{\phi}]^{-1} L_\rho \quad (\text{C.59})$$

$$= \phi[I + BK\phi + L_\rho C\phi]^{-1} L_\rho \quad (\text{C.60})$$

$$= \phi \{ I + \bar{B}[\bar{K} + \bar{R}^{-1}SC]\phi \}^{-1} \bar{B}\bar{R}^{-1}S \quad (\text{C.61})$$

$$= \phi\bar{B} \{ I + [\bar{K} + \bar{R}^{-1}SC]\phi\bar{B} \}^{-1} \bar{R}^{-1}S \quad (\text{C.62})$$

$$\rightarrow \phi\bar{B}[C\phi\bar{B}]^{-1} \quad (\text{C.63})$$

pointwisely for $s \in \mathcal{D}$ as $\epsilon \rightarrow \infty$ or $\rho \rightarrow \infty$. From (C.59) to (C.63), we used the equality $\bar{\phi} = \phi[I + BK\phi]^{-1}$, the design L_ρ , the equality $BK = \bar{B}\bar{K}$, the matrix equality $X[I + XY]^{-1} = [I + YX]^{-1}X$, and the asymptotic relation (C.46). It has been proved that $C\phi(s)\bar{B}$ is invertible for all $s \in \mathcal{D}$. Now we proceed to prove ii). Since $\phi\bar{B}[C\phi\bar{B}]^{-1}$ is a right inverse matrix of C , we can write

$$C^\dagger(s, \bar{B}) := \phi\bar{B}[C\phi\bar{B}]^{-1} = \begin{bmatrix} C_p^\dagger(s, \bar{B}) & \frac{1}{s}M_p(s, \bar{B}) \\ 0 & I_r \end{bmatrix}, \quad (\text{C.64})$$

where $C_p^\dagger(s, \bar{B})$ satisfies $C_p C_p^\dagger(s, \bar{B}) = I_{p_p}$. and $M_p(s, \bar{B}) \in \mathbb{R}^{p_p \times d}$ satisfies $C_p M_p(s, \bar{B}) = 0_{p_p \times d}$. Since $0 < |s| < +\infty$, when $L_\rho \rightarrow \infty$,

$$K \bar{\phi}_L(s) \begin{bmatrix} L_p & \frac{1}{s} L_i \end{bmatrix} \rightarrow \begin{bmatrix} K_p & \frac{1}{s} K_i \end{bmatrix} C^\dagger(s, \bar{B}) \quad (\text{C.65})$$

pointwisely for $s \in \mathcal{D}$. Combining (C.57) and (C.65) yields

$$L_o(s) \rightarrow \left(\begin{bmatrix} C_p \\ C_{pz} \end{bmatrix} \phi_p(s) B_p + \begin{bmatrix} 0 \\ D_{pz} \end{bmatrix} \right) \begin{bmatrix} K_p & \frac{1}{s} K_i \end{bmatrix} C^\dagger(s, \bar{B}) \quad (\text{C.66})$$

$$= C [L_o^*(s)] C^\dagger(s, \bar{B}) \quad (\text{C.67})$$

pointwisely for $s \in \mathcal{D}$ as $\epsilon \rightarrow \infty$ or $\rho \rightarrow \infty$, which proves ii). \blacksquare

Summary of Balanced Realization [46]

A balanced realization approach was used to reduce the order of the model. Briefly, this method can be described as

$$G_p \sim \begin{bmatrix} A_p & B_p \\ C_p & D_p \end{bmatrix} \xrightarrow{T} \hat{G}_p \sim \begin{bmatrix} \hat{A}_p & \hat{B}_p \\ \hat{C}_p & \hat{D}_p \end{bmatrix} \xrightarrow{\text{part}} \hat{G} \sim \begin{bmatrix} \hat{A}_{11} & \hat{A}_{12} & \hat{B}_1 \\ \hat{A}_{21} & \hat{A}_{22} & \hat{B}_2 \\ \hat{C}_1 & \hat{C}_2 & \hat{D} \end{bmatrix} \\ \xrightarrow{\text{Eq.(C.69)}} G_r = \begin{bmatrix} A_r & B_r \\ C_r & D_r \end{bmatrix} \quad (\text{C.68})$$

$$\begin{aligned} A_r &= \hat{A}_{11} - \hat{A}_{12}\hat{A}_{22}^{-1}\hat{A}_{21} \\ B_r &= \hat{B}_1 - \hat{A}_{12}\hat{A}_{22}^{-1}\hat{B}_2 \\ C_r &= \hat{C}_1 - \hat{C}_2\hat{A}_{22}^{-1}\hat{A}_{21} \\ D_r &= \hat{D} - \hat{C}_2\hat{A}_{22}^{-1}\hat{B}_2 \end{aligned} \quad (\text{C.69})$$

where a coordinate transformation T is used to transform G_p into its balanced realization \hat{G}_p , with $\hat{A}_p = T^{-1}A_pT$, $\hat{B}_p = T^{-1}B_p$, $\hat{C}_p = C_pT$, $\hat{D}_p = D_p$, in which the states are ranked using a metric named Hankel Singular Value (HSV) defined as

$\sigma_i \triangleq (\lambda_i(PQ))^{1/2}$, where P is the controllability gramian and Q is the observability gramian of G_p . Appropriate cut off values σ_{cutoff} will part all matrices in \hat{G} according to the rank of HSV, where $\hat{A}_{11} \in R^{n_r \times n_r}$, $\hat{B}_1 \in R^{n_r \times m}$ and $\hat{C}_1 \in R^{p \times n_r}$. The rest of $n - n_r$ states were residualized using Eq.(C.69) and the reduced-order model G_r was therefore derived. For the Vulture model, setting $\sigma_{cutoff} = 415$ selected the reduced model order to be $n_r = 80$.

Appendix D

Proof for Results in Chapter 5

Another Class of Relative Degree Two Plant Model

Another class of relative degree three plant models are those with no actuator dynamics and first-order sensors. The first order sensors are modeled as

$$\dot{w}_y + (D_s + \Theta_s^{*T})w_y = D_s y_p \quad (\text{D.1})$$

with $D_s \geq 0$ is diagonal and known, and $\Theta_s^{*T} \in \mathbb{R}^{p \times p}$ are its uncertainties. Also, for command tracking we define integral error states $e_{pz} = z - z_{cmd}$ and $w_z := \int e_{pz} dt$. Define $w_u := \Lambda^* u_p$. The augmented plan model is square and can be written as

$$\begin{aligned}
\begin{bmatrix} \dot{x}_p \\ \dot{w}_y \\ \dot{w}_z \end{bmatrix} &= \underbrace{\begin{bmatrix} A_p & 0 & 0 \\ C_p & -D_s & 0 \\ C_{pz} & 0 & 0 \end{bmatrix}}_A \underbrace{\begin{bmatrix} x_p \\ w_y \\ w_z \end{bmatrix}}_x + \underbrace{\begin{bmatrix} B_p \\ 0 \\ D_z \end{bmatrix}}_{B_1} \Theta_p^{*T} x_p + \underbrace{\begin{bmatrix} 0 \\ I \\ 0 \end{bmatrix}}_{B_2} \begin{bmatrix} -\Theta_s^{*T} \\ [y] \end{bmatrix} \\
&\quad + \underbrace{\begin{bmatrix} B_p \\ 0 \\ D_z \end{bmatrix}}_{B_1} \Lambda^* u + \underbrace{\begin{bmatrix} 0 \\ 0 \\ -I \end{bmatrix}}_{B_z} z_{cmd} \\
y &= \underbrace{\begin{bmatrix} 0 & I & 0 \\ 0 & 0 & I \end{bmatrix}}_C x, \quad z = \underbrace{\begin{bmatrix} C_{pz} & 0 & 0 \end{bmatrix}}_{C_z} x + D_z \Lambda^* u.
\end{aligned} \tag{D.2}$$

Proof of Lemma 5.1

Proof: Since the plant has uniformly relative degree two, i.e. $r = 2$, the observer canonical form (C.6) of $R(s)$ (see Definition 3.4 and proof of Lemma 4.2 in Appendix C), has the form of

$$\overline{R}(s) = \left[\begin{array}{cc|cc} sI_p - A_{11} & -A_{12} & 0 & \hat{B}_{12} \\ -A_{21} & sI_{n-p} - A_{22} & B_{21} & \hat{B}_{22} \\ \hline I_p & 0 & 0 & 0 \end{array} \right]. \tag{D.3}$$

with $B_{12} = 0$ and $A_{12}B_{22}$ of full rank. It is noted that $Z[\overline{R}(s)] = Z[\overline{R}_s(s)]$ where

$$\overline{R}_s(s) = \left[\begin{array}{c|cc} sI_{n-p} - A_{22} & B_{21} & \hat{B}_{22} \\ \hline -A_{12} & 0 & \hat{B}_{12} \end{array} \right] \tag{D.4}$$

is a submatrix of $\hat{R}(s)$. Since $A_{12}B_{21}$ is full rank, the problem is reduced to the **Case I**, as presented in proof of Lemma 4.2 in Appendix C: squaring up a plant model $\{A_{22}, B_{21}, A_{12}\}$ so that it has relative degree one. Using **Case I** of the proof of Lemma

4.2 generates a \hat{B}_{12} and a \hat{B}_{22} such that $Z[\bar{R}_s(s)]$ are stable and $\begin{bmatrix} A_{12}B_{21} & \hat{B}_{12} \end{bmatrix}$ is full rank. In this case, we have added $(p - m)$ inputs of relative degree one and the squared-up plant model has $[n - r_s - (m - p)]$ stable transmission zeros. ■

Proof of Lemma 5.2

Proof: The proof will be performed in a transformed coordinate. Similar to \bar{B}_2 , we part $C^T = \begin{bmatrix} C_2^T & C_1^T \end{bmatrix}$. For a square plant model that has nonuniform input relative degree two, there exists an invertible transformation $T_{in} = \begin{bmatrix} (\mathfrak{C}\mathfrak{B})^{-1}\mathfrak{C} \\ \mathfrak{N} \end{bmatrix}$, $T_{in}^{-1} = \begin{bmatrix} \mathfrak{B} & \mathfrak{N} \end{bmatrix}$, where $\mathfrak{C}^T = \begin{bmatrix} C_2^T & A^T C_2^T & C_1 \end{bmatrix}$, $\mathfrak{B} = \begin{bmatrix} B_2 & AB_2 & B_{s1} \end{bmatrix}$ (see Lemma 3.1), that transforms (5.4) into the input normal form coordinate (see Lemma 3.2). In this proof, matrices in input normal form coordinate will be denoted with the subscript $(\cdot)_{in}$, as in $x_{in} = T_{in}x$, $A_{in} = T_{in}AT_{in}^{-1}$, $\bar{B}_{2,in} = T_{in}\bar{B}_2$ (and therefore $B_{2,in} = T_{in}B_2$ and $B_{s1,in} = T_{in}B_{s1}$), $B_{1,in} = T_{in}B_1$, $B_{z,in} = T_{in}B_z$, $C_{in} = CT_{in}^{-1}$, $\Psi_{1,in}^{*T} = \Psi_1^{*T}T_{in}^{-1}$ and $\Psi_{2,in}^{*T} = \Psi_2^{*T}T_{in}^{-1}$. The input normal form of the plant model

(5.4) is

$$\begin{aligned}
\begin{bmatrix} \dot{\xi}_1^2 \\ \dot{\xi}_2^2 \\ \dot{\xi}_1^1 \\ \dot{\eta} \end{bmatrix} &= \underbrace{\begin{bmatrix} 0 & R_{2,1}^2 & R_{2,1}^1 & V_2 \\ I & R_{2,2}^2 & R_{2,2}^1 & 0 \\ 0 & R_{1,1}^2 & R_{1,1}^1 & V_1 \\ 0 & U_2 & U_1 & Z \end{bmatrix}}_{A_{in}} \underbrace{\begin{bmatrix} \xi_1^2 \\ \xi_2^2 \\ \xi_1^1 \\ \eta \end{bmatrix}}_{x_{in}} + \underbrace{\begin{bmatrix} I_m \\ 0 \\ 0 \\ 0 \end{bmatrix}}_{B_{2,in}} \Lambda^* u \\
&\quad + B_{2,in} \underbrace{\begin{bmatrix} \psi_2^{1*T} & \psi_2^{2*T} & \psi_{21}^{1*T} & \psi_2^{(n-r_s)*T} \end{bmatrix}}_{\Psi_{2,in}^T} x_{in} \\
&\quad + \underbrace{\begin{bmatrix} I_m \\ \frac{1}{c}I_m \\ 0 \\ 0 \end{bmatrix}}_{B_{1,in}} \underbrace{\begin{bmatrix} 0 & \psi_1^{2*T} & \psi_{11}^{1*T} & \psi_1^{(n-r_s)*T} \end{bmatrix}}_{\Psi_{1,in}^T} x_{in} + B_{z,in} z_{cmd} \quad (D.5) \\
y &= \underbrace{\begin{bmatrix} 0 & CAB_2 & CB_{s1} & 0 \end{bmatrix}}_{C_{in}} x_{in}.
\end{aligned}$$

where $r_s = \sum_{i=1}^m r_i$. It is noted that $B_{1,in} = [\times \times 0 0]^T$ and $\Psi_1^{*T} T_{in}^{-1} = [0 \times \times \times]$ since Assumption 5.5 holds.

Define $A_{in}^* = A_{in} + B_{1,in} \Psi_{1,in}^* + B_{2,in} \Psi_{2,in}^* = T_{in} A^* T_{in}^{-1}$. Examination of the elements of $\bar{B}_{2,in}^1$ and $\bar{B}_{2,in}^{1*}$, which are defined as $\bar{B}_{2,in}^{1*} = T_{in} \bar{B}_{2,in}^1$, and $\bar{B}_{2,in}^1 = T_{in} \bar{B}_{2,in}^{1*}$, respectively, shows that

$$\bar{B}_{2,in}^1 = \begin{bmatrix} B_{2,in}^1 & B_{s1,in} \end{bmatrix} = \begin{bmatrix} a_1^0 I_m & 0 \\ a_1^1 I_m & 0 \\ 0 & I_{m_s} \\ 0 & 0 \end{bmatrix}, \quad (D.6)$$

and

$$\overline{B}_{2,in}^{1*} = \begin{bmatrix} B_{2,in}^{1*} & B_{s1,in} \end{bmatrix} = \begin{bmatrix} a_1^0 I_m + a_1^1 \psi_2^{1*T} & 0 \\ a_1^1 I_m & 0 \\ \hline 0 & I_{m_s} \\ \hline 0 & 0 \end{bmatrix}. \quad (\text{D.7})$$

where $B_{2,in}^1 = T_{in}B_{2,in}^1$, $B_{s1,in} = T_{in}B_{s1}$ and $B_{2,in}^{1*} = T_{in}B_{2,in}^{1*}$. It is noted that $C_{in}\overline{B}_{2,in}^1 = C_{in}\overline{B}_{2,in}^{1*} = \begin{bmatrix} a_1^1 CAB_2 & CB_{s1} \end{bmatrix}$ has full rank by Assumption 5.3 and Lemma 5.1. Examination on elements of $\overline{B}_{2,in}^{1*}$ and $\overline{B}_{2,in}^1$ shows that

$$\overline{B}_{2,in}^{1*} = \overline{B}_{2,in}^1 + B_{2,in}a_1^1\overline{\psi}_2^{1*T}. \quad (\text{D.8})$$

where

$$\overline{\psi}_2^{1*T} = \begin{bmatrix} \psi_2^{1*T} & 0_{m \times (p-m)} \end{bmatrix} \in \mathbb{R}^{m \times p} \quad (\text{D.9})$$

where ψ_2^{1*T} is a subset of the elements in $\Psi_{2,in}^*$ as shown in (D.5). It is noted that (D.7) also holds for $(A_{in}^* - L_{in}C_{in})$ for $\forall L_{in} \in \mathbb{R}^{n \times m}$. Transformation back to the original coordinate proves the Lemma. \blacksquare

Proof of Lemma 5.3

Proof: To prove Lemma 6.6, It is equivalent to show $\{(A_{in}^* - L_{in}^*C_{in}), \overline{B}_{2,in}^{1*}, SC_{in}\}$ is SPR, where $A_{in}^* = T_{in}A^*T_{in}^{-1}$ and $\overline{B}_{2,in}^{1*} = T_{in}\overline{B}_2^{1*}$. Define $\overline{C}_{in} = SC_{in}$,

$$M_{in}^T = \begin{bmatrix} I & 0 & 0 \\ 0 & 0 & I \end{bmatrix} \quad (\text{D.10})$$

which is the null space of C_{in} , and

$$N_{in}^{1*} = (M_{in}^T M_{in})^{-1} M_{in}^T \left[I - \overline{B}_{2,in}^{1*} (\overline{C}_{in} \overline{B}_{2,in}^{1*})^{-1} \overline{C}_{in} \right], \quad (\text{D.11})$$

which is the null space of $\bar{B}_{2,in}^{1*}$ (see Lemma 3.1). Then propose a P_{in}^* as

$$\begin{aligned} P_{in}^* &= \bar{C}_{in}^T (\bar{C}_{in} \bar{B}_{2,in}^{1*})^{-1} \bar{C}_{in} + N_{in}^{1*T} P_I^* N_{in}^{1*}, \\ \text{s.t. } P^* \bar{B}_{2,in}^{1*} &= \bar{C}_{in}^T, \end{aligned} \quad (\text{D.12})$$

where P_I^* is the unique solution of a Lyapunov equation

$$P_I^* N_{in}^{1*} A_{in}^* M_{in} + (N_{in}^{1*} A_{in}^* M_{in})^T P_I^* = -I \quad (\text{D.13})$$

which always exists since $\{A_{in}^*, \bar{B}_{2,in}^{1*}, C_{in}\}$ has stable transmission zeros (see Proposition 3.1 and Lemma 3.1). Define

$$\{\emptyset\} := A_{in}^{*T} P_{in}^* + P_{in}^* A_{in}^* - P_{in}^* \bar{B}_{2,in}^{1*} R^{-1} \bar{B}_{2,in}^{1*T} P_{in}^* + Q_{in}^* \quad (\text{D.14})$$

where

$$\begin{aligned} Q_{in}^* &= -N_{in}^{1*T} H_{in}^* (\bar{C}_{in} \bar{B}_{2,in}^{1*})^{-1} \bar{C}_{in} - \bar{C}_{in}^T (\bar{C}_{in} \bar{B}_{2,in}^{1*})^{-1} H_{in}^{*T} N_{in}^{1*T} \\ &\quad + \varepsilon \bar{C}_{in}^T \bar{C}_{in} + N_{in}^{1*T} N_{in}^{1*} \\ &\quad - \bar{C}_{in}^T (\bar{C}_{in} \bar{B}_{2,in}^{1*})^{-1} [\Delta_{CAB}^* + \Delta_{CAB}^{*T}] (\bar{C}_{in} \bar{B}_{2,in}^{1*})^{-1} \bar{C}_{in} \end{aligned} \quad (\text{D.15})$$

$$\Delta_{CAB}^* = \bar{C}_{in} A_{in}^* B_{2,in}^{1*} - \bar{C}_{in} A_{in} B_{2,in}^1 = (C_{in} B_{2,in}^1)^T C_{in} B_{2,in}^1 \Psi_{in,a}^{*T} \quad (\text{D.16})$$

$$H_{in}^* = M_{in}^T A_{in}^{*T} \bar{C}_{in}^T + P_I^* N_{in}^{1*} A_{in}^* B_{2,in}^{1*}. \quad (\text{D.17})$$

and $B_{2,in}^1 = T_{in} B_2^1$, and $\Psi_{in,a}^{*T} = \begin{bmatrix} \psi_2^{1*T} & 0 \\ \psi_{21}^{1*T} & \psi_{11}^{1*T} \end{bmatrix}$. It has been proved [22, 25] that once ε in L_{in}^* is large enough, $\{\emptyset\} = 0$ holds for $P_{in}^* > 0$, $Q_{in}^* > 0$ and $R^{-1} > 0$ and therefore P_{in}^* guarantees the SPR properties of $\{(A_{in}^* - L_{in}^* C_{in}), B_{2,in}^{1*}, S_{in}^1 C_{in}\}$. We will show that one lower bound for such ε is $\bar{\varepsilon}$ in (6.56).

Using the definition of R in (6.54), the equality (D.16) and the transformation

matrix $T_B = [M_{in}, B_{2,in}^{1*}]$, it can be shown that

$$T_B^T \{\emptyset\} T_B = \begin{bmatrix} M_{in}^T \{\emptyset\} M_{in} & M_{in}^T \{\emptyset\} B_{2,in}^{1*} \\ B_{2,in}^{1*T} \{\emptyset\} M_{in} & B_{2,in}^{1*T} \{\emptyset\} B_{2,in}^{1*} \end{bmatrix} = 0, \quad (\text{D.18})$$

which implies that $\{\emptyset\} = 0$ and that P_{in}^* satisfies

$$\begin{aligned} (\bar{A}_{in}^* - L_{in}^* \bar{C}_{in})^T P_{in}^* + P_{in}^* (\bar{A}_{in}^* - L_{in}^* \bar{C}_{in}) &= -Q_{in}^* - \bar{C}_{in}^T R_{in}^{-1} \bar{C}_{in} \\ P_{in}^* B_{in}^{1*} &= \bar{C}_{in}^T. \end{aligned}$$

where $L_{in}^* = B_2^{1*} R^{-1}(\epsilon) S$. Now we will show that $R^{-1} > 0$ and $Q_{in}^* > 0$. Since $\varepsilon > \varepsilon_1$, $R^{-1} > 0$. To show $Q_{in}^* > 0$, equivalently we will show $T_B^T Q_{in}^* T_B > 0$. It is noted that

$$T_B^T Q_{in}^* T_B = \begin{bmatrix} I & -H_{in}^* \\ -H_{in}^{*T} & \varepsilon (\bar{C}_{in} B_{2,in}^{1*})^2 - [\Delta_{CAB}^* + \Delta_{CAB}^{*T}] \end{bmatrix}. \quad (\text{D.19})$$

Since $\bar{C}_{in} B_{2,in}^{1*} = \bar{C}_{in} B_{2,in}^1 = C B_2^{1*}$ and $C A^* B_2^{1*} = C_{in} A_{in}^* B_{2,in}^{1*}$, it follows $\varepsilon > \varepsilon_2$ that

$$\begin{aligned} \epsilon I &\geq (\bar{C}_{in} B_{2,in}^1)^{-1} [(C_{in} B_{2,in}^1)^T C_{in} B_{2,in}^1 \Psi_{in,a}^{*T} + \Psi_{in,a}^{*T} (C_{in} B_{2,in}^1)^T C_{in} B_{2,in}^1] (\bar{C}_{in} B_{2,in}^1)^{-1} \\ &\quad + (\bar{C}_{in} B_{2,in}^1)^{-1} H_{max}^2 (\bar{C}_{in} B_{2,in}^1)^{-1} \\ &\geq (\bar{C}_{in} B_{2,in}^{1*})^{-1} [\Delta_{CAB}^* + \Delta_{CAB}^{*T}] (\bar{C}_{in} B_{2,in}^{1*})^{-1} + (\bar{C}_{in} B_{2,in}^{1*})^{-1} H_{in}^{*T} H_{in}^* (\bar{C}_{in} B_{2,in}^{1*})^{-1} \end{aligned} \quad (\text{D.20})$$

From (D.20) to (D.21), we used the fact that

$$\|H_{in}^*\| \leq \|P_I^*\| \|N_{in}^{1*} A_{in} B_{2,in}^{1*}\| + \|\bar{C}_{in} A_{in}^* M_{in}\| \quad (\text{D.22})$$

$$\begin{aligned} N_{in}^{1*} \bar{A}_{in}^* B_{in}^{1*} &= N_{in}^1 A_{in} B_{in}^1 \\ &\quad + \begin{bmatrix} -(a_1^0 + a_1^1 R_{22}^2) \psi_2^{1*T} & \psi_2^{1*T} - \psi_2^{2*T} R_{22}^1 \\ 0 & 0 \end{bmatrix} \end{aligned} \quad (\text{D.23})$$

$$\begin{aligned} C_{in} A_{in}^* M_{in} &= C_{in} A_{in} M_{in} \\ &\quad + \begin{bmatrix} 0 & CAB_2 \psi_2^{(n-r_s)*T} + CB_1 \psi_1^{(n-r_s)*T} \end{bmatrix} \end{aligned} \quad (\text{D.24})$$

and the sensitivity of Lyapunov equation solutions [53, Example 1] as

$$\|P_I^*\| \leq (1 + 2\bar{\Psi}_{max} \|P_I\|) \|P_I\|, \quad (\text{D.25})$$

where P_I is a nominal solution to (D.13) without uncertainties. By Schur's complement, the fact that inequality (D.21) holds implies that $T_B^T Q_{in}^* T_B > 0$ and therefore $Q_{in}^* > 0$. \blacksquare

Proof of Theorem 5.1

Proof: We propose a Lyapunov function candidate

$$V = e_{mx}^T P^* e_{mx} + Tr \left[\tilde{\Omega}^T \Gamma_{\psi_\lambda}^{-1} \tilde{\Omega} |\Lambda^*| \right] + Tr \left[\tilde{\psi}_2^{1T} \Gamma_{\psi_m}^{-1} \tilde{\psi}_2^1 \right] \quad (\text{D.26})$$

where $P^* = P^{*T} > 0$ is the matrix that guarantees the SPR properties of $\{A_{L^*}^*, \bar{B}_2^{1*}, SC\}$, satisfying

$$P^* A_{L^*}^* + A_{L^*}^* P^* = -Q^* < 0 \quad (\text{D.27})$$

$$P^* \bar{B}_2^{1*} = C^T S^T, \quad (\text{D.28})$$

for a $Q^* = Q^{*T} > 0$. Partition on both sides of (D.28) yields

$$P^* [B_2^{1*} B_1] = C^T \begin{bmatrix} S_2^T & S_1^T \end{bmatrix}. \quad (\text{D.29})$$

By appealing to (5.23)(5.24)(5.25)(D.27)(D.29), the derivative of V has the following bound

$$\begin{aligned} \dot{V} &= e_{mx}^T [A_{L^*}^{*T} P^* + P^* A_{L^*}^*] e_{mx} \\ &\quad - 2e_{mx}^T [P^* B_2^{1*} - C^T S_2^T] \Lambda^* \tilde{\Omega}^T \bar{\xi} - 2e_{mx}^T [P^* B_2^{1*} - C^T S_2^T] \tilde{\psi}_2^{1T} \bar{e}_{sy} \\ &= -e_{mx}^T Q^* e_{mx} \leq 0. \end{aligned} \quad (\text{D.30})$$

Then $e_{mx}(t)$, $\tilde{\Omega}(t)$ and $\tilde{\psi}_2^1(t)$ are bounded as $t \rightarrow \infty$, which proves i). Applying Barbalat's Lemma (using the fact that $\dot{e}_{mx}(t)$ is bounded) shows that $e_{mx}(t) \rightarrow 0$ as $t \rightarrow \infty$, which proves ii). From (5.24) and (5.11), the fact $e_{mx}(t) \rightarrow 0$ implies that $e_y(t) \rightarrow 0$, $e_{sy}(t) \rightarrow 0$ and $\bar{e}_{sy}(t) \rightarrow 0$ as $t \rightarrow \infty$, which in turn implies that x_m , as well as \bar{x}_m and \bar{u}_{bl} , is bounded. Further, denote

$$e_{pz}(t) = z - z_{cmd}, \quad e_{mz}(t) = z_m - z_{cmd}. \quad (\text{D.31})$$

From (5.3), it is noted that $\int e_{pz}(t)dt$ is an element of x . From (5.9), it is noted that $\int(e_{mz}(t) - L_I e_y)dt$ is an element of x_m where L_I are the rows of L corresponding to e_{mz} dynamics. As a result, $e_{mx}(t) \rightarrow 0$ as $t \rightarrow \infty$, which, together with the definition of e_{mx} as

$$e_{mx} = e_x + B_2 \Lambda^* a_1^1 \bar{\Psi}_1^{*T} x_m + B_2 a_1^1 \left[\tilde{\psi}_2^{1T}(t) \bar{e}_{sy} \right] - B_2 \Lambda^* a_1^1 \tilde{\Omega}^T \bar{\xi}, \quad (\text{D.32})$$

implies $e_x(t) \rightarrow \int(B_2[\cdot])dt$ and therefore

$$\int(e_{pz} - e_{mz} + L_I e_y)dt \rightarrow \int(B_{2,I}[\cdot])dt = 0 \quad (\text{D.33})$$

as $t \rightarrow \infty$ (since $B_{2,I}$, the rows of B_2 corresponding to w_z dynamics, is zero). Eq.(D.33), together with the fact that

$$e_z(t) = z - z_m = e_{pz} - e_{mz} \quad (\text{D.34})$$

implies

$$\int e_z(t)dt \rightarrow - \int(L_I e_y)dt \quad (\text{D.35})$$

which has a bounded limit as $t \rightarrow \infty$ (since $e_y(t) \rightarrow 0$). Further, from (5.3) and (5.9), $\dot{e}_z(t)$ is bounded as $t \rightarrow \infty$. Applying Barbalat's Lemma shows that $e_z(t) \rightarrow 0$ as $t \rightarrow \infty$, which proves iii). \blacksquare

Proof of Corollary 5.1

Proof: It is noted that by Lemma 5.3, $\{A_{L^*}^*, B_2^{1*}, SC\}$ is SPR, and therefore by Corollary 3.3 $\{A_{L^*}^*, B_2^{0*}, SC, SCB_2^{1*}\}$ is also SPR. By Corollary 3.3, there exists a $P^* = P^{*T} > 0$ that satisfies the results of Lemma 5.3 as

$$P^* B_2^{1*} = C^T S_2^T \quad (\text{D.36})$$

results of Lemma 3.6 as

$$P^* A_{L^*}^* + A_{L^*}^{*T} P^* = -W^T W - L \quad (\text{D.37})$$

$$P B_2^{0*} = C^T S_2^T + W^T K \quad (\text{D.38})$$

$$K^T K = a_1^1 S_2 C B_2^{1*} + a_1^1 (S_2 C B_2^{1*})^T \quad (\text{D.39})$$

for a W , a K and a $L = L^T > 0$. Propose a Lyapunov function candidate

$$V = e_{mx}^T P^* e_{mx} + \text{Tr} \left[\tilde{\Omega}^T \Gamma_{\psi_\lambda}^{-1} \tilde{\Omega} |\Lambda^*| \right] + \text{Tr} \left[\tilde{\psi}_2^{1T} \Gamma_{\psi_m}^{-1} \tilde{\psi}_2^1 |\Lambda^*| \right] \quad (\text{D.40})$$

whose derivative is

$$\begin{aligned} \dot{V} &= e_{mx}^T [P^* A_{L^*}^* + A_{L^*}^{*T} P^*] e_{mx} - 2e_{mx}^T [P^* B_2^{1*} - C^T S_2^T] \tilde{\psi}_2^{1T} \bar{e}_{sy} \\ &\quad + 2e_{mx}^T [P^* B_2^{0*} - C^T S_2^T] \Lambda^* \tilde{\Omega}^T \bar{\xi} \\ &\quad - [\tilde{\Omega}^T \bar{\xi}]^T \Lambda^{*T} [2a_1^1 (S_2 C B_2^{1*})^T S_2 C B_2^{1*}] \Lambda^* \tilde{\Omega}^T \bar{\xi} \\ &= -e_{mx}^T [-W^T W - L] e_{mx} + 2e_{mx}^T [W^T K] \Lambda^* \tilde{\Omega}^T \bar{\xi} \\ &\quad - [\tilde{\Omega}^T \bar{\xi}]^T \Lambda^{*T} [K^T K] \Lambda^* \tilde{\Omega}^T \bar{\xi} \leq 0. \end{aligned} \quad (\text{D.41})$$

The above proof shows that $e_{mx}(t) \rightarrow 0$ as $t \rightarrow \infty$, which implies that $e_y(t) \in L_\infty$ as $t \rightarrow \infty$. ■

Appendix E

Proof for Results in Chapter 6

Another Class of Relative Degree Three Plant Model

Another class of relative degree three plant models are those with first-order actuators and first-order sensors. The first order actuators are modeled as

$$\dot{u}_p + (D_a + \Theta_a^{*T}) u_p = D_a u. \quad (\text{E.1})$$

where $D_a \geq 0$ is diagonal and known, and $\Theta_a^{*T} \in \mathbb{R}^{m \times m}$ are its uncertainties. The first order sensors are modeled as

$$\dot{w}_y + D_s w_y = D_s y_p \quad (\text{E.2})$$

with $D_s \geq 0$ is diagonal and known. Also, for command tracking we define integral error states $e_{pz} = z - z_{cmd}$ and $w_z := \int e_{pz} dt$. Define $w_u := \Lambda^* u_p$. The augmented plant model is square and can be written as

$$\begin{bmatrix} \dot{x}_p \\ \dot{w}_u \\ \dot{w}_y \\ \dot{w}_z \end{bmatrix} = \underbrace{\begin{bmatrix} A_p & B_p & 0 & 0 \\ 0 & -D_a & 0 & 0 \\ C_p & 0 & -D_s & 0 \\ C_{pz} & D_z & 0 & 0 \end{bmatrix}}_A \underbrace{\begin{bmatrix} x_p \\ w_u \\ w_y \\ w_z \end{bmatrix}}_x + \underbrace{\begin{bmatrix} B_p \\ 0 \\ 0 \\ D_z \end{bmatrix}}_{B_2} \Theta_p^{*T} x_p + \begin{bmatrix} 0 \\ I \\ 0 \\ 0 \end{bmatrix} \begin{bmatrix} -\Theta_a^{*T} \\ w_u \end{bmatrix} \\
+ \underbrace{\begin{bmatrix} 0 \\ D_a \\ 0 \\ 0 \end{bmatrix}}_{B_3} \Lambda^* u + \underbrace{\begin{bmatrix} 0 \\ 0 \\ 0 \\ -I \end{bmatrix}}_{B_z} z_{cmd} \\
y = \underbrace{\begin{bmatrix} 0 & 0 & I & 0 \\ 0 & 0 & 0 & I \end{bmatrix}}_C x, \quad z = \underbrace{\begin{bmatrix} C_{pz} & D_z & 0 & 0 \end{bmatrix}}_{C_z} x. \tag{E.3}$$

Proof of Proposition 6.1

Proof: Since

$$\begin{aligned}
A^* b_3 &= \begin{bmatrix} 0 \\ I \\ -(2\zeta\omega_n + \theta_{\zeta\omega}^*) \end{bmatrix} \omega_n^2 \\
A^{*2} b_3 &= \begin{bmatrix} b_p \\ -(2\zeta\omega_n + \theta_{\zeta\omega}^*) \\ (\omega_n^2 + \theta_{\zeta\omega}^*) + (2\zeta\omega_n + \theta_{\zeta\omega}^*)^2 \end{bmatrix} \omega_n^2,
\end{aligned} \tag{E.4}$$

b_1 can be spanned by $[b_3, A^* b_3, A^{*2} b_3]$ as

$$b_1 = A^{*2} b_3 \frac{1}{\omega_n^2} + A^* b_3 \frac{(2\zeta\omega_n + \theta_{\zeta\omega}^*)}{\omega_n^2} + b_3 \frac{(\omega_n^2 + \theta_{\zeta\omega}^*)}{\omega_n^2} \tag{E.5}$$

■

Proof of Lemma 6.2

Proof: From (6.3), it can be shown that

$$Ab_3 = \begin{bmatrix} 0 \\ I \\ -(2\zeta\omega_n) \end{bmatrix} \omega_n^2, \quad A^2 b_3 = \begin{bmatrix} b_p \\ -(2\zeta\omega_n) \\ (\omega_n^2) + (2\zeta\omega_n)^2 \end{bmatrix} \omega_n^2 \quad (\text{E.6})$$

Their differences from b_3^{i*} (E.4) can be written as

$$\begin{aligned} A^{*2} b_3 - A^2 b_3 &= \begin{bmatrix} 0 \\ -\theta_{\zeta\omega}^* \\ \theta_{\omega}^* + 4\zeta\omega_n\theta_{\zeta\omega}^* + \theta_{\zeta\omega}^{*2} \end{bmatrix} \omega_n^2 \\ &= A^* b_3 (-\theta_{\zeta\omega}^*) + b_3 (\theta_{\omega}^* + 2\zeta\omega_n\theta_{\zeta\omega}^*) \quad (\text{E.7}) \\ A^* b_3 - Ab_3 &= \begin{bmatrix} 0 \\ 0 \\ -\theta_{\zeta\omega}^* \end{bmatrix} \omega_n^2 = b_3 (-\theta_{\zeta\omega}^*) \end{aligned}$$

Then it is found that

$$\begin{aligned} b_3^{1*} - b_3^1 &= A^* b_3 (-\theta_{\zeta\omega}^*) + b_3 (\theta_{\omega}^* + 2\zeta\omega_n\theta_{\zeta\omega}^*) + b_3 \cdot 2(-\theta_{\zeta\omega}^*) \\ &= b_3^{2*} (-\theta_{\zeta\omega}^*) + b_3 (\theta_{\omega}^* + 2\zeta\omega_n\theta_{\zeta\omega}^*) \quad (\text{E.8}) \end{aligned}$$

$$b_3^{2*} - b_3^2 = b_3 (-\theta_{\zeta\omega}^*) \quad (\text{E.9})$$

The results follows. ■

Proof of Lemma 6.3

Proof: Using Lemma 6.2, Eq.s (6.6) and (6.12), it can be shown that

$$c^T (sI - A_{l*}^*)^{-1} f_3^2(\psi_3^1, \bar{e}_{\psi y}^{[1]}) = W_3^*(s) \left((s+1)^2 \left[\psi_3^1 \bar{e}_{\psi y}^{[1]} \right] - \psi_3^{1*} s \left[\psi_3^1 \bar{e}_{\psi y}^{[1]} \right] + (s+1)^2 \left[\psi_3^1 \bar{e}_{\psi y}^{[1][2]} \right] \right) \quad (\text{E.10})$$

Plugging in the definition of $\bar{e}_{\psi y}^{[1][2]}$ in (6.25) yields

$$c^T(sI - A_{l^*}^*)^{-1} f_3^2(\psi_3^1, \bar{e}_{\psi y}^{[1]}) = W_3^*(s)(s+1)^2 \left(\psi_3^1 \bar{e}_{\psi y}^{[1]} - \psi_3^{1*} \bar{e}_{\psi y}^{[1][2]} + \psi_3^1 \bar{e}_{\psi y}^{[1][2]} \right) \quad (\text{E.11})$$

Then apply (3.2) and the results follow. \blacksquare

Proof of Lemma 6.4

Proof: With (6.34), u_2 as in (6.32) can be rewritten as

$$\begin{aligned} u &= -\psi_1^T(t) [A^2 x_m - A l e_y] - \left(2\dot{\psi}_1^T(t) + 2\psi_1^T(t) \right) [Ax_m] \\ &\quad - \left(\ddot{\psi}_1^T(t) + 2\dot{\psi}_1^T(t) + \psi_1^T(t) \right) [x_m] - (s^2 + 2s) [\psi_1^T(t)] e_{y_1^0} \end{aligned} \quad (\text{E.12})$$

Since we design $\psi_1(t)$ as in (6.33), the following relation holds

$$\psi_1^T(t) b_3 = 0, \quad \psi_1^T(t) b_3^2 = 0 \quad (\text{E.13})$$

which leads to

$$\psi_1^T(t) \dot{x}_m = \psi_1^T(t) [Ax_m - l e_y] \quad (\text{E.14})$$

$$\psi_1^T(t) \ddot{x}_m = \psi_1^T(t) [A^2 x_m - A l e_y - l \dot{e}_y] \quad (\text{E.15})$$

This, together with $e_{y_1^0}$ in (6.35), in turn transforms (E.12) into

$$\begin{aligned} u &= -(s+1)^2 [\psi_1^T(t) x_m] - \psi_1^T(t) l \dot{e}_{y_1^0} - \left[2\dot{\psi}_1^T(t) + 2\psi_1^T(t) \right] \dot{e}_{y_1^0} \\ &\quad - ((s^2 + 2s) [\psi_1^T(t)]) e_{y_1^0} \end{aligned} \quad (\text{E.16})$$

Applying the chain rule of derivative yields

$$u = -(s+1)^2 [\psi_1^T(t) x_m] - (s+2) \cdot s \cdot [\psi_1^T(t) e_{y_1^0}] \quad (\text{E.17})$$

Applying (6.37) yields

$$u = -(s+1)^2 \left[\psi_1^T(t)x_m + \bar{e}_{\Psi_1 y_1^0}^{[1]} \right] \quad (\text{E.18})$$

which, together with (6.37), yields

$$\begin{aligned} c^T(sI - A_{l^*}^*)^{-1} & \left\{ b_3 \left[(s+1)^2 \left(\bar{\psi}_1^{*T} x_m \right) + u_2 \right] + f_{x_m}(e_y) \right\} = \\ W_3^{1*}(s)\lambda^* & \left[-\tilde{\psi}_1^{*T} x_m \right] - W_3^{1*}(s)\lambda^* \bar{e}_{\Psi_1 y_1^0}^{[1]} + c^T(sI - A^*)^{-1} f_{x_m}(e_y; s) \end{aligned} \quad (\text{E.19})$$

Now we will show that $f_{x_m}(e_y; s)$ addresses $\lambda^* \bar{e}_{\Psi_1 y_1^0}^{[1]}$. Since $\bar{e}_{\Psi_1 y_1^0}^{[1]}$ is not directly available to us, we have to design $f_{x_m}(s)$ using Lemma 6.3 as in (6.36), which yields

$$\begin{aligned} & -W_3^{1*}(s)\lambda^* \bar{e}_{\Psi_1 y_1^0}^{[1]} + c^T(sI - A^*)^{-1} f_{x_m}(e_y; s) \\ & = W_3^*(s) \left[(s+1)^2 \left[\lambda(t) \bar{e}_{\Psi_1 y_1^0}^{[1]} \right] \right] + W_3^*(s) \left[-\psi_3^{1*} s \left[\lambda(t) \bar{e}_{\Psi_1 y_1^0}^{[1]} \right] + (s+1)^2 \left[\psi_3^1(t) \bar{e}_{\Psi_1 y_1^0}^{[1][2]} \right] \right] \\ & = W_3^*(s)(s+1)^2 \left[\lambda(t) \bar{e}_{\Psi_1 y_1^0}^{[1]} - \psi_3^{1*} \bar{e}_{\Psi_1 y_1^0}^{[1][2]} + \psi_3^1(t) \bar{e}_{\Psi_1 y_1^0}^{[1][2]} \right] \end{aligned} \quad (\text{E.20})$$

where we have applied the definition of $\bar{e}_{\Psi_1 y_1^0}^{[1][2]}$ in (6.37). This directly leads to the results. \blacksquare

Proof of Theorem 6.1

Proof: For the high order tuner (6.41), define an error coordinate z_h as

$$z_h = x_h + A_h^{-1} b_h \psi_1'^T \quad (\text{E.21})$$

which allows its output as

$$c_h^T z_h = \psi_1^T(t) - \psi_1'^T(t) \quad (\text{E.22})$$

whose dynamics are

$$\dot{z}_h(t) = A_h g(x_m) z_h + A_h^{-1} b_h \dot{\psi}_1'^T(t). \quad (\text{E.23})$$

Now we will prove the stability results of Theorem 6.1. We propose a Lyapunov function as

$$V = e_{mx}^T P^* e_{mx} + (\psi'_1 - \psi_1^*)^2 + \eta z_h^T P_h z_h \quad (\text{E.24})$$

where e_{mx} is the states of error model, P^* satisfies

$$\begin{aligned} P^* (A^* - l^* c^T) + (A^* - l^* c^T)^T P^* &= -Q^* < 0 \\ P^* b_3^{1*} &= c \end{aligned} \quad (\text{E.25})$$

which are the results of SPR properties of (6.40), and P_h satisfies

$$P_h A_h + A_h P_h^T = -I. \quad (\text{E.26})$$

Using (6.40) and (E.23), \dot{V} is found to be

$$\begin{aligned} \dot{V} &= -e_{mx}^T Q^* e_{mx} + 2P^* b_3^{1*} e_{mx}^T \lambda^* \left[(\psi_1 - \psi'_1) + (\psi'_1 - \psi_1^*) \right]^T x_m \\ &\quad - 2e_y \lambda^* (\psi'_1 - \psi_1^*)^T x_m - \eta \cdot [z_h^T I z_h] g(x_m) + 2\eta \cdot [z_h^T P_h A_h^{-1} b_h e_y x_m] \end{aligned} \quad (\text{E.27})$$

which, combined with (E.25), yields

$$\begin{aligned} \dot{V} &= -e_{mx}^T Q^* e_{mx} - \eta \cdot [z_h^T z_h] g(x_m) \\ &\quad + 2e_y \lambda^* (\psi_1 - \psi'_1)^T x_m + 2\eta \cdot [z_h^T P_h A_h^{-1} b_h e_y x_m] \end{aligned} \quad (\text{E.28})$$

which is equivalent to

$$\begin{aligned} \dot{V} &= -e_{mx}^T Q^* e_{mx} - \eta \cdot [z_h^T z_h] - \eta \cdot \mu [z_h x_m]^2 \\ &\quad + 2e_y \lambda^* c_h^T z_h x_m + 2\eta \cdot [z_h^T P_h A_h^{-1} b_h e_y x_m] \end{aligned} \quad (\text{E.29})$$

using (E.22). Then we pick

$$\eta = \frac{\|c_h\| \lambda_{max}}{\|P_h A_h^{-1} b_h\|}, \quad \mu = \frac{2 \|c\|^2 \|c_h\|^2 \lambda_{max}^2}{\lambda_{min, Q^*} \eta} \quad (\text{E.30})$$

where $|\lambda^*| \leq \lambda_{max}$, which leads to

$$\begin{aligned}\dot{V} &\leq -\lambda_{min,Q^*} \|e_{mx}\|^2 - \eta \cdot [z_h^T z_h] - \eta \cdot \mu \|z_h x_m\|^2 \\ &\quad + 4 \|c\| \|e_{mx}\| \lambda_{max} \|c_h\| \|z_h x_m\|\end{aligned}\tag{E.31}$$

and therefore

$$\dot{V} \leq -\eta \cdot [z_h^T z_h] - \left(\sqrt{\lambda_{min,Q^*}} \|e_{mx}\| - \sqrt{\eta \mu} \cdot \|z_h x_m\| \right)^2.\tag{E.32}$$

As a result, $e_{mx}(t)$, $z_h(t)$, $\psi'_1(t)$ are all bounded as $t \rightarrow \infty$, and therefore $x_m(t)$ is bounded in the CRM, which proves i). This in turn implies \dot{z}_h as in (E.23) is bounded. Applying Barbalat's Lemma yields that $z_h(t) \rightarrow 0$ as $t \rightarrow \infty$, which in turns implies that in (E.32) $e_{mx}(t) \rightarrow 0$ as $t \rightarrow \infty$. Then the results of ii) follows. ■

Proof of Lemma 6.6

Proof: The proof will be very similar to the proof of Lemma 5.3 and therefore only key steps are shown in this proof. The input normal form of the plant model

(6.47) is

$$\begin{aligned}
\begin{bmatrix} \dot{\xi}_1 \\ \dot{\xi}_2 \\ \dot{\xi}_3 \\ \dot{\eta} \end{bmatrix} &= \underbrace{\begin{bmatrix} 0 & 0 & R_1 & V \\ I_m & 0 & R_2 & 0 \\ 0 & I_m & R_3 & 0 \\ 0 & 0 & U & Z \end{bmatrix}}_{A_{in}} \underbrace{\begin{bmatrix} \xi_1 \\ \xi_2 \\ \xi_3 \\ \eta \end{bmatrix}}_{x_{in}} + \underbrace{\begin{bmatrix} \times \\ \times \\ \times \\ 0 \end{bmatrix}}_{B_{1,in}} \underbrace{\begin{bmatrix} 0 & 0 & \psi_1^{3*T} & \psi_1^{(n-3m)*T} \end{bmatrix}}_{\Psi_{1,in}^{*T}} x_{in} \\
&\quad + \underbrace{\begin{bmatrix} I_m \\ 0 \\ 0 \\ 0 \end{bmatrix}}_{B_{3,in}} \underbrace{\begin{bmatrix} \psi_3^{1*T} & \psi_3^{2*T} & \psi_3^{3*T} & \psi_3^{(n-3m)*T} \end{bmatrix}}_{\Psi_{3,in}^{*T}} x_{in} \\
&\quad + B_{3,in} \Lambda^* u + B_{in,z} z_{cmd} \\
y &= \underbrace{\begin{bmatrix} 0 & 0 & CA^2 B_3 & 0 \end{bmatrix}}_{C_{in}} x_{in}
\end{aligned} \tag{E.33}$$

using $x_{in} = T_{in}x$, $A_{in} = T_{in}AT_{in}^{-1}$, $B_{3,in} = T_{in}B_3$, $B_{1,in} = T_{in}B_1$, $B_{in,z} = T_{in}B_z$, $C_{in} = CT_{in}^{-1}$, $\Psi_{1,in}^{*T} = \Psi_1^{*T}T_{in}^{-1}$, $\Psi_{3,in}^{*T} = \Psi_3^{*T}T_{in}^{-1}$ and $\begin{bmatrix} R_1^T & R_2^T & R_3^T \end{bmatrix}^T = ((\mathfrak{CB})^{-1}\mathfrak{CA}^2B)^T$, where T_{in} is defined in (3.13). It is noted that $(T_{in}B_1)^T = \begin{bmatrix} \times & \times & \times & 0 \end{bmatrix}$ since Assumption 6.4 holds, and that $\Psi_{1,in}^{*T} = \begin{bmatrix} 0 & 0 & \times & \times \end{bmatrix}$ since Assumption 6.5 holds. All equations in this proof are valid in both coordinates, and matrices in input norm form coordinate will be denoted with subscript $(\cdot)_{in}$.

To prove Lemma 6.6, It is equivalent to show $\{(A_{in}^* - L_{in}^* C_{in}), B_{3,in}^{1*}, SC_{in}\}$ is SPR, where $A_{in}^* = T_{in}A^*T_{in}^{-1}$ and $B_{3,in}^{1*} = T_{in}B_3^{1*}$. Define $\bar{C}_{in} = SC_{in}$,

$$M_{in}^T = \begin{bmatrix} I & 0 & 0 & 0 \\ 0 & I & 0 & 0 \\ 0 & 0 & 0 & I \end{bmatrix} \tag{E.34}$$

which is the null space of C_{in} . The rest of the proof is exactly following the proof of

Lemma 5.3 and noting

$$\Delta_{CAB}^* = (C_{in}B_{3,in}^1)^T C_{in}B_{in}^1 \Psi_R^{*T} \quad (\text{E.35})$$

where $\Psi_R^{*T} = (\psi_3^{1*} + a_2^1/a_2^2) + (\psi_1^{3*T} + R_3)$ and

$$\|H_{in}^*\| \leq \|P_I^*\| \|N_{in}^{1*} A_{in} B_{3,in}^{1*}\| + \|\bar{C}_{in} A_{in}^* M_{in}\| \quad (\text{E.36})$$

$$\begin{aligned} N_{in}^{1*} \bar{A}_{in}^* B_{in}^{1*} &= N_{in}^1 A_{in} B_{in}^1 \\ &+ \begin{bmatrix} (a_2^2 R_3 + a_2^1 R_2 + a_2^0 R_1)((\psi_3^{1*})^2 + \psi_3^{2*T}) \\ (a_2^2 R_3 + a_2^1 R_2) \psi_3^{1*} \\ 0 \end{bmatrix} \end{aligned} \quad (\text{E.37})$$

$$\begin{aligned} C_{in} A_{in}^* M_{in} &= C_{in} A_{in} M_{in} \\ &+ \begin{bmatrix} 0 & 0 & CA^2 B_3 \psi_1^{(n-3m)*T} \end{bmatrix} \end{aligned} \quad (\text{E.38})$$

■

Proof of Lemma 6.7

Proof: The proof is carried out in the input normal form as in (E.33) where

$$\Psi_{3,in}^{*T} = \begin{bmatrix} \psi_3^{1*T} & \psi_3^{2*T} & \psi_3^{3*T} & \psi_3^{(n-3m)*T} \end{bmatrix}. \quad (\text{E.39})$$

Following the definition of B_3^{i*} in (6.69) it can be shown that

$$\begin{aligned} &\left[\begin{array}{c|c|c} B_3^{3*} & B_3^{2*} & B_3^{1*} \end{array} \right]_{in} \\ &= \left[\begin{array}{c|c|c} a_2^2 & a_2^2 \psi_3^{1*T} + a_2^1 & a_2^2 (\psi_3^{1*2} + \psi_3^{2*T}) + a_2^1 \psi_3^{1*T} + a_2^2 \\ 0 & a_2^2 & a_2^2 \psi_3^{1*T} + a_2^1 \\ 0 & 0 & a_2^2 \\ \hline 0 & 0 & 0 \end{array} \right] \end{aligned} \quad (\text{E.40})$$

Similarly, following the definition of B_3^1 in (6.60), it can be shown that

$$\left[\begin{array}{ccc} B_3^3 & B_3^2 & B_3^1 \end{array} \right]_{in} = \left[\begin{array}{ccc} a_2^2 & a_2^1 & a_2^0 \\ 0 & a_2^2 & a_2^1 \\ 0 & 0 & a_2^2 \\ \hline 0 & 0 & 0 \end{array} \right] \quad (\text{E.41})$$

Then the results follows after some algebra. ■

Proof of Proposition 6.3

Proof: Then performing rearrangement on the uncertainties terms Ψ_1^* , Ψ_2^* and Ψ_3^* as

$$\left[\begin{array}{ccc} B_3 & 0 & B_1 \end{array} \right] \left[\begin{array}{c} \Psi_3^{*T} \\ 0 \\ \Psi_1^{*T} \end{array} \right] = \left[\begin{array}{ccc} B_3^{3*} & B_3^{2*} & B_3^{1*} \end{array} \right] \left[\begin{array}{ccc} \Lambda^* & & \\ & \Lambda^* & \\ & & \Lambda^* \end{array} \right] \left[\begin{array}{c} \bar{\Psi}_3^{*T} \\ \bar{\Psi}_2^{*T} \\ \bar{\Psi}_1^{*T} \end{array} \right]. \quad (\text{E.42})$$

Such parametrization always exists since in the input normal form,

$$\left[\begin{array}{ccc} B_3 & 0 & B_1 \end{array} \right]_{in} = \left[\begin{array}{ccc} \times & 0 & \times \\ 0 & 0 & \times \\ 0 & 0 & \times \\ \hline 0 & 0 & 0 \end{array} \right], \text{ and } \left[\begin{array}{ccc} B_3^{3*} & B_3^{2*} & B_3^{1*} \end{array} \right]_{in} = \left[\begin{array}{ccc} \times & \times & \times \\ 0 & \times & \times \\ 0 & 0 & \times \\ \hline 0 & 0 & 0 \end{array} \right] \quad (\text{E.43})$$

(see Assumption 6.5), and

$$\left[\begin{array}{c} \Psi_3^{*T} \\ \Psi_2^{*T} \\ \Psi_1^{*T} \end{array} \right]_{in} = \left[\begin{array}{ccc|c} 0 & 0 & \times & \times \\ 0 & 0 & \times & \times \\ \times & \times & \times & \times \end{array} \right]. \quad (\text{E.44})$$

The rearranged uncertainties in the input normal form coordinate also have a structure of

$$\begin{bmatrix} \overline{\Psi}_3^{*T} \\ \overline{\Psi}_2^{*T} \\ \overline{\Psi}_1^{*T} \end{bmatrix}_{in} = \left[\begin{array}{ccc|c} 0 & 0 & \times & \times \\ 0 & 0 & \times & \times \\ \times & \times & \times & \times \end{array} \right]. \quad (\text{E.45})$$

■

Proof of Lemma 6.8

Proof: The proof is very similar to the proof of Lemma 6.3, noting that

$$\begin{aligned} C(sI - A_{L^*}^*)^{-1} F(t) &= C(sI - A_{L^*}^*)^{-1} [(B_3^2 s + B_3^3) \phi^T(t) \bar{\omega}^{[1]} + \pi_2^2(s) (\psi_3^1(t) \bar{\omega}^{[1][2]}(t))] \\ &= W_3^*(s) \pi_2^2(s) (\phi^T(t) \bar{\omega}^{[1]} + \tilde{\psi}_3^1(t) \bar{\omega}^{[1][2]}(t)) \end{aligned} \quad (\text{E.46})$$

where we have used the property of B_3^2 in Lemma 6.7, the equivalent realization of B_3^{2*} in Lemma 3.3, and the definition of $\bar{\omega}^{[1][2]}(t)$ in (6.75). It is noted that each time Lemma 3.3 is used to generate zeros in the error model analysis, Eq.(3.18) has to be used to change the state coordinate, which yields (6.77). ■

Proof of Lemma 6.9

Proof: The proof will be a direct extension of the derivation in Section 6.1.2 and therefore only a brief step is shown below. The first portion of the proof follows the proof of Lemma 6.8. Replacing L with

$$L^* = B_3^{1*} R^{-1} S \quad (\text{E.47})$$

in the error model (6.67), using Eq.(6.71) to specify the difference and applying Proposition 6.3 yields

$$\begin{aligned}
\dot{e}_x &= (A^* - L^* C)e_x \\
&\quad + B_3^{2*} \psi_3^{1*T} e_{sy} + B_3^{3*} \psi_3^{2*T} e_{sy} - F_L(e_y; s) \\
&\quad + B_3^{1*} \Lambda^* \bar{\Psi}_1^{*T} x_m + B_3^{2*} \Lambda^* \bar{\Psi}_2^{*T} x_m + B_3^{3*} \Lambda^* \bar{\Psi}_3^{*T} x_m \\
&\quad + B_3 \Lambda^* (u_{bl} + u_{ad}) - B_3 u_{bl} + F_{x_m}(e_y; s)
\end{aligned} \tag{E.48}$$

Plugging in (6.59) and applying Lemma 6.8 transforms (E.48) into

$$\begin{aligned}
\dot{e}'_x &= A_{L^*}^* e'_x - B_3^{1*} \tilde{\psi}_3^{1T} \left[\bar{e}_{y\psi}^{[1]} + \bar{e}_{y\psi}^{[1][2]} \right] - B_3^{1*} \tilde{\psi}_3^{2T} \bar{e}_{y\psi}^{[2]} \\
&\quad + B_3^{1*} \Lambda^* \bar{\Psi}_1^{*T} x_m + B_3^{2*} \Lambda^* \bar{\Psi}_2^{*T} x_m + B_3^{3*} \Lambda^* \bar{\Psi}_3^{*T} x_m \\
&\quad + B_3 \Lambda^* [-\Lambda^{*-1} u_{bl} + u_{bl} + u_{ad}] + F_{x_m}(e_y; s).
\end{aligned} \tag{E.49}$$

Applying Lemma 3.3 and substituting (6.66) yields

$$\begin{aligned}
\dot{e}''_x &= A_{L^*}^* e''_x - B_3^{1*} \tilde{\psi}_3^{1T} \left[\bar{e}_{\psi y}^{[1]} + \bar{e}_{\psi y}^{[1][2]} \right] - B_3^{1*} \tilde{\psi}_3^{2T} \bar{e}_{\psi y}^2 \\
&\quad + B_3 \Lambda^* \pi_2^2(s) \left[-\Lambda^{*-1} \bar{u}_{bl}^{[2]} + \bar{\Psi}_1^{*T} x_m + \bar{\Psi}_2^{*T} \bar{x}_m^{[1]} + \bar{\Psi}_3^{*T} \bar{x}_m^{[2]} \right] \\
&\quad + B_3 \Lambda^* [u_{bl} + u_{ad}] + F_{x_m}(e_y; s).
\end{aligned} \tag{E.50}$$

The rest of the proof follows that of Lemma 6.4. Since $\Psi_1(t)$ has a special structure as in (6.65), $\Psi_1^T(t)F_L(e_y; s) = 0$ and $\Psi_1^T(t)F_{x_m}(e_y; s) = 0$ and therefore

$$\begin{aligned}
\Psi_1^T(t) \dot{x}_m &= \Psi_1^T(t) [Ax_m + B_m z_{cmd} - Le_y] \\
\Psi_1^T(t) \ddot{x}_m &= \Psi_1^T(t) [A^2 x_m + AB_m z_{cmd} - AL e_y + B_m \dot{z}_{cmd} - L \dot{e}_y]
\end{aligned} \tag{E.51}$$

All terms, except $L\dot{e}_y$, in (E.51) are available for control and therefore are put in u_{ad} . Expansion of the compact form of u_{ad} as in (6.63) shows

$$\begin{aligned} u_{ad} = & -u_{bl} + \pi_2^2(s) \left[\Lambda^T(t) \bar{u}_{bl}^{[2]} - \Psi_2^T(t) \bar{x}_m^{[1]} - \Psi_3^T(t) \bar{x}_m^{[2]} \right] \\ & - a_2^2 d_2^0 \Psi_1^T(t) [A^2 x_m + AB_m z_{cmd} - AL e_y + B_m \dot{z}_{cmd}] \\ & - \left(a_2^2 d_2^1 \dot{\Psi}_1^T(t) + a_2^1 d_1^0 \Psi_1^T(t) \right) [Ax_m + B_m z_{cmd}] \\ & - \left(a_2^2 d_2^2 \ddot{\Psi}_1^T(t) + a_2^1 d_1^1 \dot{\Psi}_1^T(t) + a_2^0 d_0^0 \Psi_1^T(t) \right) [x_m] \\ & - (a_2^2 d_2^2 s^2 + a_2^1 d_1^1 s) [\Psi_1^T(t)] e_{y_1^0} \end{aligned} \quad (\text{E.52})$$

Applying Eq.(E.51), substituting the definition of $e_{y_1^0}$ in (6.62), applying the chain rule of derivative yields

$$\begin{aligned} u_{ad} = & -u_{bl} + \pi_2^2(s) \left[\Lambda^T(t) \bar{u}_{bl}^{[2]} - \Psi_1^T(t) x_m - \Psi_2^T(t) \bar{x}_m^{[1]} - \Psi_3^T(t) \bar{x}_m^{[2]} \right] \\ & - (a_2^2 s + a_2^1) \cdot s [\Psi_1^T(t) e_{y_1^0}] \end{aligned} \quad (\text{E.53})$$

Substituting u_{ad} (E.52), $F_{x_m}(e_y; s)$ (6.58) in (E.50), and applying Lemma 6.8 yields

$$\begin{aligned} \dot{e}_{mx} = & A_{L^*}^* e_{mx} - B_3^{1*} \tilde{\psi}_3^{1T} \left[\bar{e}_{\psi y}^{[1]} + \bar{e}_{\psi y}^{[1][2]} \right] - B_3^{1*} \tilde{\psi}_3^{2T} \bar{e}_{\psi y}^{[2]} \\ & + B_3^{1*} \Lambda^* \left[\tilde{\Lambda}^T \bar{u}_{bl}^{[2]} - \tilde{\Psi}_1^T(t) x_m - \tilde{\Psi}_2^T \bar{x}_m^{[1]} - \tilde{\Psi}_3^T \bar{x}_m^{[2]} \right] \\ & + B_3^{1*} \tilde{\Lambda}^T \bar{e}_{\Psi_1 y_1^0}^{[1]} + B_3^{1*} \tilde{\psi}_3^{1T} \bar{e}_{\Psi_1 y_1^0}^{[1][2]} \end{aligned} \quad (\text{E.54})$$

Grouping terms, and noting that Lemma 6.6 guarantees that $\{A_{L^*}^*, B_3^{1*}, SC\}$ is SPR, yields the results. ■

Proof of Theorem 6.2

Proof: Without loss of generality, we consider the error model as

$$\begin{aligned} \dot{e}_{mx} = & A_{L^*}^* e_{mx} + B_3^{1*} \Lambda^* \tilde{\Omega}^T \bar{\xi} \\ e_y = & C e_{mx}. \end{aligned} \quad (\text{E.55})$$

The following proof will be very similar to the proof of Lemma 6.1 and therefore only brief steps are listed. First we define a new tuner state as

$$Z_\Omega = X_\Omega + A_H^{-1} B_H \Omega'^T \quad (\text{E.56})$$

whose dynamics are

$$\dot{Z}_\Omega = A_H Z_\Omega g(\bar{\xi}; \mu_\xi) + A_H^{-1} B_H \dot{\Omega}'^T. \quad (\text{E.57})$$

and g is defined in (6.83). Then the difference between Ω and Ω' can be written as

$$\Omega^T - \Omega'^T = C_H Z_\Omega \quad (\text{E.58})$$

since $C_H A_H^{-1} B_H = -I$.

Let P^* be the matrix that guarantees the SPR properties of $\{A_{L^*}^*, B_3^{1*}, SC\}$ as

$$\begin{aligned} P^* A_{L^*}^* + A_{L^*}^{*T} P^* &= -Q^* < 0 \\ P^* B_3^{1*} &= C^T S^T \end{aligned} \quad (\text{E.59})$$

We propose a Lyapunov function

$$\begin{aligned} V &= e_{mx}^T P^* e_{mx} + Tr \left[\left(\Omega' - \Omega^* \right)^T \Gamma^{-1} \left(\Omega' - \Omega^* \right) |\Lambda^*| \right] \\ &\quad + \delta_\xi \cdot Tr [Z_\Omega^T P_H Z_\Omega] > 0 \end{aligned} \quad (\text{E.60})$$

whose derivatives are derived by applying (E.55)(E.59) as

$$\begin{aligned} \dot{V} &\leq -\delta_\xi \cdot \sum_{j=1}^{m+3n} z_\Omega^{jT} z_\Omega^j \\ &\quad - \sum_{j=1}^{m+3n} \left[\frac{n\lambda_Q}{m+3n} e_{mx}^2 - 4 \|SC\| \|C_H\| \|e_{mx}\| \|z_\Omega^j\| \|\bar{\xi}^j\| + \delta_\xi \mu_\xi z_\Omega^{jT} z_\Omega \bar{\xi}^2 \right] \end{aligned} \quad (\text{E.61})$$

where z_Ω^1 is an element of Z_Ω

$$Z_\Omega = \begin{bmatrix} z_\Omega^1 & z_\Omega^2 & \cdots & z_\Omega^{[m+3n]} \end{bmatrix}, \quad (\text{E.62})$$

and we have used the fact that $Q > Q^*$. Plugging in the definition of δ_ξ and δ_ν yields

$$\dot{V} \leq -\delta_\xi \cdot \sum_{j=1}^{m+3n} z_\Omega^{jT} z_\Omega^j - \sum_{j=1}^{m+3n} \left[\sqrt{\frac{n\lambda_Q}{m+3n}} \|e_{mx}\| - \sqrt{\delta_\xi \mu_\xi} \|z_\Omega^{jT}\| \|\bar{\xi}^{jT}\| \right]^2 \leq 0$$

As a result, all signals in (E.60) are bounded and therefore signals in CRM are also bounded, which proves i). One can follow the proof of Theorem 6.1 and shows that $e_x(t) \rightarrow 0$ and $e_y(t) \rightarrow 0$ as $t \rightarrow \infty$, which proves ii).

Following the derivation of recursive adaptation as in (6.77), e_x and e_{mx} is related as

$$e_{mx} = e_x + [B_3^{2*} + B_3^{3*} s] [\tilde{\Omega}^T \bar{\xi} + \dots] \quad (\text{E.63})$$

where some terms similar to $\tilde{\Omega}^T \bar{\xi}$ are omitted. It is noted that since all signals in V are bounded and in particular, $z_\Omega(t) \rightarrow 0$ as $t \rightarrow \infty$, $[B_3^{2*} + B_3^{3*} s] \tilde{\Omega}^T \bar{\xi}$ is guaranteed to be bounded. It is also noted that $\int (z - z_{cmd}) dt$ is an element of x and $\int [(z_m - z_{cmd}) + L_I e_y] dt$, where L_I is the rows of L corresponding to z_m , is an element of x_m . It follows $e_{mx}(t) \rightarrow 0$ and x_m is bounded that e_x is bounded, and therefore $\int (z - z_m) dt$ is bounded. Also it is noted that \ddot{x}_m is bounded and therefore $(z - z_m)^{(1)}$ is bounded. Applying Barbalat's Lemma proves iii). ■

Appendix F

Proof for Results in Chapter 7

Proof of Lemma 7.2

Proof: Lemma 3.3 says that

$$\begin{aligned}\dot{e}_x &= A_L^* e_x + B_r^{i*} \phi^{*T} \omega(t) - F(t) \\ e_y &= C e_x\end{aligned}$$

is equivalent to

$$\begin{aligned}\dot{e}'_x &= A_L^* e'_x + B_r \phi^{*T} \pi_{r-1}^{r-1-i}(s) [\omega(t)] - F(t) \\ e_y &= C e_x\end{aligned}\tag{F.1}$$

in terms of transfer function matrix.

Step 1: Substituting the definition of $\bar{\omega}^{[i-1]}(t)$ yields

$$e'_x = A_L^* e'_x + B_r \phi^{*T} \pi_{r-1}^{r-1}(s) [\bar{\omega}^{[i-1]}(t)] - F(t)\tag{F.2}$$

Step 2: Substituting the definition of $F(t)$ and F_r^i in (7.6) applying Proposition 6.7

yields

$$\begin{aligned}
\dot{e}_x'' &= A_L^* e_x'' + B_r \phi^{*T} \pi_2^2(s) [\bar{\omega}^{[i-1]}(t)] - B_3 \pi_2^2(s) [\phi^T(t) \bar{\omega}^{[i-1]}(t)] \\
&\quad + \sum_{j=1}^{r-i} B_r \psi_r^{[j]*} \pi_{r-1}^{r-i-j}(s) \cdot s^{i-1} [\phi^T(t) \bar{\omega}^{[i-1]}(t)] \\
&\quad - \sum_{j=1}^{r-1-i} [F_r^{i+j}(\psi_r^{jT}(t) \bar{\omega}^{[i-1][i-1+j]}(t)) + \\
&\quad + \sum_{k=1}^{r-i-j} F_r^{i+j+k}(\psi_r^{kT}(t) \bar{\omega}^{[i-1][i-1+j][i-1+j+k]}(t)) + \dots]
\end{aligned} \tag{F.3}$$

Substituting the definition of $\bar{\omega}^{[i-1][i-1+j]}(t)$ as in Eq.(7.10) and applying Proposition 3.2 yields

$$\begin{aligned}
\dot{e}_x'' &= A_L^* e_x'' - B_r \pi_{r-1}^{r-1}(s) [\tilde{\phi}^T(t) \bar{\omega}^{[i-1]}(t)] \\
&\quad + \sum_{j=1}^{3-i} B_r \psi_3^{[j]*} \pi_{r-1}^{r-1}(s) [\bar{\omega}^{[i-1][i-1+j]}(t)] \\
&\quad - \sum_{j=1}^{r-1-i} [F_r^{i+j}(\psi_r^{jT}(t) \bar{\omega}^{[i-1][i-1+j]}(t)) + \\
&\quad + \sum_{k=1}^{r-i-j} F_r^{i+j+k}(\psi_r^{kT}(t) \bar{\omega}^{[i-1][i-1+j][i-1+j+k]}(t)) + \dots]
\end{aligned} \tag{F.4}$$

Then repeating Step 1-2 on $\bar{\omega}^{[i-1][i-1+j]}(t)$ and so on until the last index of $\bar{\omega}^{[i]\dots[j][k]}$ hits $[r-1]$, will yield the results. \blacksquare